Selection Based List Detection with Approximate Matrix Inversion for Large-Scale MIMO Systems

Tianpei Chen

Department of Electrical & Computer Engineering
McGill University
Montreal, Québec, Canada

August 2016

A thesis submitted to McGill University in partial fulfillment of the requirements for the degree of Master of Engineering.

2016/08/01

Abstract

Large-scale multiple-input multiple-output (LS-MIMO) technology constitutes a foundation for next generation wireless communication system. Selection based list detection is attractive for practical LS-MIMO system because of its massively parallelizable nature. In this paper, we propose an improved high performance selection based list algorithm, which takes into account the channel hardening phenomenon making it suitable for LS-MIMO. First, we propose a low latency approximate matrix inversion scheme, for replacing the time consuming large dimensional complex matrix inversion, that is widely used not only in selection based list detections but also in many other LS-MIMO detection techniques. To assess the performance of the proposed approximate matrix inversion scheme for detection in LS-MIMO we consider its application for a linear detector (LD) and propose a hybrid technique inspired by channel hardening to reduce the error floor induced by this approximation. The proposed approximate matrix inversion scheme can be integrated into selection based list detection for achieving a lower processing latency and deeper parallelism. Then our analysis of the impact of channel hardening on selection based list detection motivates the use of an improved ordering scheme for the successive interference cancellation (SIC) sub-detector. We compare the improved selection based list algorithm with other two state-of-art high performance low complexity LS-MIMO detection techniques, namely multistage likelihood ascent search (LAS) and message passing detection (MPD). Computer simulation shows that the proposed selection based list detection algorithm performs better than multistage LAS and has just a fraction of dB performance loss compared with MPD. The complexity of the proposed algorithm, multistage-LAS and MPD are in the same order of magnitude and the last two do not have the advantage of being massively parallelizable.

Sommaire

La technologie MIMO à grande échelle (LS-MIMO) forme une base pour la prochaine génération de systèmes de communication sans fil. La détection de liste en fonction de sélection est attrayante pour les systèmes LS-MIMO pratiques, dû à leur nature fortement parallélisable. Dans cet article, nous proposons un algorithme amélioré et à haute performance pour la détection de liste en fonction de sélection, qui prend en compte le phénomène de durcissement de canaux, le rendant approprié pour le LS-MIMO. En premier lieu, nous proposons un schème d'inversion matricielle approximative a faible latence, ainsi permettant de sauver du temps par rapport à l'application de l'inversion matricielle complexe a large dimension, couramment utilisee non seulement dans la détection de liste en fonction de sélection, mais aussi dans d'autres techniques de detection de LS-MIMO. Afin d'évaluer la performance de le schème d'inversion matricielle approximative dans la détection de LS-MIMO, on considère son application pour un détecteur linéaire (LD) et on propose une technique hybride inspirée par le durcissement de canaux, visant à réduire le plancher d'erreur induit par cette approximation. Le schème d'inversion matricielle approximative peut être intégrée dans la détection de liste en fonction de sélection afin d'atteindre une plus faible latence dans le traitement et un parallélisme plus profond. Ainsi, notre analyse de l'impact du durcissement des canaux sur la détection de liste en fonction de sélection incite à l'utilisation d'un schème de commande amélioré pour le sub-détecteur successive interference cancellation (SIC). Nous comparons la détection de liste en fonction de sélection avec deux autres techniques modernes de détection LS-MIMO à haute performance faible complexité, notamment le multistage likelihood ascent search (LAS) et le message passing detection (MPD). La simulation informatique démontre que la détection de liste en fonction de sélection proposé performe mieux qu'une détection multiétage LAS, et n'enregistre qu'une faible perte de performance dB par rapport à la détection MPD. La complexité de l'algorithme proposé, les détections multiétage-LAS et MPD se trouvent dans le même ordre de grandeur, les deux derniers ne possédant pas l'avantage d'être fortement parallélisables.

Acknowledgments

First and foremost, I would like to express my sincere gratitude to my supervisor, Prof Harry Leib, for his patient instructions, insightful advices and financial support during my master program. I have learned a lot from his earnest attitude and acute inspirations for research.

Furthermore, I would like to thank my lab colleagues, my course instructors, my friends and all the people who provide kindly help to my work and life during these years.

At last, I am deeply indebted to my parents for their continuous support and encouragement. Without them, this work would not have been completed successfully.

Contents

List of Figures

List of Tables

List of Acronyms

AWGN	Additive White Gaussian Noise
APP	A Posterior Probability
BER	Bit Error Rate
CSCG	Circularly Symmetric Complex Gaussian
GIG	Generalize Integer Gaussian Distribution
LS-MIMO	Large-Scale Multiple-Input Multiple-Output
LD	Linear Detector
MLD	Maximum Likelihood Detector
MED	Minimum Euclidean Distance
MAP	Maximum A Posterior
MU	Multiuser
MMSE	Minimum Mean Square Error
OM	Orthogonality Measure
QAM	Quadrature Amplitude Modulation
SNR	Signal to Noise Ratio
SINR	Signal to Interference plus Noise Ratio
SD	Sphere Decoder
SIC	Successive Interference Cancellation
V-BLAST	Vertical Bell Labs Layered Space-Time
ZF	Zero Forcing

Notation Convention

$\mathbf{X}$	Matrix $\mathbf{X}$
$\mathbf{I}_N$	$N \times N$ identity matrix
$\mathbf{0}$	Zero vector or matrix
$\mathbf{x}_i$	ith column of matrix $\mathbf{X}$
$[\mathbf{X}]_{ij}$	Component of matrix $\mathbf{X}$ at ith row jth column
$(\cdot)^H$	Conjugate transpose
$det(\mathbf{X})$	Determinant of matrix $\mathbf{X}$
$Tr(\mathbf{X})$	Trace of matrix $\mathbf{X}$
$\lambda_{max}(\mathbf{X})$	Maximum eigenvalue of matrix $\mathbf{X}$
$\lambda_{min}(\mathbf{X})$	Minimum eigenvalue of matrix $\mathbf{X}$
$\mathbb{E}(\cdot)$	Expectation
$Var(\cdot)$	Variance
$\|\| \cdot \|\|$	Euclidean norm
$\|\| \cdot \|\|_F$	Frobenius norm
$\mathbb{A}$	set $\mathbb{A}$
$\|\mathbb{A}\|$	size of set $\mathbb{A}$
$\mathbb{A}^N$	N dimensional vector space with each component of the vector drawn from $\mathbb{A}$
$\mathbb{O}(\cdot)$	Order of magnitude
$\mathcal{Q}(\cdot)$	Quantization
$\Re(\cdot)$	Real part

$\Im(\cdot)$	Imaginary part
$Pr(A)$	Probability that event A occurs
P_e	Average frame error probability
$f_X(x)$	Probability density function of random variable X
$F_X(x)$	Cumulative distribution function of random variable X
$\varphi_X(t)$	Characteristic function of random variable X

Chapter 1

Introduction

The sharp increase of rich multimedia data traffic in wireless communication and the shortage of radio spectrum resources motivate the demand for novel technologies that can accommodate this trend while providing high reliability. Constituting one of the principal technologies for fifth generation (5G) wireless communication system, large-scale multiple-input multiple-output (LS-MIMO) is an important candidate for providing impressive advances [1–4]. As outlined in [1], for LS-MIMO systems with large number of base station antennas serving a small number of single-antenna users under time-division duplex (TDD) mode, high spectral efficiency and link reliability can be achieved. The potential of LS-MIMO systems for higher spectral efficiency, higher energy efficiency at both transmitting and receiving sides as well as improved system robustness is summarized in [2] and [3]. Close relation among LS-MIMO and other fundamental technologies in 5G wireless communication systems such as millimetre wave communications and small-cell based heterogeneous network (HetNet) is pointed out in [4]. LS-MIMO multiuser (MU) systems, that employ hundreds of antennas at the Base Station (BS) serving tens of geophysically distributed single antenna users, is an enabling technology for 5G systems.

Although LS-MIMO technology can provide significant benefits, issues still exist for its integration into practical communication systems. One that of paramount importance is

the design of high performance detectors for the uplink. Techniques such as maximum likelihood detection (MLD) [5] and sphere decoder (SD) [6,7] have asymptotic complexities that scale exponentially with the number of transmit antennas [5, 8], and therefore are infeasible for practical LS-MIMO. In recent years, several low complexity high performance detectors were proposed for LS-MIMO systems, such as the block-iterative generalized decision feedback equalizer (BI-GDFE) [9–11], likelihood ascend search (LAS) algorithm and its variations [12–14], Reactive Tabu search (RTS) and its variations [15, 16], message passing detectors (MPD) [17–20], Monte-Carlo sampling based algorithms [21, 22], and element-based lattice reduction (ELR) aided linear detector [23]. To elaborate a little further, BI-GDFE detects the transmitted symbols by using a feed forward equalizer (FFE) and a feed backward equalizer (FBE) in a block-iterative manner [9]. Asymptotic analysis of BI-GDFE, which relies heavily on random matrix theory, demonstrates that its performance can approach the single-user matched-filter bound (MFB) at sufficient high SNR region [9, 10]. In [11], its asymptotic performance was compared with that of MMSE-SIC for LS-MIMO. It was shown that they have similar convergence behaviour and are capable of approaching the single-user MFB at sufficient high SNR region. LAS and RTS algorithms both belong to the class of metaheuristics based local search algorithms. In LS-MIMO systems with extremely large number of antennas (e.g. 600 transmit and receive antennas), LAS is capable of achieving nearly single-input single-output AWGN performance with low complexity [12]. A hardware implementation of the LAS algorithm was reported in [13]. In [14], the authors proposed an improved LAS algorithm by first generating multiple possible solution candidates, and then selecting the best one among them. Compared with LAS algorithms, RTS algorithms perform better because of the exploitation of an efficient local minima escape strategy. Randomly-restart reactive tabu search (R3TS), which makes use of the random restart technique, obtains a set of possible final solution candidates from the randomly generated initial solutions [15]. Layered tabu search (LTS) detects the symbols in a sequential manner [16]. In each layer, the decision of whether tabu search

is launched or not is made based on the reliability of the symbol detected by a decision feedback equalizer. MPD is a belief propagation based algorithm which works on graphical models. An approximate message passing detection technique based on a factor graph was presented in [17]. In [18], a message passing algorithm that works on a tree model, which approximates the fully-connected MIMO graph, was proposed. In [19], a MPD algorithm that works with the matched-filter received vector was combined with a simple channel estimation scheme that estimates $\mathbf{H}^H\mathbf{H}$ directly instead of the channel propagation matrix $\mathbf{H}$, resulting in a novel detection algorithm for LS-MIMO systems. MPD was also extended to large scale multiuser MIMO-OFDM systems in [20]. In [21], a randomized MCMC algorithm that can achieve near-optimal performance in LS-MIMO systems with 4-QAM was presented. A Monte-Carlo sampling based detector that exploits a mixed Gibbs sampling (MGS) technique and multiple restart strategy was proposed in [22]. The ELR aided linear detector is another low complexity high performance detection algorithm proposed in recent years. Different from the other conventional lattice reduction (LR) based algorithms, the ELR aided linear detector proposed in [23] aims to reduce the symbol-wise asymptotic pair wise error probability (PEP) rather than just find another more orthogonal basis $\tilde{\mathbf{H}}$ that defines the same lattice as $\mathbf{H}$.

Selection based list detection for MIMO has the advantage for massively parallelization [24–26], allowing for high data throughput implementations. In general, selection based list detection comprises of three main stages—channel partition, candidate list generation and final decision. At the channel partition stage, the channel is partitioned into two subsets based on a certain selection scheme. At the candidate list generation stage, for the first channel subset, all the corresponding possible transmitted symbol sub-vectors are considered. For the second channel subset, instead of considering all the corresponding possible transmitted symbol sub-vectors, low complexity linear detector (LD) with successive interference cancellation (SIC) is used to obtain the decisions of the symbol sub-vectors. Therefore, a list of candidate transmitted symbol vectors is generated at this stage. Then

the best candidate in the list, using the minimum Euclidean distance (MED) rule, is chosen as the final decision. In [24], a selection based list algorithm called generalized parallel interference cancellation (GPIC) was proposed, which performs channel partition based on the postprocessing signal to noise ratio (SNR) using zero forcing (ZF). In [25], it was shown theoretically that the channel partition procedure is crucial for the performance of selection based list detection in conventional small MIMO. Based on this analysis, the authors proposed an improved scheme of GPIC, named Sel-MMSE-OSIC, that exploits diversity maximization channel selection (DMS) for channel partition and derived a sufficient condition for the new scheme to achieve optimal asymptotic diversity. The scheme proposed in [26] uses an simpler incremental channel partition technique to replace the DMS scheme and employs a tree search algorithm for candidate list generation, resulting in lower complexity compared with Sel-MMSE-OSIC. The schemes in [25] and [26] can achieve very close performance to MLD in conventional small MIMO systems.

In LS-MIMO systems, the schemes in [25] and [26] achieve optimal diversity (which is large due to large N_r [5]) at very high SNR region. However, such asymptotic diversity may never be achieved over practical operational SNR ranges in LS-MIMO systems. The most prominent factor that contributes to the memory consumption and complexity of selection based list detection is the size of the candidate list. Therefore, in LS-MIMO, it is of paramount importance to have an good achievable diversity over practical BER ranges (i.e. no less than 10^{-7}) while keeping the size of the list feasible for practical implementations.

Complex matrix inversion is widely used not only in selection based list detections but also other detection techniques for LS-MIMO systems. However, even for conventional MIMO systems, complex matrix inversion is cumbersome to implement [27–29], let along in LS-MIMO systems, where the numbers of receive (N_r) and transmit (N_t) antennas are much larger. It is worth to point out that in practical hardware implementations of detection algorithms, the measure of asymptotic complexity is not sufficient. Processing latency (parallel time units), memory consumption, power consumption and hardware cost are also

important measures. Generally speaking, exact matrix inversion schemes such as Gaussian Elimination (GE), Cholesky decomposition (CD) and QR decomposition based algorithms requiring $\mathbb{O}(N_t)$ parallel time units [28], may exceed the channel coherence interval. In order to address this issue, the channel hardening phenomenon [1, 30] can be exploited in approximate matrix inversion techniques that based on L-term Neumann series expansion (SE) [31–33] for LS-MIMO detection. As we show later, the processing latency of SE based approximate matrix inversion is of order $\mathbb{O}(a\log(N_t))$, where a is a constant, which is much lower compared with that of exact matrix inversions when N_t is large. One reason that results in channel hardening phenomenon is that when the system loading factor $\alpha = \frac{N_t}{N_r}$ decreases, the orthogonality between the columns of the channel matrix increases, rendering the diagonal components of the associated Gram matrix of the channel become increasingly stronger compared with the off diagonal components (i.e. the Gram matrix becomes closer to diagonal). Based on this quasi-diagonal structure of the Gram matrix, L-term SE approximation only requires matrix-wise multiplications that enables parallel and efficient hardware implementations [31–33]. In [31] and [32], L-term SE based approximate matrix inversion was firstly considered for linear detections in low loaded (e.g. 64×4, 128×8 and 256×12) LS-MIMO systems. A corresponding FPGA implementation was also presented in [32], which is able to achieve 600Mb/s throughput for a 128×8 3GPP LTE advanced LS-MIMO system. Besides, compared with exact matrix inversions, its saving in hardware resources and simpler implementation structure ware also assessed. In [33], L-term SE based approximate matrix inversion was also considered for linear pre-coding in LS-MIMO systems. The comparison between L-term SE approximate matrix inversion and QR decomposition based exact matrix inversion reveals the advantages of the former scheme in energy efficiency and implementation difficulty. Nevertheless, there are two major drawbacks of L-term SE approximation that hinder its practical usage. Firstly, the conventional L-term SE approximation converges to the exact matrix inverse very slowly (linearly with the number of expansion terms). Secondly, the L-term SE approximation is only valid in

a system whose system loading factor satisfies the convergence condition constraint (i.e. the condition to guarantee the asymptotic convergence of L-term SE approximation to the exact matrix inversion with high probability is $\alpha < (\sqrt{2}-1)^2$ [34]), which results in a loss in spatial multiplexing gain.

1.1 Thesis Contribution

In this thesis, we first propose a refined approximate matrix inversion technique based on 2-term SE approximation and Newton Iteration [35–38], named K-step series expansion Newton iteration approximation (K-SENIA). The proposed technique converges much faster (exponentially with the number of iterations) than conventional L-term SE approximation by making use of the fast convergence property of Newton iteration [35–38]. We further relax the convergence constraint of K-SENIA by using a matrix inversion inflate updates (IU) technique [39], allowing for higher system loading factors to be achieved. We also apply K-SENIA/IU in linear MMSE detection, termed as MMSE-SENIA. Based on our analysis of its residual estimation error and the study of statistical distribution of the channel parameter-orthogonality measure, a hybrid MMSE detector is proposed, which can effectively reduce the error floor induced by this approximation. The K-SENIA/IU technique is then integrated into selection based list algorithms so that low latency and deeper parallelism can be obtained. Based on the analyse the impact of the channel hardening phenomenon, we show that when the dimension of channel matrix increases, the DMS rule and V-BLAST ordering for SIC based on the postprocessing SINR of the sub-data streams become less effective, and hence in LS-MIMO systems, DMS can be replaced by channel independent selection (CIS) with negligible performance loss. We also find that when the system is not extremely large (e.g. 128×32 and 128×96 MIMO), ordering strategy has larger impact on performance than channel partition scheme. Capitalizing on these results, we propose an improved selection based list algorithm by employing Type-L reliability ordering [40] in SIC sub-detectors. Simulation results reveal significant perfor-

mance improvement of such an approach. The improved selection based list algorithm is also compared with two state-of-art detection algorithms for LS-MIMO, multistage LAS algorithm [12, 41] and the MPD scheme [19]. It is shown that our algorithm performs better than the former one and has just a fraction of dB loss compared with the latter one with comparable complexity. Furthermore, we analysis the structures of multistage LAS and MPD algorithms, and show that the selection based list algorithm is more suitable for parallel implementation over them, and hence is capable of providing processing latency advantages.

1.2 Thesis Outline

The rest of the thesis is organized as follows. Chapter 2 introduces a large-scale MIMO system model and presents the channel hardening phenomenon. Chapter 3 presents the K-SENIA/IU scheme, their complexity/latency analysis as well as their applications in linear MMSE detection. The impact of channel hardening on selection based list detection in LS-MIMO is analysed in chapter 4. Chapter 5 presents the improved selection based list detection technique and a comprehensive comparison of the proposed algorithm with the multistage LAS and MPD algorithms. Chapter 6 concludes this thesis.

Chapter 2

Large-Scale MIMO Multiuser Uplink System Model

This chapter first describes the LS-MIMO multiuser (MU) uplink system model as well as the generic detection problem. Then we give a brief introduction to the successive interference cancellation (SIC) technique that is used in selection based list detectors. Furthermore, we also introduce the channel hardening phenomenon in LS-MIMO channels, which is further exploited in Chapter 3 for developing the low latency approximate matrix inversion scheme and explored in Chapter 4 for studying its impact on selection based list detections.

2.1 Generic Mathematical System Model

Consider an uncoded complex LS-MIMO MU uplink system with N_r BS antennas serving N_t geophysically distributed single-antenna users. The system loading factor is defined as $\alpha = \frac{N_t}{N_r}$. Independent information streams from each user, in the form of bit sequences, are mapped to complex symbols in groups of n_c consecutive bits. The complex symbols are statistically independent belonging to a finite signal constellation alphabet $\mathbb{A}$ (e.g., 4-QAM, 16-QAM, 64-QAM) of size $|\mathbb{A}| = M = 2^{n_c}$ with average energy E_s. Then the complex

symbols are transmitted by N_t antennas over a Rayleigh flat fading matrix channel. With perfect synchronization between receiving and transmitting sides, the generic discrete time mathematical model for the MIMO detection problem is characterized by a N_t input linear system, represented by a channel matrix and its N_r outputs that are contaminated by additive white Gaussian noise (AWGN). The input-output relation of the channel is given by:

$$\mathbf{y} = \mathbf{H}\mathbf{s} + \mathbf{n}, \tag{2.1}$$

where $\mathbf{y} \in \mathbb{C}^{N_r \times 1}$ is the received signal vector, and $\mathbf{s} \in \mathbb{C}^{N_t \times 1}$ is the transmitted symbol vector. Each component of $\mathbf{s}$ is drawn independently from $\mathbb{A}$ with equal probability. Hence $\mathbf{s}$ satisfies $\mathbb{E}[\mathbf{s}\mathbf{s}^H] = \mathbf{I}_{N_t} E_s$, where $\mathbb{E}[\cdot]$ denotes the expectation operation, $(\cdot)^H$ denotes the Hermitian transpose, and $\mathbf{I}_{N_t}$ denotes the identity matrix of size $N_t \times N_t$. Furthermore $\mathbf{H} \in \mathbb{C}^{N_r \times N_t}$ denotes the Rayleigh fading channel propagation matrix, and $[\mathbf{H}]_{ij}$ denotes the component of $\mathbf{H}$ at the ith row and jth column, representing the fading coefficient from the jth transmit antenna to the ith receive antenna. The components of $\mathbf{H}$ are independent identically distributed (i.i.d) circularly symmetric complex Gaussian (CSCG) random variables with zero mean and unit variance, $[\mathbf{H}]_{ij} \sim \mathbb{C}\mathcal{N}(0, 1)$. Finally, $\mathbf{n} \in \mathbb{C}^{N_r \times 1}$ is the AWGN vector whose components are i.i.d CSCG random variables with zero mean and variance σ_o^2. Hence $\mathbb{E}[\mathbf{n}\mathbf{n}^H] = \mathbf{I}_{N_r}\sigma_o^2$. The average symbol signal to noise ratio (SNR) is defined as $\rho_s = \frac{E_s}{\sigma_o^2}$, and the average SNR at each receive antenna is defined as $\rho_r = \frac{N_t E_s}{\sigma_o^2}$. Fig. 2.1 illustrates LS-MIMO MU uplink system model. The basic task of a MIMO detector is to estimate the transmitted symbol vector $\mathbf{s}$, based on the knowledge of received signal vector $\mathbf{y}$ and channel matrix $\mathbf{H}$.

2.2 LD/SIC

Linear detectors (LD), which are known for their appealingly low complexity [5], generate soft estimates of the transmitted symbol vector $\mathbf{s}$ by applying a linear transformation on

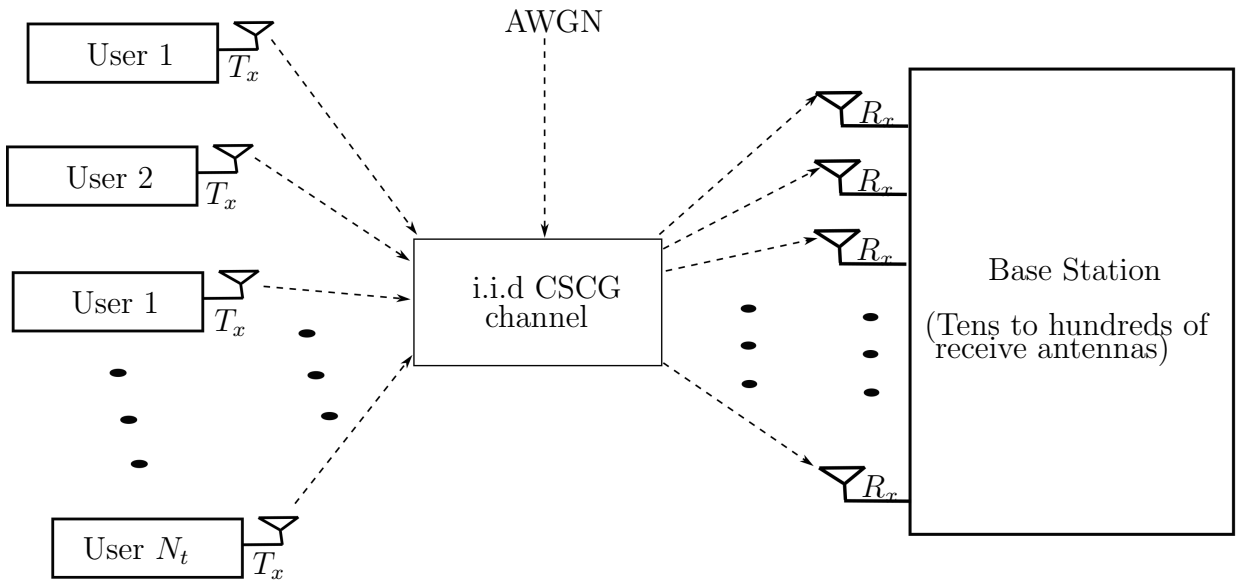

Fig. 2.1 LS-MIMO MU uplink system model

the received signal vector $\mathbf{y}$ and then quantize each component of the soft estimate vector to the closest point in the symbol constellation $\mathbb{A}$. Let $\mathbf{G} \in \mathbb{C}^{N_t \times N_r}$ denote the linear transformation matrix, $\hat{\mathbf{s}}^{LD}$ denote the output of LD, then the general form of a LD is given by

$$\hat{\mathbf{s}}^{LD} = \mathcal{Q}[\mathbf{G}\mathbf{y}], \tag{2.2}$$

where $\mathcal{Q}[\cdot]$ denotes the quantization operator based on the corresponding symbol constellation. The most prominent LDs are zero forcing (ZF) and minimum mean square error (MMSE) detectors [5]. The linear transformation matrix for ZF detection is

$$\mathbf{G}_{ZF} = (\mathbf{H}^H\mathbf{H})^{-1}\mathbf{H}^H \tag{2.3}$$

and for MMSE detection is

$$\mathbf{G}_{MMSE} = (\mathbf{H}^H\mathbf{H} + \rho_s^{-1}\mathbf{I})^{-1}\mathbf{H}^H \tag{2.4}$$

Nevertheless, the performance of LD is inferior compared with MLD [42]. Successive interference cancellation (SIC), also known as nulling-cancelling technique [43], may be applied to improve the error performance of LD. In SIC, the sub-datastreams are detected serially by a MMSE/ZF equalizer. At each layer, the interference of the detected symbol is cancelled from the received signal vector, thus increasing the reliabilities of the remaining estimates. Since MMSE/MMSE-SIC techniques can achieve significant performance gains over ZF/ZF-SIC [44, 45], in this work, we only consider MMSE/MMSE-SIC.

2.3 Channel Hardening Phenomenon

When the number of antennas (N_r, N_t or both of them) increases, the variance of the MIMO channel mutual information grows very slowly or even shrinks compared with its mean. This phenomenon is referred to as "Channel Hardening" [30]. One reason that results in channel hardening is when the system loading factor $\alpha = \frac{N_t}{N_r}$ decreases, the orthogonality between the columns of $\mathbf{H}$ increases, rendering the diagonal components of the Gram matrix $\mathbf{W} = \mathbf{H}^H\mathbf{H}$ become increasingly stronger compared with its off diagonal components, and hence $\mathbf{W}$ becomes closer to diagonal [1].

To elaborate a little further, when $N_r, N_t \to \infty$, with α fixed, the empirical distribution of the eigenvalues of $\frac{1}{N_r}\mathbf{W} = \frac{1}{N_r}\mathbf{H}^H\mathbf{H}$ converges almost surely, to a distribution named Marčenko-Pastur law [46], with probability density function (p.d.f)

$$f_\alpha(x) = (1 - \frac{1}{\alpha})^+\delta(x) + \frac{\sqrt{(x-a)^+(b-x)^+}}{2\pi\alpha x}, \tag{2.5}$$

where $(z)^+ = \max(0, z)$ and

$$a = (1 - \sqrt{\alpha})^2 \quad b = (1 + \sqrt{\alpha})^2. \tag{2.6}$$

Then following [47], let $\lambda_{max}(\mathbf{X})$ and $\lambda_{min}(\mathbf{X})$ denote the largest and smallest eigenvalues of

$\mathbf{X}$ respectively. When $N_r, N_t \to \infty$ with α fixed (we only consider the cases with $N_r \geq N_t$, therefore $\alpha \in (0, 1]$), we have

$$\lambda_{max}(\frac{1}{N_r}\mathbf{W}) \overset{a.s}{\to} (1+\sqrt{\alpha})^2 \quad \lambda_{min}(\frac{1}{N_r}\mathbf{W}) \overset{a.s}{\to} (1-\sqrt{\alpha})^2, \tag{2.7}$$

where $\overset{a.s}{\to}$ denotes convergence almost surely, that yields

$$\lambda_{max}(\frac{1}{(1+\alpha)}\frac{1}{N_r}\mathbf{W}) \overset{a.s}{\to} (1+\frac{2\sqrt{\alpha}}{1+\alpha}) \quad \lambda_{min}(\frac{1}{(1+\alpha)}\frac{1}{N_r}\mathbf{W}) \overset{a.s}{\to} (1-\frac{2\sqrt{\alpha}}{1+\alpha}). \tag{2.8}$$

Given a diagonalizable Hermitian matrix $\mathbf{A} \in \mathbb{C}^{n\times n}$, then its eigendecomposition is [48]

$$\mathbf{A} = \mathbf{Q}\mathbf{\Lambda}\mathbf{Q}^{-1}, \tag{2.9}$$

where $\mathbf{Q} \in \mathbb{C}^{n\times n}$ is the matrix whose ith column $\mathbf{q}_i$ is the ith eigenvector of $\mathbf{A}$ ($i = 1, 2, \cdots n$), and $\mathbf{\Lambda}$ is the diagonal eigenvalue matrix formed by the eigenvalues of $\mathbf{A}$. From (2.8), we see that the eigenvalues of $\mathbf{I}_{N_t} - \frac{1}{N_r(1+\alpha)}\mathbf{W} = \mathbf{I}_{N_t} - \frac{1}{N_r+N_t}\mathbf{W}$, lie approximately in the range of $[\frac{-2\sqrt{\alpha}}{1+\alpha}, \frac{2\sqrt{\alpha}}{1+\alpha}]$. If $\alpha \to 0$, then $[\frac{-2\sqrt{\alpha}}{1+\alpha}, \frac{2\sqrt{\alpha}}{1+\alpha}] \to [0, 0]$, and hence its diagonal eigenvalue matrix converges to a zero matrix, therefore this matrix convergences to a zero matrix element-wise

$$\lim_{N_r,N_t\to\infty,\alpha\to 0}(\mathbf{I}_{N_t} - \frac{1}{N_r+N_t}\mathbf{W}) = \mathbf{0}, \tag{2.10}$$

where $\mathbf{0}$ denotes the zero matrix. Then from (2.10)

$$\lim_{N_r,N_t\to\infty,\alpha\to 0}\frac{1}{N_r+N_t}\mathbf{W} = \mathbf{I}_{N_t} \overset{N_r\gg N_t}{=} \frac{1}{N_r}\mathbf{W}, \tag{2.11}$$

indicating that when N_r and N_t both grow to infinity and $\alpha = \frac{N_t}{N_r} \to 0$, $\mathbf{W}$ converges to a diagonal matrix (large magnitude disparity between its diagonal and off-diagonal components). This quasi-diagonal structure of $\mathbf{W}$ allows the exploitation of the Neumann series expansion technique to approximate $\mathbf{W}^{-1}$ invoked in various MIMO detection algorithms.

Chapter 3

Improved Approximate Matrix Inversion Exploiting Channel Hardening

This chapter first presents a low latency approximate matrix inversion scheme—K-step series expansion Newton iteration approximation (K-SENIA). We relax the convergence constraint of K-SENIA by using a matrix inversion inflate update (IU) technique making it suitable for high loaded LS-MIMO systems. The analysis of the complexity and latency of K-SENIA/IU is also provided. Then, we consider the applications of the improved approximate matrix inversion in linear MMSE detection. We characterize the error floor effect of MMSE detection aided by K-SENIA and propose a hybrid MMSE detector to reduce the error floor based on our study on statistical distribution of orthogonality measure (OM) of the MIMO channel.

3.1 Improved Approximate Matrix Inversion Scheme: K-SENIA/IU

3.1.1 Neumann Series Expansion and Newton Iteration

Neumann Series Expansion

Considering an invertible matrix $\mathbf{B} \in \mathbb{C}^{N\times N}$ that satisfies $\lim_{L\to\infty}(\mathbf{I}-\mathbf{B})^L = \mathbf{0}$, we have

$$\mathbf{B}^{-1} = \sum_{k=0}^{\infty}(\mathbf{I}-\mathbf{B})^k. \tag{3.1}$$

Let $\mathbf{S}_L = \sum_{k=0}^{L-1}(\mathbf{I}-\mathbf{B})^k$ denote the L-term SE approximation of $\mathbf{B}^{-1}$. Its approximation residual matrix, denoted by $\mathbf{R}_L$ is given by

$$\begin{aligned}\mathbf{R}_L &= \mathbf{I}-\mathbf{S}_L\mathbf{B}\\ &= \{\mathbf{I}-[\sum_{k=0}^{L-1}(\mathbf{I}-\mathbf{B})^k - \sum_{k=0}^{L-1}(\mathbf{I}-\mathbf{B})^{k+1}]\}\\ &= (\mathbf{I}-\mathbf{B})^L,\end{aligned} \tag{3.2}$$

Therefore, if $\lim_{L\to\infty}(\mathbf{I}-\mathbf{B})^L = \mathbf{0}$, then (3.1) holds, showing that the L-term SE approximation convergences to the exact matrix inverse asymptotically when L increases.

Consider invertible matrices $\mathbf{A} \in \mathbb{C}^{N\times N}$ and $\mathbf{X} \in \mathbb{C}^{N\times N}$, that satisfy $\lim_{L\to\infty}(\mathbf{I}-\mathbf{X}^{-1}\mathbf{A})^L = \mathbf{0}$. Then applying (3.1), we have [32]

$$(\mathbf{X}^{-1}\mathbf{A})^{-1} = \sum_{n=0}^{\infty}(\mathbf{I}-\mathbf{X}^{-1}\mathbf{A})^n, \tag{3.3}$$

and hence

$$\mathbf{A}^{-1} = \sum_{n=0}^{\infty}(\mathbf{I}-\mathbf{X}^{-1}\mathbf{A})^n\mathbf{X}^{-1}. \tag{3.4}$$

The L-term SE approximation of $\mathbf{A}^{-1}$, denoted by $\tilde{\mathbf{A}}_L^{-1}$, is given by

$$\tilde{\mathbf{A}}_L^{-1} = \sum_{n=0}^{L-1} (\mathbf{I} - \mathbf{X}^{-1}\mathbf{A})^n \mathbf{X}^{-1}, \tag{3.5}$$

and the approximation residual matrix of $\tilde{\mathbf{A}}_L^{-1}$, is

$$\tilde{\mathbf{R}}_L = \mathbf{I} - \tilde{\mathbf{A}}_L^{-1}\mathbf{A} = (\mathbf{I} - \mathbf{X}^{-1}\mathbf{A})^L. \tag{3.6}$$

The Gram matrix $\mathbf{W}$ can be decomposed as $\mathbf{W} = \mathbf{D} + \mathbf{E}$, where $\mathbf{D}$ is a diagonal matrix whose diagonal components are those of $\mathbf{W}$, and $\mathbf{E}$ is a zero diagonal matrix with the off diagonal components of $\mathbf{W}$. Therefore, with $\mathbf{A} = \mathbf{W}$ and $\mathbf{X} = \mathbf{D}$ in (3.5), the L-term SE approximation of $\mathbf{W}^{-1}$ is given by

$$\tilde{\mathbf{W}}_L^{-1} = \sum_{n=0}^{L-1} (-\mathbf{D}^{-1}\mathbf{E})^n \mathbf{D}^{-1}. \tag{3.7}$$

Based on (3.6), the L-term approximation residual matrix of $\tilde{\mathbf{W}}_L^{-1}$, denoted by $\tilde{\mathbf{R}}_L$, is given by

$$\tilde{\mathbf{R}}_L = (-\mathbf{D}^{-1}\mathbf{E})^L, \tag{3.8}$$

If $N_r, N_t \to \infty, \alpha \to 0$, $\mathbf{W}$ becomes diagonal as shown in (2.11) and hence $\mathbf{D}^{-1}\mathbf{E}$ tends to be a zero matrix. Then $\tilde{\mathbf{R}}_L$ in (3.8) becomes $\mathbf{0}$, so we can conclude that the performance of L-term SE approximation improves when the system loading factor α decreases or L increases [34]. Furthermore, the condition for α to ensure asymptotic convergence of the SE approximation (i.e., $\lim_{L\to\infty} \tilde{\mathbf{W}}_L^{-1} = \mathbf{W}^{-1}$) with high probability is $\alpha < (\sqrt{2}-1)^2$ [34]. Consider the 2-term SE approximation $\tilde{\mathbf{W}}_2^{-1} = \mathbf{D}^{-1} - \mathbf{D}^{-1}\mathbf{E}\mathbf{D}^{-1}$ and notice that $\mathbf{D}^{-1}$ is a diagonal matrix. Thus the computation of $\tilde{\mathbf{W}}_2^{-1}$ only requires scalar-vector multiplications, with complexity in order of $\mathbb{O}(N_t^2)$.

Newton Iteration

Newton iteration is a recursive matrix inverse approximation method [35–37]. In large dimensional matrix inversion problems, the Newton iteration algorithm can converge very fast, and it is massively parallelizable with good numerical stability. Let $\mathbf{M}_{k+1}$ denote the approximate matrix inverse computed by Newton iteration at $k+1$ step. Then

$$\mathbf{M}_{k+1} = (2\mathbf{I} - \mathbf{M}_k\mathbf{A})\mathbf{M}_k, \quad k = 0, 1, 2, \ldots \tag{3.9}$$

and the approximation residual matrix at step $k+1$ is

$$\mathbf{R}_{k+1} = \mathbf{I} - \mathbf{M}_{k+1}\mathbf{A} = (\mathbf{I} - \mathbf{M}_k\mathbf{A})^2 = \mathbf{R}_k^2. \tag{3.10}$$

Therefore, Newton iteration scheme can converge to exact matrix inversion in exponential speed.

3.1.2 K-term Series Expansion Newton Iteration Approximation (K-SENIA)

The approximation residual matrix of L-term SE approximation, as shown in (3.8), is $(-\mathbf{D}^{-1}\mathbf{E})^L$, which indicates that L-term SE approximation only converges to the exact matrix inverse in a linear speed. Therefore, large L is required to guarantee an acceptable performance when α is not extremely small. However, in view of hardware implementation, a larger L results in more latency (parallel time units) [32]. Therefore, L-term SE approximation is competitive for small L only in the system whose system loading factor is extremely low [31–33].

Conventional L-term SE approximation can be refined by using the Newton iteration. The more computationally economical approximation $\tilde{\mathbf{W}}_2^{-1}$ is used as the initial input to Newton iteration, denoted by $\check{\mathbf{M}}_0$. Let $\check{\mathbf{M}}_k$ denote the refined output after kth step Newton

iteration. With $\check{\mathbf{M}}_k = \tilde{\mathbf{W}}_L^{-1}$ from (3.7) and using (3.6) and (3.9) we have

$$\check{\mathbf{M}}_{k+1} = (2\mathbf{I} - \check{\mathbf{M}}_k\mathbf{W})\check{\mathbf{M}}_k = (\mathbf{I} + \mathbf{I} - \tilde{\mathbf{W}}_L^{-1}\mathbf{W})\tilde{\mathbf{W}}_L^{-1} = (\mathbf{I} + \tilde{\mathbf{R}}_L)\tilde{\mathbf{W}}_L^{-1}. \tag{3.11}$$

Then the use of (3.7) and (3.8) in (3.11) yields

$$\check{\mathbf{M}}_{k+1} = \sum_{n=0}^{L-1}(-\mathbf{D}^{-1}\mathbf{E})^n\mathbf{D}^{-1} + \sum_{n=L}^{2L-1}(-\mathbf{D}^{-1}\mathbf{E})^n\mathbf{D}^{-1} = \tilde{\mathbf{W}}_{2L}^{-1}. \tag{3.12}$$

Hence because of (3.12), we can use Newton iteration to calculate (3.7). With $\check{\mathbf{M}}_0 = \tilde{\mathbf{W}}_2^{-1}$, applying (3.12) iteratively, we have $\check{\mathbf{M}}_1 = \tilde{\mathbf{W}}_4^{-1}$, $\check{\mathbf{M}}_2 = \tilde{\mathbf{W}}_8^{-1}$, $\cdots$, $\check{\mathbf{M}}_k = \tilde{\mathbf{W}}_{2^{k+1}}^{-1}$ and the corresponding approximation residual matrix, denoted by $\check{\mathbf{R}}_k$, is given by

$$\check{\mathbf{R}}_k = \tilde{\mathbf{R}}_{2^{k+1}} = (-\mathbf{D}^{-1}\mathbf{E})^{2^{k+1}}. \tag{3.13}$$

Hereinafter the refined method proposed is termed as the K-step series expansion Newton iterative approximation (K-SENIA), where K denotes the number of Newton iterations.

3.1.3 Achieving Higher System Loading factor: Matrix Inversion Inflate Update (IU)

Similarly to conventional L-term SE approximation, K-SENIA is only effective in the LS-MIMO with α satisfying the asymptotic convergence condition (i.e., if $\alpha < (\sqrt{2}-1)^2$ then $\lim_{L\to\infty} \tilde{\mathbf{W}}_L^{-1} = \mathbf{W}$ with high probability [34]). This asymptotic convergence condition is limiting (e.g., with $N_r = 32$, we must have $N_t \leq 4$, and with $N_r = 128$, we must have $N_t \leq 21$), which significantly limits spatial multiplexing gain. Next we propose a scheme that combines a matrix inversion inflate update (IU) technique and K-SENIA, hence relaxes this convergence constraint.

Matrix Inversion Inflate Update (IU)

When the channel matrix is modified by adding a new column, IU efficiently updates the inflated Gram matrix inverse from the previous matrix inverse, rather than recomputing it from scratch [39]. Here we extend the ZF-IU technique from [39] to MMSE-IU. Assume $\mathbf{W}^{-1} = (\mathbf{H}^H\mathbf{H}+\rho_s^{-1}\mathbf{I}_{N_t})^{-1}$ is already computed (by exact or approximate matrix inversion). Then a new column $\mathbf{h}_n$ is added to $\mathbf{H}$, resulting in the new inflated matrix is $\mathbf{H}_e = [\mathbf{H}, \mathbf{h}_n]$. To find $\mathbf{W}_e^{-1} = (\mathbf{H}_e^H\mathbf{H}_e + \rho^{-1}\mathbf{I}_{N_t+1})^{-1}$, notice that

$$\mathbf{W}_e^{-1} = \begin{bmatrix} \mathbf{H}^H\mathbf{H} + \rho_s^{-1}\mathbf{I}_{N_t}, \mathbf{H}^H\mathbf{h}_n \\ \mathbf{h}_n^H\mathbf{H}, \qquad \mathbf{h}_n^H\mathbf{h}_n + \rho_s^{-1} \end{bmatrix}^{-1}. \tag{3.14}$$

Using the inverse of the partitioned matrix, we have [49]

$$\mathbf{P}^{-1} = \begin{bmatrix} \mathbf{P}_{11}, \mathbf{P}_{12} \\ \mathbf{P}_{21}, \mathbf{P}_{22} \end{bmatrix}^{-1} = \begin{bmatrix} \mathbf{F}_{11}^{-1}, & -\mathbf{P}_{11}^{-1}\mathbf{P}_{12}\mathbf{F}_{22}^{-1} \\ -\mathbf{F}_{22}^{-1}\mathbf{P}_{21}\mathbf{P}_{11}^{-1}, & \mathbf{F}_{22}^{-1} \end{bmatrix}, \tag{3.15}$$

where

$$\mathbf{F}_{11} = \mathbf{P}_{11} - \mathbf{P}_{12}\mathbf{P}_{22}^{-1}\mathbf{P}_{21}, \tag{3.16}$$

and

$$\mathbf{F}_{22} = \mathbf{P}_{22} - \mathbf{P}_{21}\mathbf{P}_{11}^{-1}\mathbf{P}_{12}. \tag{3.17}$$

The use of (3.15), (3.16) and (3.17) in (3.14) yields

$$\mathbf{W}_e^{-1} = \begin{bmatrix} \mathbf{F}_{11}^{-1}, & -c\mathbf{W}^{-1}\mathbf{H}^H\mathbf{h}_n \\ -c\mathbf{h}_n^H\mathbf{H}\mathbf{W}^{-1}, & c \end{bmatrix}, \tag{3.18}$$

where

$$c = \mathbf{F}_{22}^{-1} = 1/(\mathbf{h}_n^H\mathbf{h}_n + \rho_s^{-1} - \mathbf{h}_n^H\mathbf{H}\mathbf{W}^{-1}\mathbf{H}^H\mathbf{h}_n), \tag{3.19}$$

$$\mathbf{F}_{11}^{-1} = (\mathbf{W} - \mathbf{H}^H\mathbf{h}_n(\mathbf{h}_n^H\mathbf{h}_n + \rho_s^{-1})^{-1}\mathbf{h}_n^H\mathbf{H})^{-1}. \tag{3.20}$$

Let $\mathbf{A} \in \mathbb{C}^{n\times n}$, $\mathbf{X} \in \mathbb{C}^{n\times r}$, $\mathbf{R} \in \mathbb{C}^{r\times r}$ and $\mathbf{Y} \in \mathbb{C}^{r\times n}$, then based on Sherman-Morrison formula [49], the inverse of $\mathbf{A}+\mathbf{XRY}$ can be computed by

$$(\mathbf{A}+\mathbf{XRY})^{-1} = \mathbf{A}^{-1} - \mathbf{A}^{-1}\mathbf{X}(\mathbf{R}^{-1}+\mathbf{YA}^{-1}\mathbf{X})^{-1}\mathbf{YA}^{-1}, \tag{3.21}$$

and (3.20) can be rewritten as

$$\mathbf{F}_{11}^{-1} = \mathbf{W}^{-1} + c\mathbf{W}^{-1}\mathbf{H}^H\mathbf{h}_n\mathbf{h}_n^H\mathbf{H}\mathbf{W}^{-1}. \tag{3.22}$$

Therefore, each IU step of MMSE detector can be summarized as:

$$\mathbf{t}_1 = \mathbf{H}^H\mathbf{h}_n, \mathbf{t}_2 = \mathbf{W}^{-1}\mathbf{T}_1, c = 1/(\mathbf{h}_n^H\mathbf{h}_n + \rho_s^{-1} - \mathbf{t}_1^H\mathbf{t}_2), \mathbf{t}_3 = -c\mathbf{t}_2,$$

$$\mathbf{F}_{11}^{-1} = \mathbf{W}^{-1} + c\mathbf{t}_2\mathbf{t}_2^H, \mathbf{W}_e^{-1} = \begin{bmatrix} \mathbf{F}_{11}^{-1}, \mathbf{t}_3 \\ \mathbf{t}_3^H, \quad c \end{bmatrix},$$

where only vector wise multiplication is required.

Combining K-SENIA and IU

The combined scheme of K-SENIA and IU is termed as K-SENIA-IU. Capitalizing on the fact that a good approximation performance can be achieved by K-SENIA in the MIMO systems with α satisfying the convergence condition [34], the K-SENIA inverse for a sub-matrix composed of arbitrary N_i columns from $\mathbf{H}$, is firstly computed and fed to IU as the initial input. Then the matrix inverse is updated using IU by adding the remaining channel columns. To elaborate further, assume a LS-MIMO MU system whose system loading factor exceeds the asymptotic convergence constraint. First the channel matrix $\mathbf{H}$ is partitioned into two sub channel matrices $\mathbf{H}_{ini}$ and $\mathbf{H}_{rem}$. $\mathbf{H}_{ini} \in \mathbb{C}^{N_r\times N_i}$ is composed of arbitrary N_i columns of $\mathbf{H}$, where $\frac{N_i}{N_r}$ satisfies the convergence condition [34], and $\mathbf{H}_{rem} \in \mathbb{C}^{N_r\times(N_t-N_i)}$ is

composed of the remaining columns from $\mathbf{H}$. Then K-SENIA is performed to approximate $(\mathbf{H}_{ini}^H\mathbf{H}_{ini}+\rho^{-1}\mathbf{I}_{N_i})^{-1}$, resulting in $\check{\mathbf{W}}_{N_i}^{-1}$. Then IU is performed recursively to update $\check{\mathbf{W}}_{N_i}^{-1}$ by adding the remaining channel columns extracted from $\mathbf{H}_{rem}$, until $\check{\mathbf{W}}_{N_t}^{-1}$ is obtained. Let $\check{\mathbf{W}}_{N_i+j}^{-1}$ denote the updated matrix inverse at the $j$the step with $j=1,2,\ldots,N_t-N_i$. The K-SENIA-IU algorithm can be summarized in the pseudo code as follow

Algorithm 1 pseudo code of K-SENIA-IU

procedure K-SENIA-IU($\mathbf{H}$, ρ_r, N_i)
  Partition $\mathbf{H}$ into $\mathbf{H}_{ini}\in\mathbb{C}^{N_r\times N_i}$ and $\mathbf{H}_{rem}\in\mathbb{C}^{N_r\times(N_t-N_i)}$
  $\mathbf{W}_{N_i}\leftarrow\mathbf{H}_{ini}^H\mathbf{H}_{ini}+\rho_r^{-1}\mathbf{I}_{N_i}$
  $\check{\mathbf{W}}_{N_i}^{-1}\leftarrow$ **K-SENIA**$(\mathbf{W}_{N_i},k)$ ▷ Compute $\check{\mathbf{W}}_{N_i}^{-1}$ via K-SENIA
  $\mathbf{H}_{curr}\leftarrow\mathbf{H}_{ini}$
  for $j\leftarrow 1$ to (N_t-N_i) **do**
    $\check{\mathbf{W}}_{N_i+j}^{-1}\leftarrow$ **IU**$(\check{\mathbf{W}}_{N_i+j-1}^{-1})$ ▷ update the matrix inverse via IU
    $\mathbf{H}_{curr}\leftarrow[\mathbf{H}_{curr},\mathbf{h}_{p^i}]$ ▷ Inflate $\mathbf{H}_{curr}$ by adding column $\mathbf{h}_{p^i}$, which is extracted from $\mathbf{H}_{rem}$
  end for
  return $\check{\mathbf{W}}_{N_t}^{-1}$
end procedure

Error propagation in K-SENIA-IU

Next we discuss the impact of the combination of K-SENIA and IU to the approximation performance. Let $\mathbf{W}^{-1}=(\mathbf{H}^H\mathbf{H}+\rho_s^{-1}\mathbf{I})^{-1}$ and $\check{\mathbf{M}}_k$ denote the approximation of $\mathbf{W}^{-1}$ by K-SENIA. Assume the convergence condition of K-SENIA is satisfied (i.e., $\mathbf{W}^{-1}=\tilde{\mathbf{W}}_{\infty}^{-1}$) and let $\mathbf{W}_{\triangle}^{-1}$ denote the approximation error matrix of K-SENIA, which is given by

$$\mathbf{W}_{\triangle}^{-1}=\mathbf{W}^{-1}-\check{\mathbf{M}}_k, \tag{3.23}$$

where $\mathbf{W}^{-1}=\tilde{\mathbf{W}}_{\infty}^{-1}$, $\check{\mathbf{M}}_k=\tilde{\mathbf{W}}_{2^{k+1}}^{-1}$. The use of (3.7) in (3.23) yields

$$\mathbf{W}_{\triangle}^{-1}=\sum_{n=2^{k+1}}^{\infty}(-\mathbf{D}^{-1}\mathbf{E})^n\mathbf{D}^{-1}=(-\mathbf{D}^{-1}\mathbf{E})^{2^{k+1}}\sum_{n=0}^{\infty}(-\mathbf{D}^{-1}\mathbf{E})^n\mathbf{D}^{-1}=(-\mathbf{D}^{-1}\mathbf{E})^{2^{k+1}}\mathbf{W}^{-1}. \tag{3.24}$$

Let $\mathbf{W}_e^{-1} = (\mathbf{H}_e^H \mathbf{H}_e + \rho_s^{-1}\mathbf{I})^{-1}$ denote the exact matrix inversion of the inflated regularized Gram matrix, where $\mathbf{H}_e = [\mathbf{H}, \mathbf{h}_n]$. Recall (3.18), (3.19) and (3.22)

$$\mathbf{W}_e^{-1} = \begin{bmatrix} \mathbf{F}_{11}^{-1}, & -c\mathbf{W}^{-1}\mathbf{H}^H\mathbf{h}_n \\ -c\mathbf{h}_n^H\mathbf{H}\mathbf{W}^{-1}, & c \end{bmatrix}, \tag{3.25}$$

where

$$c = 1/(\mathbf{h}_n^H\mathbf{h}_n + \rho_s^{-1} - \mathbf{h}_n^H\mathbf{H}\mathbf{W}^{-1}\mathbf{H}^H\mathbf{h}_n), \tag{3.26}$$

$$\mathbf{F}_{11}^{-1} = \mathbf{W}^{-1} + c\mathbf{W}^{-1}\mathbf{H}^H\mathbf{h}_n\mathbf{h}_n^H\mathbf{H}\mathbf{W}^{-1}. \tag{3.27}$$

Then let $\check{\mathbf{W}}_e^{-1}$ denote the approximation of $\mathbf{W}_e^{-1}$ by K-SENIA-IU (with $\mathbf{W}^{-1}$ replaced by $\check{\mathbf{M}}_k$), that is

$$\check{\mathbf{W}}_e^{-1} = \begin{bmatrix} \check{\mathbf{F}}_{11}^{-1}, & -\check{c}\check{\mathbf{M}}_k\mathbf{H}^H\mathbf{h}_n \\ -\check{c}\mathbf{h}_n^H\mathbf{H}\check{\mathbf{M}}_k, & \check{c} \end{bmatrix}, \tag{3.28}$$

where

$$\check{c} = 1/(\mathbf{h}_n^H\mathbf{h}_n + \rho_s^{-1} - \mathbf{h}_n^H\mathbf{H}\check{\mathbf{M}}_k\mathbf{H}^H\mathbf{h}_n), \tag{3.29}$$

$$\check{\mathbf{F}}_{11}^{-1} = \check{\mathbf{M}}_k + \check{c}\check{\mathbf{M}}_k\mathbf{H}^H\mathbf{h}_n\mathbf{h}_n^H\mathbf{H}\check{\mathbf{M}}_k. \tag{3.30}$$

First we compare c in (3.26) and $\check{c}$ in (3.29). The use of (3.23) in (3.29) yields

$$\check{c} = 1/(\mathbf{h}_n^H\mathbf{h}_n + \rho_s^{-1} - \mathbf{h}_n^H\mathbf{H}\mathbf{W}^{-1}\mathbf{H}^H\mathbf{h}_n + \mathbf{h}_n^H\mathbf{H}\mathbf{W}_{\triangle}^{-1}\mathbf{H}^H\mathbf{h}_n). \tag{3.31}$$

Compare (3.26) and (3.31), if approximation of K-SENIA is accurate ($\mathbf{W}_{\triangle}^{-1}$ is close to a zero matrix element-wise), then the differential term $\mathbf{h}_n^H\mathbf{H}\mathbf{W}_{\triangle}^{-1}\mathbf{H}^H\mathbf{h}_n$ in the denominator is negligible. Therefore hereinafter we can assume $c = \check{c}$. Then consider $\check{\mathbf{F}}_{11}^{-1}$ in (3.30). The

use of (3.23) in (3.30) yields

$$\begin{aligned}\check{\mathbf{F}}_{11}^{-1} &= \mathbf{W}^{-1} - \mathbf{W}_{\triangle}^{-1} + c(\mathbf{W}^{-1} - \mathbf{W}_{\triangle}^{-1})\mathbf{H}^H\mathbf{h}_n\mathbf{h}_n^H\mathbf{H}(\mathbf{W}^{-1} - \mathbf{W}_{\triangle}^{-1}) \\ &= \mathbf{W}^{-1} + c\mathbf{W}^{-1}\mathbf{H}^H\mathbf{h}_n\mathbf{h}_n^H\mathbf{H}\mathbf{W}^{-1} - \mathbf{W}_{\triangle}^{-1} + c\mathbf{W}_{\triangle}^{-1}\mathbf{H}^H\mathbf{h}_n\mathbf{h}_n^H\mathbf{H}\mathbf{W}_{\triangle}^{-1} \\ &- c\mathbf{W}_{\triangle}^{-1}\mathbf{H}^H\mathbf{h}_n\mathbf{h}_n^H\mathbf{H}\mathbf{W}^{-1} - c\mathbf{W}^{-1}\mathbf{H}^H\mathbf{h}_n\mathbf{h}_n^H\mathbf{H}\mathbf{W}_{\triangle}^{-1}, \end{aligned} \tag{3.32}$$

the use of (3.24) and (3.27) in (3.32) yields

$$\begin{aligned}\mathbf{F}_{11}^{-1} - \check{\mathbf{F}}_{11}^{-1} &= \mathbf{W}_{\triangle}^{-1} + c\mathbf{W}_{\triangle}^{-1}\mathbf{H}^H\mathbf{h}_n\mathbf{h}_n^H\mathbf{H}\mathbf{W}^{-1} + c\mathbf{W}^{-1}\mathbf{H}^H\mathbf{h}_n\mathbf{h}_n^H\mathbf{H}\mathbf{W}_{\triangle}^{-1} \\ &- c(-\mathbf{D}^{-1}\mathbf{E})^{2^{k+1}}\mathbf{W}^{-1}\mathbf{H}^H\mathbf{h}_n\mathbf{h}_n^H\mathbf{H}\mathbf{W}_{\triangle}^{-1}. \end{aligned} \tag{3.33}$$

Consider the difference between the off-diagonal parts of $\mathbf{W}_e^{-1}$ in (3.25) and $\check{\mathbf{W}}_e^{-1}$ in (3.28)

$$c\mathbf{W}^{-1}\mathbf{H}^H\mathbf{h}_n - c\check{\mathbf{M}}_k\mathbf{H}^H\mathbf{h}_n = c\mathbf{W}_{\triangle}^{-1}\mathbf{H}^H\mathbf{h}_n. \tag{3.34}$$

We can observe from (3.33) and (3.34) that the approximation error terms of $\check{\mathbf{W}}_e^{-1}$ are linear transformations of the original approximation error matrix of K-SENIA $\mathbf{W}_{\triangle}^{-1}$. Notice that in both (3.33) and (3.34), the components of $\mathbf{H}^H\mathbf{h}_n$ are the off-diagonal components of $\mathbf{W}_e$, which are close to zero when $\mathbf{W}_e$ is close to diagonal. Therefore, we can conclude that the error propagation of IU process has a small impact to the approximation accuracy.

3.1.4 Complexity and Latency Analysis

Similar to [12], complexity in this work is defined as the number of complex arithmetic operations, here we use $\mathbb{O}$-notation to measure the asymptotic complexity. $\mathbb{O}$-notation defines the asymptotically tight bound of a function, given by [50]

$$\begin{aligned}\mathbb{O}(g(n)) &= \{f(n) : \text{there exist positive constants } c_1, c_2 \text{ and } n_0 \text{ such that for all } n \geq n_0, \\ 0 &\leq c_1 g(n) \leq f(n) \leq c_2 g(n), g(n) = \log(n) \text{ or } n \text{ or } n^2 \text{ etc.}\}. \end{aligned} \tag{3.35}$$

Let $\mathbb{O}(g_1(n)) = f_1(n)$ with $c_1^1 g_1(n) \leq f_1(n) \leq c_2^1 g_1(n)$ and $\mathbb{O}(g_2(n)) = f_2(n)$ with $c_1^2 g_2(n) \leq f_2(n) \leq c_2^2 g_2(n)$, where $c_1^1, c_2^1, c_1^2, c_2^2$ are positive constants. The addition operation of $\mathbb{O}$-notation is given by [50]

$$\mathbb{O}(g_1(n)) + \mathbb{O}(g_2(n)) \triangleq \mathbb{O}(g_3(n)), \tag{3.36}$$

if $g_1(n) = g_2(n)$, then

$$(c_1^1 + c_1^2) g_1(n) \leq \mathbb{O}(g_3(n)) = f_1(n) + f_2(n) \leq (c_2^1 + c_2^2) g_1(n), \tag{3.37}$$

based on (3.35), we have $\mathbb{O}(g_3(n)) = \mathbb{O}(g_1(n))$, e.g. $\mathbb{O}(n^2) + \mathbb{O}(n^2) = \mathbb{O}(n^2)$.
if $g_1(n) > g_2(n)$, then

$$c_1^1 g_1(n) < c_1^1 g_1(n) + c_1^2 g_2(n) \leq \mathbb{O}(g_3(n)) = f_1(n) + f_2(n) \leq c_2^1 g_1(n) + c_2^2 g_2(n) < (c_2^1 + c_2^2) g_1(n), \tag{3.38}$$

based on (3.35), we have $\mathbb{O}(g_3(n)) = \mathbb{O}(g_1(n))$ e.g. $\mathbb{O}(n^2) + \mathbb{O}(n) = \mathbb{O}(n^2)$.

The K-SENIA scheme is composed of two main parts. The first part is the computation of $\tilde{\mathbf{W}}_2^{-1}$, which only requires scalar-vector multiplication, with complexity that scales as $\mathbb{O}(N_t^2)$. The second part consists of k step Newton iteration as in (3.9), that each requires two matrix-matrix multiplications with complexity that scales as $\mathbb{O}(2N_t^3)$. Therefore the overall complexity of K-SENIA is of order $\mathbb{O}(2kN_t^3)$, which has the same magnitude order as exact matrix inversion [28]. Concerning processing latency, matrix-matrix multiplication requires $\mathbb{O}(\log(N_t))$ parallel time units [36] and the latency of computing $\tilde{\mathbf{W}}_2^{-1}$ is negligible compared with matrix-matrix multiplication [32]. Thus the processing latency of K-SENIA scales as $\mathbb{O}(2k\log(N_t))$, which is much lower than the processing latency of exact matrix inversion, that is $\mathbb{O}(N_t)$ [28]. With L-term SE approximation, a 2^{k+1}-term expansion is required. The L-term SE approximation comprises two main parts. The first part is the computation of $\tilde{\mathbf{W}}_2^{-1}$, with complexity $\mathbb{O}(N_t^2)$ and negligible processing latency compared

with matrix-matrix multiplication. Secondly, for $L \geq 3$, $\tilde{\mathbf{W}}_L^{-1}$ is updated by $\tilde{\mathbf{W}}_L^{-1} = (-\mathbf{D}^{-1}\mathbf{E})\tilde{\mathbf{W}}_{L-1}^{-1} + \mathbf{D}^{-1}$, thus in total, $2^{k+1} - 2$ matrix-matrix multiplications are required. Hence, we can conclude K-SENIA requires $2k$ matrix-matrix multiplications while 2^{k+1}-term SE approximation requires $2^{k+1} - 2$ matrix-matrix multiplications, the complexity and latency gain achieved by K-SENIA over L-term SE approximation are both $\frac{2^k-1}{k}$.

Consider IU, from Algorithm 1, with the initial size of approximate matrix inversion $\check{\mathbf{W}}_{N_i}^{-1} \in \mathbb{C}^{N_i \times N_i}$, to obtain $\check{\mathbf{W}}_{N_t}^{-1}$, there are $N_t - N_i$ IU steps, at the $j$the step, with $\check{\mathbf{W}}_{N_i+j-1}^{-1} \in \mathbb{C}^{(N_i+j-1)\times(N_i+j-1)}$ to be updated, the computation complexities of $\mathbf{t}_1, \mathbf{t}_2$ and $\mathbf{t}_3$ scale as $\mathbb{O}(N_r(N_i + j - 1))$, $\mathbb{O}((N_i + j - 1)^2)$ and $\mathbb{O}(N_i + j - 1)$ respectively. Then the complexity of computing c is of order $\mathbb{O}(N_r + N_i + j - 1)$. Finally, the complexity of computing $\mathbf{F}_{11}^{-1}$ is of order $\mathbb{O}((N_i + j - 1)^2)$. Therefore, the overall complexity required by the jth IU step is of order $\mathbb{O}(N_r(N_i + j - 1))$. Concerning processing latency, notice that IU only requires matrix-vector and vector-vector multiplication, thus compared with K-SENIA the latency of IU can be ignored. Then we consider the complexity of K-SENIA-IU. Let $\triangleq$ denotes the anonymous equality for $\mathbb{O}$-notation [50]. The computation of $\check{\mathbf{W}}_{N_i}^{-1}$ by K-SENIA requires a complexity of order $\mathbb{O}(2kN_i^3)$, and the complexity of $N_t - N_i$ steps of IU is of order $\mathbb{O}(N_rN_t^2 - N_rN_i^2)$ (the complexity of the jth step is of order $\mathbb{O}(N_r(N_i + j - 1))$, for $j = 1, 2, \cdots, N_t - N_i$, the overall complexity is of order $\sum_{j=1}^{N_t-N_i} \mathbb{O}(N_r(N_i + j - 1)) \triangleq \mathbb{O}(N_rN_t^2 - N_rN_i^2)$). Thus the overall complexity of K-SENIA-IU scales as $\mathbb{O}(N_rN_t^2)$ ($\mathbb{O}(N_rN_t^2 - N_rN_i^2) + \mathbb{O}(2kN_i^3) \triangleq \mathbb{O}(N_rN_t^2 + (2kN_i - N_r)N_i^2)$, since $2kN_i$ is close to N_r, the overall complexity after simplification is of order $\mathbb{O}(N_rN_t^2)$.

From the analysis above, we can see that the processing latency of K-SENIA scales as $\mathbb{O}(2k\log(N_t))$, that is much lower than that of exact matrix inversion schemes ($\mathbb{O}(N_t)$ [28]) when N_t is large. Furthermore, the hardware implementations of K-SENIA and IU is more economical than the exact matrix inversion schemes. K-SENIA and IU only require scalar-vector, matrix-vector and matrix-matrix multiplications, that can be implemented using generic, parallelizable and reusable Multiply-and-Accumulated (MAC) structure. In [32],

it is shown that the VLSI implementation of the L-term SE approximation using matrix multiplications can save various types hardware resources compared with the exact matrix inversions using Cholesky factorization. Gauss-Jordan elimination requires expensive floating point implementation to obtain good mathematical properties (dynamic range, stability) [51]. QR decomposition requires complicated data flow mechanism [27]. In addition, Gasuss-Jordan elimination, Cholesky and QR decompositions all require more division and square root operations than SE approximation [28]. Finally, [33] shows that the hardware implementation of matrix multiplication based SE approximate matrix inversion is more energy efficient than that of QR decomposition based exact matrix inversions.

3.2 Applications of Improved Approximate Matrix Inversion to Linear MMSE Detection

In order to assess the performance of the approximate matrix inversion technique for detections in LS-MIMO, in this section, we consider the simple MMSE detector, which is capable to achieve near-optimal performance in low loaded (very small α) systems with low complexity $\mathbf{O}(N_r N_t^2)$ [12] and hence considered as a potential candidate for practical receiver design [2].

3.2.1 Residual Estimation Error Analysis

We start by characterizing the approximation error in the estimated transmitted symbol vector when exact matrix inversion is replaced by K-SENIA in MMSE detectors, resulting in MMSE-SENIA. For the LDs with approximate matrix inversions, at low SNR, the multi-user interference (MUI) and noise are the dominant factors that influence detection performance [38] obscuring the errors due to approximate matrix inversion. Thus our analysis is carried out at high SNR ($\rho_r \to \infty$), where the approximation error becomes the major factor for performance loss. Let $\mathbf{W} = \mathbf{H}^H\mathbf{H} + \rho_s^{-1}\mathbf{I}$ denote the regularized Gram matrix.

The soft estimates of the original MMSE detector and MMSE detector with K-SENIA, denoted by $\hat{\mathbf{s}}^{MMSE}$ and $\hat{\mathbf{s}}^{MMSE-SENIA}$ respectively, are given by $\hat{\mathbf{s}}^{MMSE} = \mathbf{W}^{-1}\mathbf{H}^H\mathbf{y}$ and $\hat{\mathbf{s}}^{MMSE-SENIA} = \check{\mathbf{M}}_k\mathbf{H}^H\mathbf{y}$. The residual estimation error (mean square error) ϵ of this approximation is defined as

$$\epsilon = \mathbb{E}(||\hat{\mathbf{s}}^{MMSE} - \hat{\mathbf{s}}^{MMSE-SENIA}||^2), \tag{3.39}$$

the use of (3.24) in (3.39) yields

$$\epsilon = \mathbb{E}(||(\mathbf{W}^{-1} - \check{\mathbf{M}}_k)\mathbf{H}^H\mathbf{y}||^2) = \mathbb{E}(||\mathbf{W}_{\triangle}^{-1}\mathbf{H}^H\mathbf{y}||^2) = \mathbb{E}(||(-\mathbf{D}^{-1}\mathbf{E})^{2^{k+1}}\mathbf{W}^{-1}\mathbf{H}^H\mathbf{y}||^2), \tag{3.40}$$

and at high SNR this is

$$\epsilon_\infty = E_s\mathbb{E}[||(\mathbf{D}^{-1}\mathbf{E})^{2^{k+1}}||_F^2]. \tag{3.41}$$

where $||\cdot||_F$ denotes the Frobenius norm. The proof of (3.41) can be found in Appendix A.

The insights provided by (3.41) are twofold. Firstly, since $\epsilon_\infty > 0$, the residual estimation error in (3.41) does not vanish with increasing SNR, which indicates the existence of an error floor in the BER-SNR curves of MMSE-SENIA at high SNR. Secondly, the level of the error floor is determined by two factors: the iteration time of K-SENIA and magnitude disparity between the diagonal and off-diagonal components in $\mathbf{W}$ (i.e., how close the magnitudes of the components in $(\mathbf{D}^{-1}\mathbf{E})^{2^{k+1}}$ are to zero, or the orthogonality between the columns of $\mathbf{H}$).

3.2.2 Reducing the Error Floor

From the analysis of the residual estimation error of MMSE-SENIA in the previous section, it is straightforward that the error floor can be reduced by increasing the iteration time of K-SENIA. Besides this, we can also consider an alternative solution that takes into account

the second factor. If the orthogonality between the columns of $\mathbf{H}$ increases, the diagonal components of $\mathbf{W}$ would become increasingly stronger than its off-diagonal components, then from (3.41), the error floor becomes lower. Capitalizing on this result, we next propose a hybrid MMSE detector that can reduce the error floor by considering the real-time channel orthogonality.

Hybrid MMSE detection

The Orthogonality Measure (OM) of $\mathbf{H}$ is defined by

$$\breve{\phi} = \frac{\det(\mathbf{H}^H\mathbf{H})}{\prod_{i=1}^{N_t} ||\mathbf{h}_i||^2}, \tag{3.42}$$

where $\mathbf{h}_i$ denotes the i th column of $\mathbf{H}$, $\det(\cdot)$ denotes determinant operator, $||\cdot||$ denotes the Euclidean norm (another related definition is orthogonality deficiency [42] $\tilde{\phi} = 1 - \breve{\phi}$). Based on the Hadamard's inequality $\det(\mathbf{H}^H\mathbf{H}) \leq \prod_{i=1}^{N_t} [\mathbf{H}^H\mathbf{H}]_{ii}^2 = \prod_{i=1}^{N_t} ||\mathbf{h}_i||^2$, we have $0 \leq \breve{\phi} \leq 1$. If $\mathbf{H}^H\mathbf{H}$ is singular then $\breve{\phi} = 0$ and if all the columns in $\mathbf{H}$ are mutually orthogonal then $\breve{\phi} = 1$.

The hybrid MMSE detector uses exact matrix inversion when the channel is not orthogonal enough (i.e., where the OM of this channel realization is below a certain threshold) in order to avoid approximation performance loss in this extreme case and if the OM is above the threshold, the hybrid MMSE detector uses approximate matrix inversion. Such hybrid MMSE detector can be defined as

$$\text{Hybird MMSE} = \begin{cases} \text{MMSE-SENIA}, & \text{if } \breve{\phi} \geq \zeta \\ \text{MMSE}, & \text{if } \breve{\phi} < \zeta \end{cases} \tag{3.43}$$

where ζ is the threshold. By selecting a proper ζ, we can tune the usage percentage of MMSE-SENIA, thus making a trade-off between the performance and latency of the hybrid MMSE detector. The selection of ζ requires the knowledge of the distribution of OM.

Statistical Distribution of Orthogonality Measure (OM)

Consider an alternative form of (3.42), using the Cholesky factorization [52], $\mathbf{H}^H\mathbf{H} = \mathbf{R}^H\mathbf{R}$, where $\mathbf{R} \in \mathbb{C}^{N_t \times N_t}$ is an upper triangular matrix. Let $\mathbf{r}_i$ denote the ith column of $\mathbf{R}$, $r_{ji} = [\mathbf{R}]_{ji}, j \leq i$ and r_{ji}^* denote the conjugate of r_{ji}. Then (3.42) can be rewritten as

$$\breve{\phi} = \frac{\det(\mathbf{R}^H)\det(\mathbf{R})}{\prod_{i=1}^{N_t}||\mathbf{r}_i||^2} = \frac{\prod_{i=1}^{N_t} r_{ii}^* \prod_{i=1}^{N_t} r_{ii}}{\prod_{i=1}^{N_t}||\mathbf{r}_i||^2} = \prod_{i=1}^{N_t}\{\frac{|r_{ii}|^2}{|r_{ii}|^2 + \sum_{j<i}|r_{ji}|^2}\}. \tag{3.44}$$

Let $\chi^2(k)$ denotes the Chi-square distribution with k degrees of freedom and $Gamma(k,\theta)$ denotes the Gamma distribution with shape parameter k and scale parameter θ. From [53] r_{ji} are independent, for $1 \leq i \leq N_t$, $|r_{ii}|^2 \sim Gamma(N_r - i + 1, 1)$ and for $1 \leq j < i \leq N_t$, $r_{ji} \sim \mathbb{CN}(0,1)$, hence $\Re(r_{ji}), \Im(r_{ji}) \sim \mathcal{N}(0, \frac{1}{2})$. Therefore $2\sum_{j<i}|r_{ji}|^2 = \sum_{j<i}[(\sqrt{2}\Re(r_{ji}))^2 + (\sqrt{2}\Im(r_{ji}))^2] \sim \chi^2(2(i-1)) \sim Gamma((i-1), 2)$ and $\sum_{j<i}|r_{ji}|^2 \sim Gamma(i-1, 1)$ $(i \geq 2)$. Thus (3.44) can be rewritten as

$$\breve{\phi} = \prod_{i=1}^{N_t}\frac{\alpha_i}{\alpha_i + \beta_i} \tag{3.45}$$

$$\alpha_i = |r_{ii}|^2 \sim Gamma(k_1^i, 1), \quad k_1^i = N_r - i + 1, \quad i = 1, 2 \ldots N_t \tag{3.46}$$

$$\beta_i = \begin{cases} 0 \quad i = 1 \\ \sum_{j<i}|r_{ji}|^2 \sim Gamma(k_2^i, 1), \quad k_2^i = i - 1, \quad i = 2, 3, \ldots N_t \end{cases} \tag{3.47}$$

Furthermore, if $X \sim Gamma(k_1, \theta)$ and $Y \sim Gamma(k_2, \theta)$ are independent, then $\frac{X}{X+Y} \sim Beta(k_1, k_2)$, that is the Beta distribution with shape parameters $k_1, k_2 > 0$ [54]. Let $\eta_i = \frac{\alpha_i}{\alpha_i + \beta_i}$, $i = 1, 2, \ldots, N_t$. Since $\beta_1 = 0$, we have

$$\eta_i = \begin{cases} 1, \quad i = 1 \\ \frac{\alpha_i}{\alpha_i + \beta_i}, \quad i = 2, 3, \ldots, N_t \end{cases} \tag{3.48}$$

Then (3.45) can be rewritten as

$$\breve{\phi} = \prod_{i=1}^{N_t} \eta_i = \prod_{i=2}^{N_t} \eta_i, \tag{3.49}$$

and for sake of simplicity, we change the indexing of (3.49) by defining

$$\tilde{\eta}_i = \eta_{i+1} \sim Beta(\tilde{k}_1^i, \tilde{k}_2^i), \quad i = 1, 2, \ldots, N_t - 1 \tag{3.50}$$

where $\tilde{k}_1^i = k_1^{i+1} = N_r - i$ and $\tilde{k}_2^i = k_2^{i+1} = i$. Thus $\breve{\phi} = \prod_{i=1}^{N_t-1} \tilde{\eta}_i$ is the product of $N_t - 1$ independent beta random variables.

The distribution of the product of independent beta random variables plays an important role in the likelihood ratio test statistics [55–58] and the exact expressions of its distribution have been studied by many researchers. There are three main types of expressions of this distribution, Meijer G or Fox's H function [59], series summation representation [60] and the infinite mixture of the beta distribution [61]. However, these expressions all suffer from various drawbacks that limit their practical use such as long computation time, highly complicated structure and coefficients [62]. Recently an approximate expression of this distribution, called near-exact approximate distribution, was proposed [62]. The near-exact approximate distribution keeps intact the part of the exact distribution, and approximates the remaining part asymptotically. In our case of interest, where all the $\tilde{k}_2^i$ are integers, the approximate part in the near-exact approximate distribution vanishes. Therefore, the exact distribution of $\breve{\phi}$ can be presented in an explicit and highly manageable form.

The exact expressions of probability density function (p.d.f.) $f_{\breve{\phi}}(x)$ and cumulative distribution function (c.d.f.) $F_{\breve{\phi}}(x)$ of $\breve{\phi}$ are given by,

$$f_{\breve{\phi}}(x) = x^{-1} f^{GIG}(-\ln(x)|g, \{\mu_l\}_{l=1:g}, \{\tau_l\}_{l=1:g}). \tag{3.51}$$

$$F_{\breve{\phi}}(x) = 1 - F^{GIG}(-\ln(x)|g, \{\mu_l\}_{l=1:g}, \{\tau_l\}_{l=1:g}), \tag{3.52}$$

where $f^{GIG}(x|g,\{\mu_l\}_{l=1:g},\{\tau_l\}_{l=1:g})$ and $F^{GIG}(x|g,\{\mu_l\}_{l=1:g},\{\tau_l\}_{l=1:g})$ denote p.d.f. and c.d.f. of Generalized Integer Gamma (GIG) distribution [63] respectively with the depth $g = N_t - 1$, shape parameters $\mu_l = N_t - l$ and rate parameters $\tau_l = N_r - l$, $l = 1, 2, \ldots, g$.

Proof. See Appendix B.1.

However, (3.51) and (3.52) are still too complicated for practical computations and analysis. Therefore, next we provide an accurate approximate distribution form. Based on the central limit theorem [64], the distribution of $\breve{\phi}$ converges to log-normal [65] asymptotically,

$$\lim_{N_t\to\infty} \breve{\phi}_{N_t} \sim \ln\mathcal{N}(-U_{N_t}, S^2_{N_t}), \tag{3.53}$$

where

$$U_{N_t} = \sum_{i=1}^{N_t-1} u_i = (N_t-1)\psi(N_r) - \sum_{i=1}^{N_t-1}\psi(N_r-i), \tag{3.54}$$

and

$$S^2_{N_t} = \sum_{i=1}^{N_t-1}\sigma_i^2 = \sum_{i=1}^{N_t-1}\psi_1(N_r-i) - (N_t-1)\psi_1(N_r). \tag{3.55}$$

where $u_i = \mathbb{E}(-\ln(\tilde{\eta}_i))$ and $\sigma_i^2 = Var(-\ln(\tilde{\eta}_i))$, with $Var()$ denotes the variance and $\psi_1(x) = \frac{d\psi(x)}{dx}$ denotes the trigamma function.

Proof. See Appendix B.2

The log-normal approximate p.d.f. and c.d.f of $\breve{\phi}$, denoted by $f^{\ln\mathcal{N}}_{\breve{\phi}}(x)$ and $F^{\ln\mathcal{N}}_{\breve{\phi}}(x)$ respectively, are given by [65]

$$f^{\ln\mathcal{N}}_{\breve{\phi}}(x) = \frac{1}{xS_{N_t}\sqrt{2\pi}}\exp[-\frac{(\ln(x)+U_{N_t})^2}{2S^2_{N_t}}]. \tag{3.56}$$

$$F^{\ln\mathcal{N}}_{\breve{\phi}}(x) = \Phi(\frac{\ln(x)+U_{N_t}}{S_{N_t}}), \tag{3.57}$$

where Φ is the cumulative distribution function of the standard normal distribution.

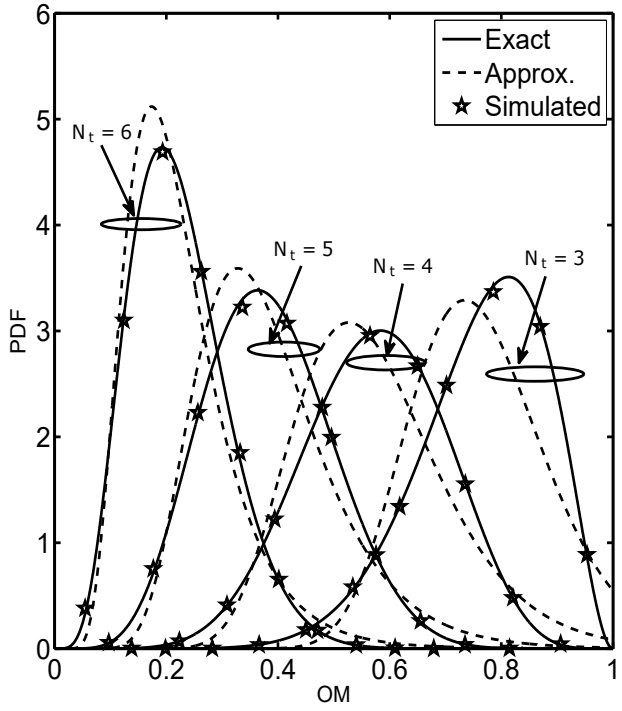

(a)

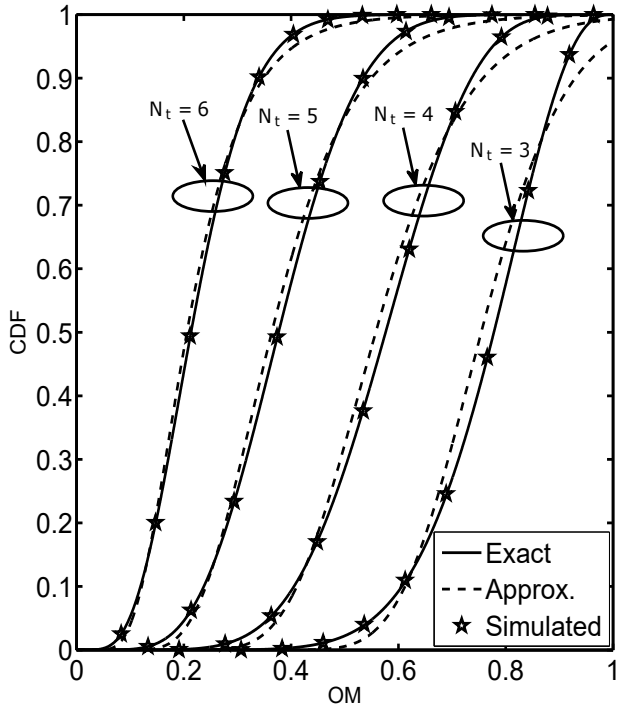

(b)

Fig. 3.1 Exact, approximate and simulated distributions of OM with $N_r = 12$ and $N_t = 3, 4, 5, 6$, (a) p.d.f. (b) c.d.f.

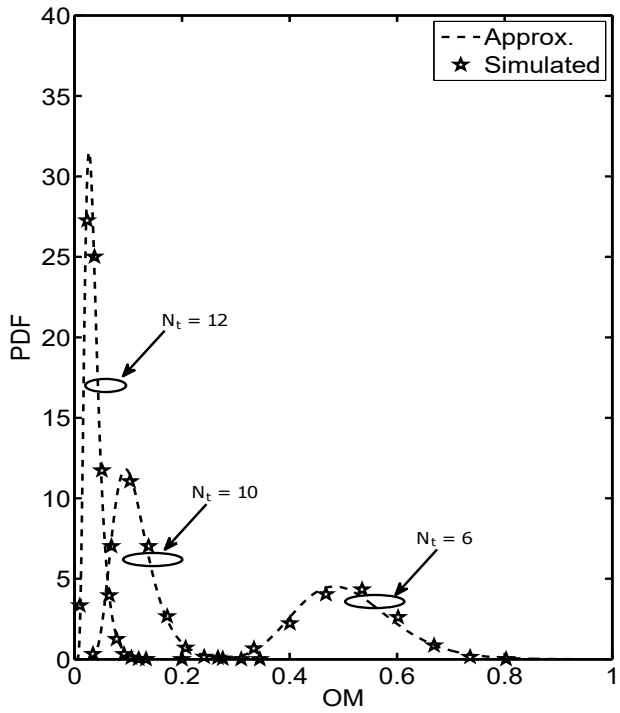

Fig. 3.2 Approximate and simulated distributions of OM with $N_r = 24$ and $N_t = 6, 10, 12$

Fig. 3.1 presents the exact and approximate distribution forms of OM (Fig. 3.1(a) p.d.f. and Fig. 3.1(b) c.d.f.) of i.i.d CSCG MIMO channel with $N_r = 12$ and $N_t = 3, 4, 5, 6$. In addition, we also provide the simulated p.d.f. and c.d.f. of OM, which are generated based on 10^5 independent channel realizations. It is observed that, firstly, the exact theoretical p.d.f. and c.d.f. match the simulated results very well, secondly, the log-normal approximation gets closer to exact distribution with increasing N_t. Fig. 3.2 presents the approximate and simulated pdf of OM with $N_r = 24$ and $N_t = 6, 10, 12$. It is observed that with N_t increasing, the log-normal approximation matches simulated results well. For example, for $N_t = 10$ and $N_t = 12$ all the simulated points lie on the log-normal approximation curves. These results demonstrate the effectiveness of the log-normal approximation for practical analysis and computations.

3.2.3 BER Performance of MMSE detection Aided by Improved Approximate Matrix Inversion

The general setup of the computer simulations is detailed in Appendix C. Firstly we consider the BER performance of MMSE-SENIAk, where k denotes the number of Newton iterations. For comparison, MMSE detector with exact matrix inversion and MMSE detectors exploiting 3-term SE approximation, referred to as MMSE-EMI and MMSE-SE3 respectively, are also considered. Fig. 3.3 presents the results for 64×8 and 128×16 16-QAM MIMO systems where the convergence condition are satisfied. As we can observe from Fig. 3.3, MMSE-SENIA1/2/3 all outperform MMSE-SE3 significantly. For example, in 64×8 MIMO system, at BER= 6.13×10^{-4}, the SNR gain provided by MMSE-SENIA1/2/3 over MMSE-SE3 are 2.2dB, 3.4dB and 3.5dB respectively and in the 128×16 MIMO system, at BER= 6.79×10^{-4}, the SNR gain provided by MMSE-SENIA1/2/3 over MMSE-SE3 are 2.3dB, 3.4dB and 3.5dB respectively. Furthermore, in both system configurations, the performance of MMSE-SENIA improves rapidly with k and are almost indistinguishable for $k = 3$ from that of MMSE-EMI with only a fraction of dB loss at low BER region. For example, in 64×8 MIMO system, at BER= 1.89×10^{-4}, MMSE-SENIA with $k = 3$ can provide about 2.4dB and 2.5dB over MMSE-SENIA1 respectively. When BER$\geq 1.09 \times 10^{-4}$, MMSE-SENIA with $k = 2, 3$ perform indistinguishable from MMSE-EMI and only exhibits about 0.8dB and 0.3dB performance loss at BER= 1.19×10^{-5}. In 128×16 MIMO system, at BER= 1.55×10^{-4}, the SNR gain provided by MMSE-SENIA with $k = 2, 3$ over MMSE-SENIA1 is 2.4dB and 2.5dB respectively. And when BER$\geq 7.85 \times 10^{-5}$, MMSE-SENIA with $k = 2, 3$ have indistinguishable performances from that of MMSE-EMI, and exhibits about 0.6dB and 0.2dB performance loss at BER= 5.14×10^{-6} respectively. In Fig. 3.4 we consider 32×4 16-QAM MIMO system. Error floor can be observed when SNR$\geq$ 14dB for MMSE-SE3 and MMSE-SENIA1, which is caused by the residual estimation error ϵ_∞ of (3.41). The levels of the error floors become lower with improving approximation performance [32] [34]. For example, with MMSE-SE3, the error floor occurs at BER= 2.35×10^{-4},

while with MMSE-SENIA1, the error floor occurs at BER= 7.63×10^{-5}. With MMSE-SENIA2/3, no error floors are observed for BER$\geq 10^{-6}$.

Next we consider the BER performance of MMSE detectors exploiting K-SENIA-IU in 64×16, 128×32 and 32×10 16-QAM MIMO systems, where the system loading factors α exceed the convergence constraint. The MMSE detectors employing K-SENIA-IU with size of the initial approximate matrix inverse N_i and k iterations of K-SENIA, are referred to as MMSE-SENIAk-IU ($N_t = N_i + (N_t - N_i)$). For comparison, we also consider MMSE-EMI , MMSE-EMI employing IU, referred to as MMSE-EMI-IU, MMSE-SE3, MMSE-SENIAk and MMSE that exploits SE3-IU, referred to as MMSE-SE3-IU ($N_t = N_i + (N_t - N_i)$), where the initial approximate matrix inverse is computed by 3-term SE approximation. Fig. 3.5 presents the corresponding results for 64×16 and 128×32 MIMO systems. As we can observe, because of higher system loading factors, the BER performances of MMSE-SE3 and MMSE-SENIA-(1/3) fail to converge to MMSE-EMI, as demonstrated by the fact that BER does not decrease when ρ_r increases. However, MMSE-SENIA1/3-IU performs much better, and the performance of MMSE-SENIA3-IU is almost indistinguishable from that of MMSE-EMI with just a fraction of dB loss at low BER region. For example, in the 64×16 system, MMSE-SENIA3-IU performs indistinguishable from MMSE-EMI for BER$\geq 6.02 \times 10^{-5}$ and is about 0.5dB worse at BER= 3.01×10^{-6}. In the 128×32 system, the performance of MMSE-SENIA3-IU is indistinguishable from that of MMSE-EMI for BER$\geq 5.14 \times 10^{-5}$ and exhibits about 0.2dB performance loss at BER= 1.17×10^{-6}. In addition, it can be observed from Fig. 3.5(a) that the performances of MMSE-EMI-IU and MMSE-EMI are the same, this is because if the initial input of IU is the exact matrix inverse, the output of IU is also exact, thus hereinafter we do not present the results for MMSE-EMI-IU. Fig. 3.6 presents the results in 32×10 system. Error floors occur when SNR$\geq$ 18dB. These error floors are induced by the approximation error of $\check{\mathbf{W}}_{N_i}^{-1}$. In addition, the error floor can be vanished at BER$\geq 10^{-6}$ with increasing k in MMSE-SENIA-IU. Furthermore, by comparing MMSE-SENIA3 (for 64×8 and 128×16 systems) in Fig. 3.3 and MMSE-

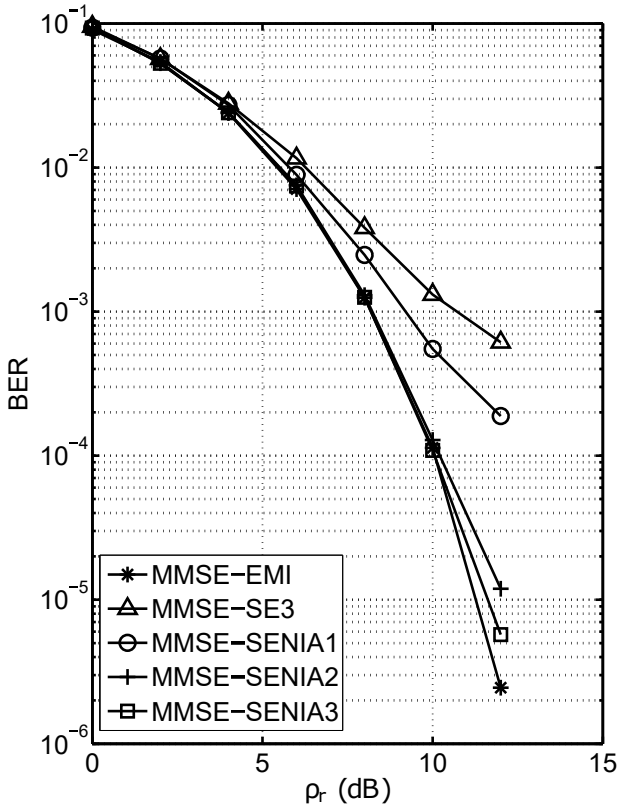

(a)

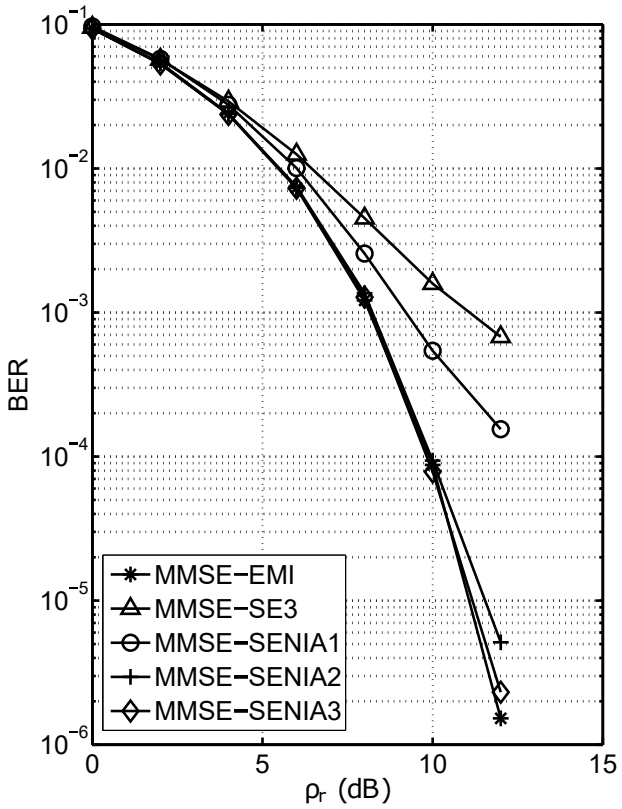

(b)

Fig. 3.3 BER performance of MMSE-EMI, MMSE-SE3 and MMSE-SENIA1/2/3 in (a) 64×8 MIMO and (b) 128×16 16-QAM MIMO systems

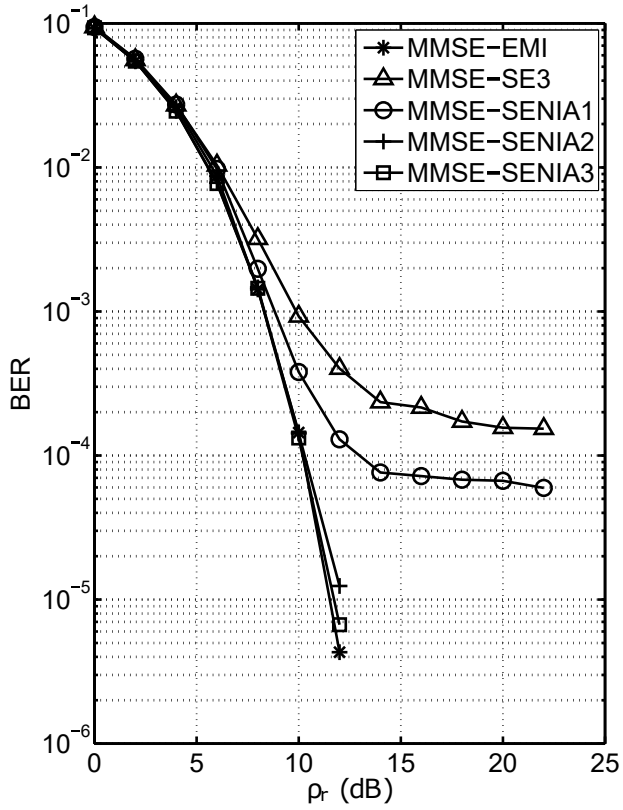

Fig. 3.4 BER performance of MMSE-EMI, MMSE-SE3 and MMSE-SENIA1/2/3 in a 32×4 16-QAM MIMO system

SENIA3-IU (for $64\times(8+8)$ and $128\times(16+16)$ systems) in Fig. 3.5, we can observe that the combination of K-SENIA and IU does not induce observable approximation performance degradation compared with original K-SENIA. This corroborates the error propagation analysis of K-SENIA-IU in 3.1.3.

In Fig. 3.7 we present the BER performance of the hybrid MMSE detector, referred to as MMSE-HYB, in 128×20, $4, 16$ and 64-QAM MIMO systems. For comparison, MMSE-EMI and MMSE-SENIA3 are also considered. The usage percentages of the channel realizations decoded by MMSE-SENIA3 considered are 0.25, 0.50 and 0.75, which is tuned by setting the threshold ζ of (3.43) based on the approximate log-normal distribution of OM of (3.53). Fig. 3.7 demonstrates that compared to MMSE-SNEIA, MMSE-HYB can effectively reduce error floors. For example, in the 4-QAM system, the error floor of MMSE-SENIA3 occurs at BER$= 5.19\times 10^{-6}$, while for MMSE-HYB $(0.75, 0.50, 0.25)$, no error floor is observed at BER$\geq 5.65\times 10^{-8}$. In the 16-QAM system, the error floor of MMSE-SENIA3 occurs at 10^{-4}, while for MMSE-HYB $(0.75, 0.50, 0.25)$, the error floors are reduced to 1.29×10^{-5}, 2.48×10^{-6} and 4.09×10^{-7} respectively. For the 64-QAM system, the error floor of MMSE-SENIA3 occurs at BER$= 2.95\times 10^{-4}$, which can be reduced to 1.12×10^{-4}, 2.22×10^{-5} and 3.32×10^{-6} by MMSE-HYB $(0.75, 0.50, 0.25)$ respectively.

The results in this chapter demonstrate the capacity of K-SENIA-IU matrix inversion to provide good performance at BER ranges of practical interest in higher loaded LS-MIMO systems. In the next chapter we show how such approximate matrix inversion can be integrated into other high performance MIMO detection techniques.

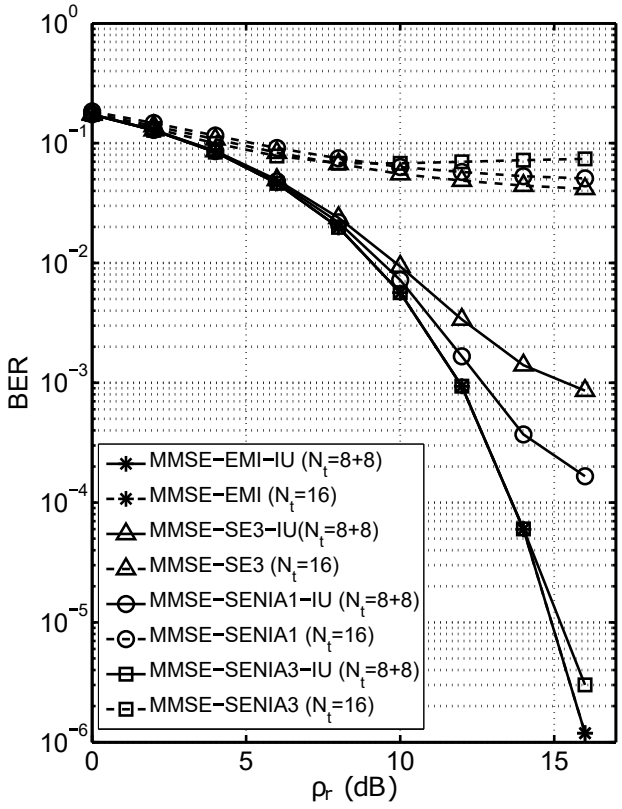

(a)

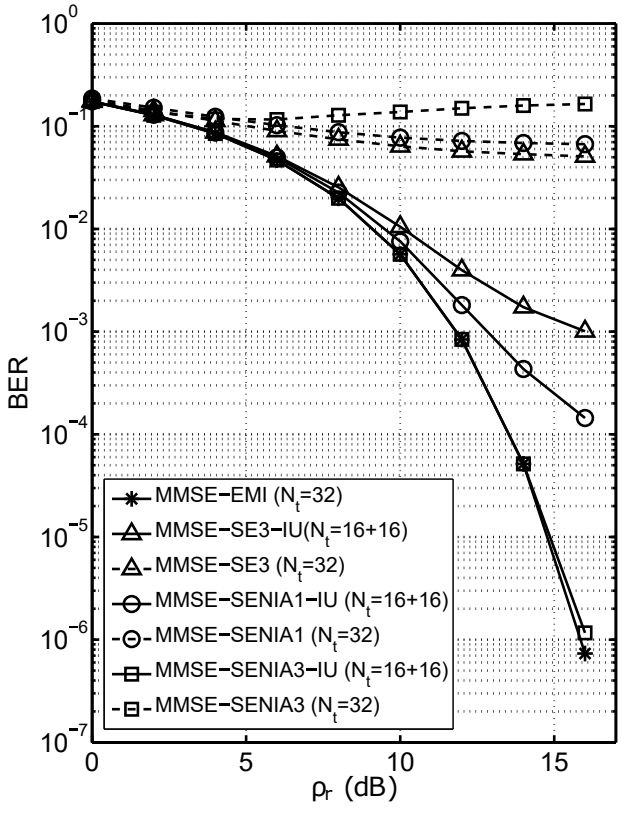

(b)

Fig. 3.5 BER performance of MMSE-EMI/EMI-IU, MMSE-SE3/SE3-IU and MMSE-SENIA(1/3)/SENIA(1/3)-IU in (a) 64×16 (b) 128×32 16-QAM MIMO systems

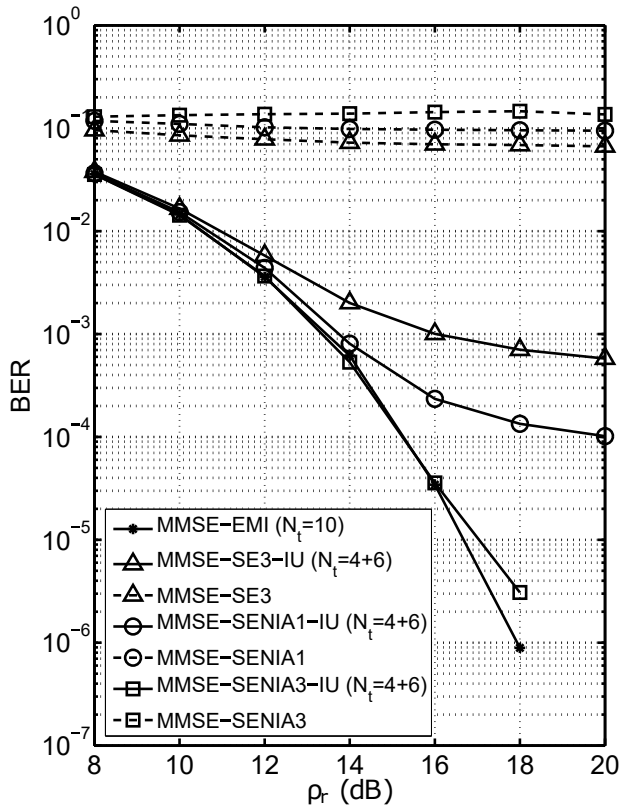

Fig. 3.6 BER performance of MMSE-EMI, MMSE-SE3-IU and MMSE-SENIA1/2/3-IU in a 32×10 16-QAM MIMO system

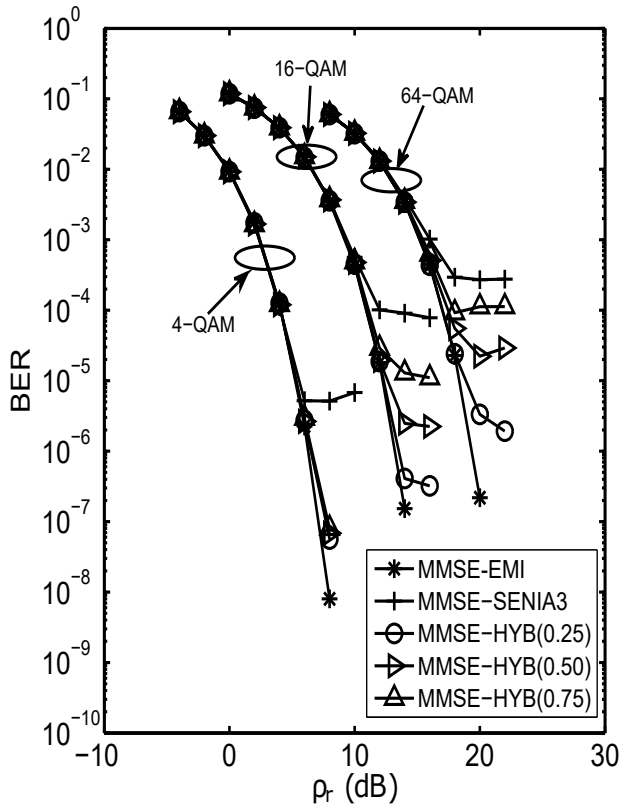

Fig. 3.7 BER performance of hybrid MMSE detectors in 128×20, 4, 16 and 64-QAM MIMO systems

Chapter 4

Selection Based List Detections for Large-Scale MIMO

4.1 General Structure of Selection Based List Detector

At the receiving side, a frame error (detection error) occurs if there is at least one erroneous estimate in the estimated symbol vector. The optimal detector (in the sense of lowest average detection error probability) when $\mathbf{H}$ is known, is the maximum likelihood detector (MLD), that is using the minimum Euclidean distance (MED) rule [5]

$$\hat{\mathbf{s}}^{ML} = \arg \min_{\hat{\mathbf{s}} \in \mathbb{A}^{N_t}} ||\mathbf{y} - \mathbf{H}\hat{\mathbf{s}}||^2, \tag{4.1}$$

where $||\cdot||$ denotes the Euclidean norm. Consider an alternative representation of MLD in (4.1). Let $\mathbf{H}_1 \in \mathbb{C}^{N_r \times N}$ denote a sub-matrix composed of N columns from $\mathbf{H}$, where $1 \leq N \leq N_t$, and let $\mathbf{s}_1 \in \mathbb{C}^{N \times 1}$ denote the symbol sub-vector whose components are transmitted over the channel corresponding to $\mathbf{H}_1$. Similarly, let $\mathbf{H}_2 \in \mathbb{C}^{N_r \times (N_t - N)}$ denote the sub-matrix composed of the remaining columns from $\mathbf{H}$ and $\mathbf{s}_2 \in \mathbb{C}^{(N_t - N) \times 1}$ denote the symbol sub-vector whose components are transmitted over the channel corresponding to

$\mathbf{H}_2$. Thus (2.1) can be rewritten as

$$\mathbf{y} = \mathbf{H}_1\mathbf{s}_1 + \mathbf{H}_2\mathbf{s}_2 + \mathbf{n}. \tag{4.2}$$

Let $\hat{\mathbf{s}}_1, \hat{\mathbf{s}}_2$ denote the estimates of $\mathbf{s}_1, \mathbf{s}_2$. Let $[\hat{\mathbf{s}}_1^1, \hat{\mathbf{s}}_1^2, \dots \hat{\mathbf{s}}_1^K]$, $K = M^N$ denote all the possible values of $\hat{\mathbf{s}}_1$ and $[\hat{\mathbf{s}}_2^1, \hat{\mathbf{s}}_2^2, \dots, \hat{\mathbf{s}}_2^Q]$, $Q = M^{N_t - N}$ denote all the possible values of $\hat{\mathbf{s}}_2$. Then the ML solution of (4.1) can be rewritten as

$$(\hat{\mathbf{s}}^{ML})^T = [(\hat{\mathbf{s}}_1^{ML})^T, (\hat{\mathbf{s}}_2^{ML})^T] \text{ where } \hat{\mathbf{s}}_1^{ML} = \hat{\mathbf{s}}_1^{\tilde{k}}, \quad \hat{\mathbf{s}}_2^{ML} = \hat{\mathbf{s}}_2^{\tilde{q}}, \tag{4.3}$$

and

$$[\tilde{k}, \tilde{q}] = \arg \min_{k \in [1,2 \dots K]} \min_{q \in [1,2,\dots,Q]} ||\mathbf{y} - \mathbf{H}_1\hat{\mathbf{s}}_1^k - \mathbf{H}_2\hat{\mathbf{s}}_2^q||^2. \tag{4.4}$$

The process of obtaining the ML solution based on such equivalent representation can be divided into three steps. First consider all the possible sub-vector hypotheses $\hat{\mathbf{s}}_1^k$ of $\mathbf{s}_1$, and perform corresponding interference cancellations in $\mathbf{y}$ to obtain the residual observations $\mathbf{y}^k, k \in [1, 2, \dots, K]$

$$\mathbf{y}^k = \mathbf{y} - \mathbf{H}_1\hat{\mathbf{s}}_1^k, \quad k = 1, 2, \dots, K. \tag{4.5}$$

Then solve

$$\hat{\mathbf{x}}_2^k = \arg \min_{\tilde{\mathbf{s}}_2 \in [\hat{\mathbf{s}}_2^1, \hat{\mathbf{s}}_2^2 \dots, \hat{\mathbf{s}}_2^Q]} ||\mathbf{y}^k - \mathbf{H}_2\tilde{\mathbf{s}}_2||^2, \quad k = 1, 2, \dots, K \tag{4.6}$$

$$\tilde{k} = \arg \min_{k \in [1,2,\dots,K]} ||\mathbf{y}^k - \mathbf{H}_2\hat{\mathbf{x}}_2^k||^2, \tag{4.7}$$

Finally form $\hat{\mathbf{s}}_1^{ML} = \hat{\mathbf{s}}_1^{\tilde{k}}, \hat{\mathbf{s}}_2^{ML} = \hat{\mathbf{x}}_2^{\tilde{k}}$.

The selection based list detection first generates a list of candidates for possible transmitted symbol vectors estimates $\hat{\mathbf{s}}^k, k = 1, 2, \cdots, M^N$, then the best candidate in the list, is chosen using MED rule as the final decision. Fig. 4.1 depicts the block diagram of selection based list detection with DMS channel partition and V-BLAST ordered MMSE-SIC (V-BLAST-SIC) [66] sub-detector. As we can see from Fig. 4.1, selection based list detection

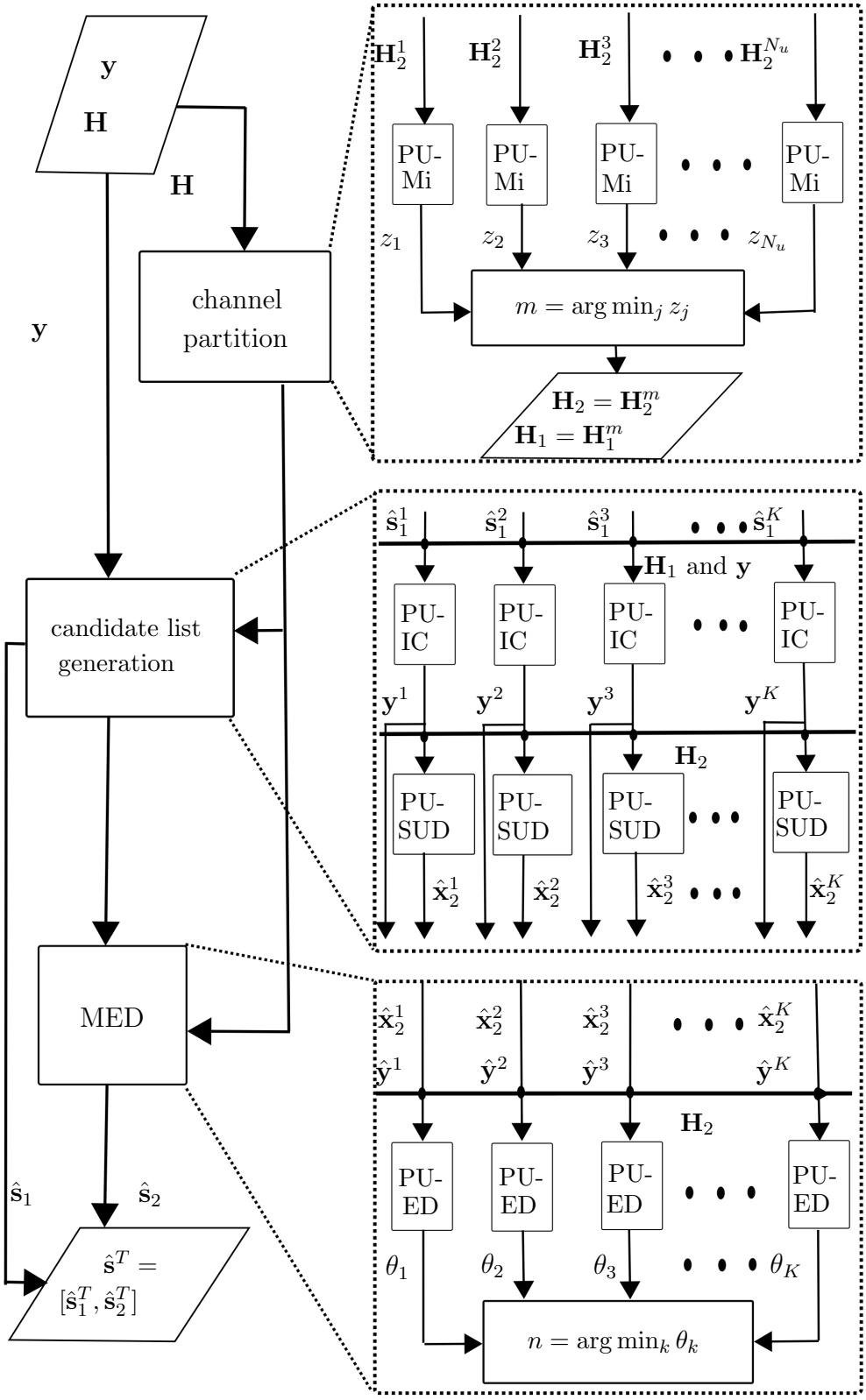

Fig. 4.1 Block diagram of selection based list detector with DMS channel partition and V-BLAST-SIC sub-detection

can be divided into three parallelizable stages:

- Channel Partition: The sub-matrices $\mathbf{H}_1$ and $\mathbf{H}_2$ in (4.4) are first obtained by the channel partition rule. The DMS rule [67] chooses the subset of the columns of $\mathbf{H}$ with strongest weakest sub-datastream (in the sense of postprocessing SINR using MMSE criterion [68]) and forms $\mathbf{H}_2$. Define the possible subsets $\mathbf{H}_2^j, j = [1, 2, \cdots, N_u]$, where $N_u = \binom{N_t}{N}$. The subset chosen by DMS rule $\mathbf{H}_2^m$ is given by

$$m = \arg \min_{j=1,2,\cdots,N_u} z_j \tag{4.8}$$

$$z_j = \max_{k=1,2,\cdots,N_t-N} [((\mathbf{H}_2^j)^H \mathbf{H}_2^j + \rho_s \mathbf{I})^{-1}]_{kk} \tag{4.9}$$

  The parallel structure of this procedure is shown in Fig. 4.1. In the first phase, the matrix inversions in (4.9) are computed by the processing units (PU) of matrix inversion (Mi) in parallel, in which the fast K-SENIA-IU can be used instead of exact matrix inversion. Then in the second phase, the subset is chosen based on (4.8).

- Candidate list generation: Use (4.5) to obtain K residual observations $\mathbf{y}^k$, then instead of performing an exhaustive search in (4.6), V-BLAST-SIC is employed to obtain the estimates $\hat{\mathbf{x}}_2^k, k \in [1, 2, \ldots, K]$. As shown in Fig. 4.1, interference cancellations and V-BLAST-SIC are performed in parallel by PU of interference cancellation (IC) and PU of sub-detector (SUD) respectively. The number of parallel pipelines required is M^N. The inverse $(\mathbf{H}_2^H \mathbf{H}_2 + \rho_s \mathbf{I})^{-1}$ required by V-BLAST-SIC is already computed at the channel partition stage. Besides V-BLAST-SIC, other sub-optimal detection techniques can also serve as sub-detectors.

- Final decision: Based on the MED decision rule in (4.7), the Euclidean distances $\theta_k, k = [1, 2, \cdots, M^N]$ of all symbol vector candidates in the list are computed by the PU of Euclidean distance (ED), and the best candidate is chosen as the final decision.

The sufficient condition for the selection based list algorithm with DMS channel partition

and V-BLAST-SIC sub-detector to achieve optimal asymptotic diversity N_r is [25]

$$N = N_{min} = \lceil \sqrt{\frac{(N_r - N_t)^2}{4} + N_r} - \frac{(N_r - N_t)}{2} - 1 \rceil, \tag{4.10}$$

where $\lceil x \rceil$ denote the minimum integer no less than x. Table.4.1 presents the values of N_{min} in various system configurations (for $\alpha \leq 1$).

Table 4.1 Values of N_{min} in different system configurations

N_t \ N_r	32	64	96	128
16	1	1	1	1
32	5	1	1	1
64	N/A	7	1	1
96	N/A	N/A	9	3

4.2 Impact of Channel Hardening on Channel Partition and V-BLAST Ordering

Let $P_r(\mathrm{A})$ denotes the probability that event A occurs. Let P_e^{ML} denote the average frame error probability of MLD, defined by $P_e^{ML} = \mathbb{E}_{\mathbf{H},\mathbf{y}}[\Pr(\hat{\mathbf{s}}^{ML} \neq \mathbf{s}|\mathbf{H},\mathbf{y})]$, $P_{et} = \mathbb{E}_{\mathbf{H},\mathbf{y}}[\Pr(\hat{\mathbf{s}} \neq \mathbf{s}|\mathbf{H},\mathbf{y})]$ denote the average frame error probability of the selection based list algorithm and $P_{e2} = \mathbb{E}_{\mathbf{H}_2,\mathbf{y}^{k_1}}[\Pr(\hat{\mathbf{s}}_2^{k_1} \neq \mathbf{s}_2|\mathbf{H}_2,\mathbf{y}^{k_1})]$ denote the average sub-frame error probability of the sub-detector for the sub-system $[\mathbf{H}_2,\mathbf{y}^{k_1}]$, where $\mathbf{y}^{k_1}$ is the residual observation signal vector of (4.5) with the interference from $\mathbf{s}_1$ perfectly cancelled from $\mathbf{y}$, that is

$$\mathbf{y}^{k_1} = \mathbf{y} - \mathbf{H}_1\hat{\mathbf{s}}_1^{k_1}, \tag{4.11}$$

where $\hat{\mathbf{s}}_1^{k_1} = \mathbf{s}_1$, hence

$$\mathbf{y}^{k_1} = \mathbf{H}_2\mathbf{s}_2 + \mathbf{H}_1(\mathbf{s}_1 - \hat{\mathbf{s}}_1^{k_1}) + \mathbf{n} = \mathbf{H}_2\mathbf{s}_2 + \mathbf{n}. \tag{4.12}$$

P_{et} of selection based list detections is bounded by [25]

$$\max(P_e^{ML}, P_{e2}) \leq P_{et} \leq P_e^{ML} + P_{e2}, \tag{4.13}$$

From (4.13), we see that the lower and upper bounds of P_{et} are determined by P_e^{ML} and P_{e2}. P_e^{ML} is a fixed value and P_{e2} is determined by the performance of the sub-detector. Therefore, the performance of selection based list detection is determined by the performance of the sub-detector. For selection based list detection with OSIC sub-detection, the performance of such sub-detector is determined by two factors: channel partition scheme and ordering strategy. Next we consider, in LS-MIMO, how DMS channel partition and V-BLAST ordering are influenced by the channel hardening phenomenon.

The DMS and V-BLAST ordering rules both use the postprocessing SINR of MMSE [68] as a reliability measure of the symbol sub-datastreams. For the kth estimate of MMSE detection, the postprocessing SINR γ_k is [40, 69]

$$\gamma_k = \frac{\rho_s}{[(\mathbf{H}^H\mathbf{H} + \rho_s^{-1}\mathbf{I})^{-1}]_{kk}} - 1 = \frac{1}{1 - \mathbf{h}_k^H\mathbf{R}_y^{-1}\mathbf{h}_k} - 1, \tag{4.14}$$

where $\mathbf{R}_y = (\mathbf{H}\mathbf{H}^H + \rho_s^{-1}\mathbf{I})$ is the autocorrelation matrix of $\mathbf{y}$. The V-BLAST-SIC algorithm [66], at each layer, measures the reliabilities of the symbol sub-datastreams in the sense of postprocessing SINR, and detects the symbol sub-datastream with the strongest postprocessing SINR. Then, the interference from the detected symbol is cancelled from the received signal vector. Let $[\mathbf{A}]_k$ denote the kth row of $\mathbf{A}$, then the process of V-BLAST-SIC is given by the following pseudo code

Algorithm 2 V-BLAST-SIC

procedure $(\mathbf{H}, \mathbf{y})$
$\mathbf{B}^{(0)} = \mathbf{H}, \mathbf{y}^{(0)} = \mathbf{y}$
for $i = 1 \to N_t$ **do**
$\phi^i = \arg\min_{k=1,2,\cdots,N_t-i+1}[(\mathbf{W}^{-1})^{(i)}]_{kk}$ ▷ find the index of the sub-datastream with the strongest postprocessing SINR, where $(\mathbf{W}^{-1})^{(i)} = [(\mathbf{B}^{(i-1)})^H\mathbf{B}^{(i-1)} + \rho_s^{-1}\mathbf{I}]^{-1}$
$\mathbf{g}_{MMSE} = [(\mathbf{W}^{-1})^{(i)}]_{\phi^i}(\mathbf{B}^{i-1})^H$ ▷ compute the MMSE equalization vector
$\hat{\mathbf{s}}_{\phi^i} = \mathcal{Q}[\mathbf{g}_{MMSE}\mathbf{y}^{(i-1)}]$ ▷ detect ϕ^ith symbol
$\mathbf{y}^{(i)} = \mathbf{y}^{(i-1)} - \mathbf{h}_{\phi^i}\hat{\mathbf{s}}_{\phi^i}$ ▷ cancel the interference of the detected symbol from the received signal vector, where $\mathbf{h}_{\phi^i}$ is the ϕ^ith column of $\mathbf{B}^{(i-1)}$
update $\mathbf{B}^{(i)}$ by removing $\mathbf{b}_{\phi^i}$ from $\mathbf{B}^{(i-1)}$
end for
end procedure

A fast recursive implementation of V-BLAST-SIC can be found in [70]. In Algorithm 2, $(\mathbf{W}^{-1})^{(i)}$ denotes the Regularized Gram matrix inversion of the updated channel matrix $\mathbf{B}^{(i-1)}$ at the ith layer. Firstly, $(\mathbf{W}^{-1})^{(1)} = [(\mathbf{H}^H\mathbf{H} + \rho_s^{-1}\mathbf{I})]^{-1}$ is computed, then at ith $(i \geq 2)$ layer. $(\mathbf{W}^{-1})^{(i)}$ is updated from $(\mathbf{W}^{-1})^{(i-1)}$ instead of being recomputed from scratch, so that only one complete matrix inversion is required in V-BLAST-SIC. The complexity of this implementation scales as $\mathbb{O}((N_t)^3)$.

Both DMS and V-BLAST ordering are effective only if the measured reliabilities of the symbol sub-datastreams are highly diverse [67, 69]. However, in LS-MIMO, due to channel hardening of (2.11), the diagonal elements of $((\mathbf{H}_2^j)^H\mathbf{H}_2^j + \rho_s^{-1}\mathbf{I})^{-1}$ for all the possible $\mathbf{H}_2^j$ in (4.9) and $((\mathbf{B}^{(i)})^H\mathbf{B}^{(i)} + \rho_s^{-1}\mathbf{I})^{-1}$ at each layer of V-BLAST-SIC converge uniformly to constants, that is

$$\lim_{N_r,N_t\to\infty,\alpha\to 0}((\mathbf{H}_2^j)^H\mathbf{H}_2^j + \rho_s^{-1}\mathbf{I})^{-1} = \frac{1}{N_r + \rho_s^{-1}}\mathbf{I}_{N_t-N}, \tag{4.15}$$

$$\lim_{N_r,N_t\to\infty,\alpha\to 0}((\mathbf{B}^{(i)})^H\mathbf{B}^{(i)} + \rho_s^{-1}\mathbf{I})^{-1} = \frac{1}{N_r + \rho_s^{-1}}\mathbf{I}_{N_t-N-i}. \tag{4.16}$$

Therefore, with $N_r, N_t \to \infty, \alpha \to 0$, postprocessing SINR becomes less effective as a reliability measure, rendering DMS performs equally as channel independent selection (CIS) and V-BLAST ordering performs equally as random ordering.

4.3 Integration of K-SENIA/IU into Selection Based List Detection

Although DMS and V-BLAST ordering perform equally as CIS and random ordering asymptotically (i.e. $N_r, N_t \to \infty, \alpha \to 0$), when the size of the system is not extremely large, they are still effective for performance improvement. Large matrix inversion is heavily used in DMS channel partition stage, and the result is reused in the candidate list generation stage as $(\mathbf{W}^{-1})^{(1)}$ of V-BLAST-SIC, where the fast and highly accurate K-SENIA/IU can be exploited to replace exact matrix inversions. The advantages of using K-SENIA/IU are twofold. Firstly, as we analysed in chapter 3.1, the large processing latency of exact matrix inversion may causes a delay exceeding the channel coherence time, while K-SENIA/IU provides much lower latency and its hardware implementation is simpler and more energy efficient [32, 33]. Secondly, K-SENIA/IU only requires vector-wise and matrix-wise multiplications, which can be conveniently parallelized, meaning that a deeper parallelism can be obtain in each PU-Mi in Fig. 4.1.

4.4 BER Performance of Selection Based List Detections in Large-Scale MIMO

The general computer simulation setup is detailed in Appendix C. We consider the impact of channel hardening on selection based list detection by comparing different channel partition schemes (DMS and CIS), different matrix inversion schemes (exact matrix inversion (Ei) and K-SENIA-IU (Ai)) and different ordering strategies of SIC (V-BLAST-SIC and SIC without ordering). The schemes considered are CIS-Ai-SIC, CIS-Ai-VBLAST-SIC, DMS-Ai-SIC, DMS-Ai-VBLAST-SIC and DMS-Ei-VBLAST-SIC.

Fig. 4.2 presents the results for 128×32 and 128×96 4-QAM MIMO systems (i.e. system loading factor $\alpha = 0.25$ and 0.75), where the number of antenna selected at channel partition stage is $N = 1$, the number of iterations of K-SENIA is 3 and the initial size of

matrix inverse for IU N_{ini} is 16. It can be observed that for both configurations, DMS-Ai-VBLAST-SIC have almost indistinguishable performance from DMS-Ei-VBLAST-SIC and no error floor is observed in the BER $\geq 10^{-6}$. This demonstrates the suitability of the integration of K-SENIA-IU in selection based list detectors. Then, by comparing CIS-Ai-SIC and DMS-Ai-SIC, CIS-Ai-VBLAST-SIC and DMS-Ai-VBLAST-SIC, we can conclude that in LS-MIMO, when N is small, the channel partition scheme has a very small impact on performance. The ordering strategy, however, has a larger impact on performance. For example, in Fig. 4.2(a), CIS-Ai-VBLAST-SIC performs about 0.4dB better than CIS-Ai-SIC at BER$= 2.86 \times 10^{-6}$, in Fig. 4.2(b), the SNR gain achieved by CIS-Ai-VBLAST-SIC over CIS-Ai-SIC is about 1.1dB at BER$= 1.60 \times 10^{-5}$.

Therefore, hereinafter, we use CIS in selection based list detections, such that the considerable computational complexity required by the DMS of (4.8) and (4.9) (i.e., the computation of N_u matrix inversions) can be reduced with negligible performance loss.

Fig. 4.3 considers the effect of different N on the performance of CIS-Ai-SIC and CIS-Ai-VBLAST-SIC in a 128×96 4-QAM MIMO system. As we can observe, when the system size is large, for CIS-Ai-SIC and CIS-Ai-VBLAST-SIC, increasing $N = 1$ to $N = 2$ has a very small improvement on performance.

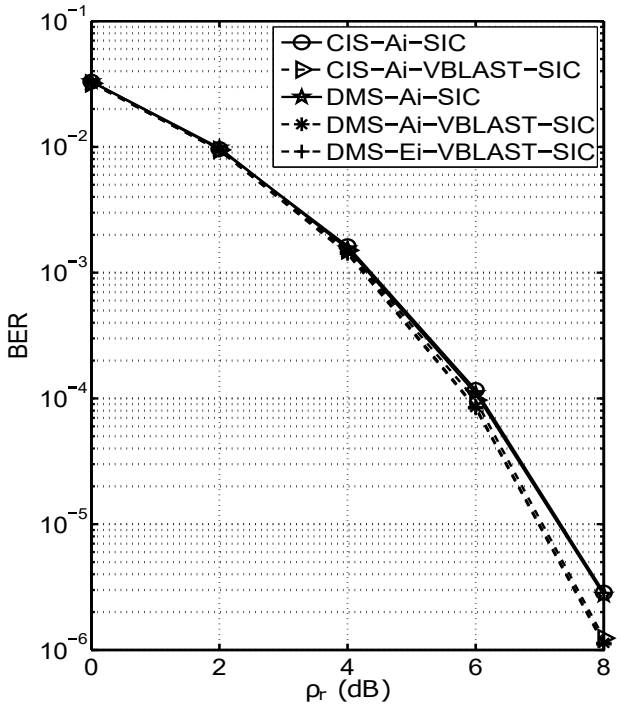

(a)

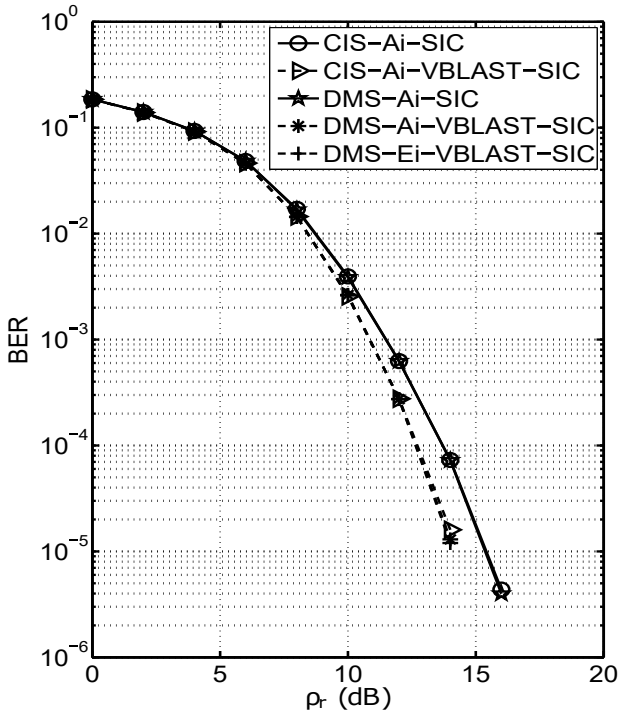

(b)

Fig. 4.2 BER performance of selection based list detections in (a) 128×32 MIMO and (b) 128×96 4-QAM MIMO systems with $N = 1$

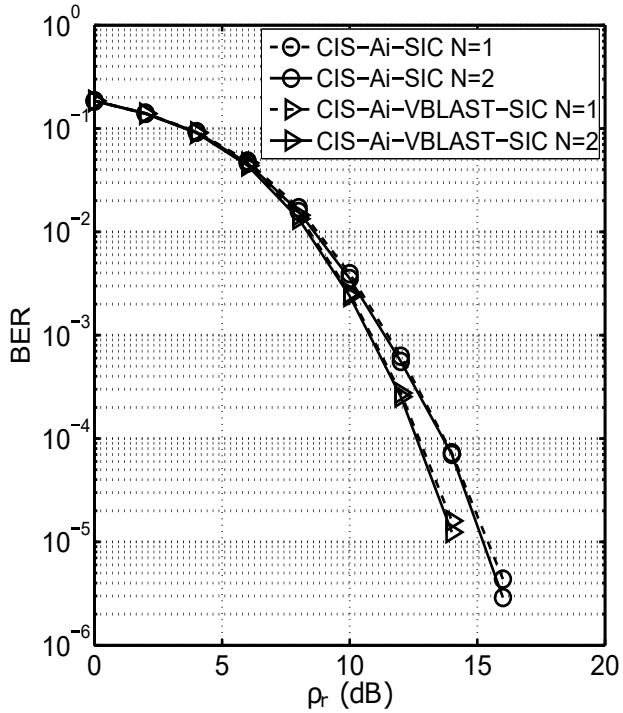

Fig. 4.3 BER performance of CIS-Ai-SIC/VBLAST-SIC with different N in a 128×96 4-QAM MIMO system

Chapter 5

Selection Based List detection with Improved OSIC Sub-detection

In this chapter, we first present a selection based list detection using an improved ordering scheme for SIC sub-detection. Simulation results demonstrate that in LS-MIMO systems it performs better than the selection based list detection with V-BLAST-SIC sub-detection. Furthermore, a comprehensive comparison including performance, complexity and structure are made between the proposed algorithm and the other two state-of-art LS-MIMO detection schemes, namely multistage LAS algorithm [12, 41] and MPD algorithm [19].

5.1 The Improved Ordering Scheme for SIC Sub-detectors

From chapter 4, we see that in LS-MIMO systems with selection based list detection, the ordering scheme used in sub-detectors affects performance more significantly than the channel partition strategy. We also see that V-BLAST ordering become less effective due to the channel hardening phenomenon. Therefore to improve performance we consider an improved ordering (IO) scheme based on the simplified Maximum a Posterior (MAP) based log-likelihood ratio reliability of the decision bit and approximate Gaussian distribution of MMSE soft estimate of $\tilde{\mathbf{s}} = \mathbf{G}_{MMSE}\mathbf{y}$ [40], namely Type-L reliability. For the modulation

schemes with multiple bits per symbol, Type-L reliability of the kth decision symbol is [40]

$$L_k = (1+\gamma_k)(|\Re(\tilde{\mathbf{s}}_k)| + |\Im(\tilde{\mathbf{s}}_k)|), \quad k = 1, 2, \cdots, N_t \tag{5.1}$$

and the use of (4.14) in (5.1) yields

$$L_k \triangleq \frac{|\Re(\tilde{\mathbf{s}}_k)| + |\Im(\tilde{\mathbf{s}}_k)|}{[(\mathbf{H}^H\mathbf{H} + \rho_s^{-1}\mathbf{I})^{-1}]_{kk}}, \quad k = 1, 2, \cdots, N_t \tag{5.2}$$

where $\Re(\cdot)$ and $\Im(\cdot)$ denote the real and imaginary parts. The Type-L reliability measure takes into account postprocessing SINR and the magnitude of $\tilde{\mathbf{s}}_k$, which reflect the channel variation and received signal vector respectively. In selection based list detectors, V-BLAST-SIC only considers the sub-matrix $\mathbf{H}_2$ that results in the same detection order for all the sub-detectors. The detection order with improved ordering SIC (IO-SIC) is also influenced by residual observations $\mathbf{y}^k$ of (4.5), and thus varies for different sub-detectors. Therefore, selection based list detection with IO-SIC as the sub-detector can provide more diverse candidate symbol vectors in the list. Type-L reliabilities are formed for the undetected symbol sub-datastreams, and the most reliable sub-datastream is selected to be quantized for hard decisions. Pseudo code Algorithm 3 summarizes the procedure employing IO-SIC.

We can see from Algorithm 3, at ith layer of IO-SIC, soft estimates of the undetected symbol sub-datastreams are required in order to evaluate their Type-L reliabilities, in which the computation of the estimate $(\mathbf{B}^{(i-1)})^H\mathbf{y}^{(i-1)}$ is a matrix-vector multiplication that has a complexity scales as $\mathbb{O}(N_r(N_t - i + 1))$. Next, we show that this estimate can be updated from the previous layer with lower complexity. To elaborate further, given the estimate at

Algorithm 3 IO-SIC

procedure $(\mathbf{H}, \mathbf{y})$
$\mathbf{B}^{(0)} = \mathbf{H}, \mathbf{y}^{(0)} = \mathbf{y}$
for $i = 1 \rightarrow N_t$ **do**
$\tilde{\mathbf{s}}^{(i)} = (\mathbf{W}^{-1})^{(i)}(\mathbf{B}^{(i-1)})^H \mathbf{y}^{(i-1)}$ ▷ Obtain the soft estimates of the undetected symbol sub-datastreams, where $(\mathbf{W}^{-1})^{(i)} = ((\mathbf{B}^{(i-1)})^H \mathbf{B}^{(i-1)} + \rho_s^{-1}\mathbf{I})^{-1}$
for $j = 1 \rightarrow N_t - i + 1$ **do**
$L_j = \frac{|\Re(\tilde{\mathbf{s}}_k^{(i)})| + |\Im(\tilde{\mathbf{s}}_k^{(i)})|}{[(\mathbf{W}^{(i)})^{-1}]_{kk}}$ ▷ compute Type-L reliabilities of undetected symbol sub-datastreams
end for
$\phi^i = \arg\max_{j=1,2,\cdots,N_t-i+1} L_j$ ▷ find the index of the most reliable sub-datastream
$\hat{\mathbf{s}}_{\phi^i} = \mathcal{Q}[\tilde{\mathbf{s}}_{\phi^i}^{(i)}]$ ▷ Quantize ϕ^ith component of $\tilde{\mathbf{s}}^{(i)}$
$\mathbf{y}^{(i)} = \mathbf{y}^{(i-1)} - \mathbf{h}_{\phi^i}\hat{\mathbf{s}}_{\phi^i}$ ▷ cancel the interference of the detected symbol from the received signal vector, where $\mathbf{h}_{\phi^i}$ is the ϕ^ith column of $\mathbf{H}$
update $\mathbf{B}^{(i)}$ by removing $\mathbf{h}_{\phi^i}$ from $\mathbf{B}^{(i-1)}$
end for
end procedure

the ith layer

$$[(\mathbf{B}^{(i-1)})^H \mathbf{y}^{(i-1)}] = \begin{bmatrix} \mathbf{h}_1^H \mathbf{y}^{(i-1)} \\ \mathbf{h}_2^H \mathbf{y}^{(i-1)} \\ \vdots \\ \mathbf{h}_{\phi^i}^H \mathbf{y}^{(i-1)} \\ \vdots \\ \mathbf{h}_{N_t-i+1}^H \mathbf{y}^{(i-1)}]^T \end{bmatrix} \tag{5.3}$$

where ϕ^i is the index of the most reliable sub-data stream that is chosen to be detected at

the ith layer. At the $i+1$ layer, using $\mathbf{y}^{(i)} = \mathbf{y}^{i-1} - \mathbf{h}_{\phi^i}\hat{\mathbf{s}}_{\phi^i}$, we have

$$(\mathbf{B}^{(i)})^H\mathbf{y}^{(i)} = \begin{bmatrix} \mathbf{h}_1^H\mathbf{y}^{(i)} \\ \mathbf{h}_2^H\mathbf{y}^{(i)} \\ \vdots \\ \mathbf{h}_{\phi^i-1}^H\mathbf{y}^{(i)} \\ \mathbf{h}_{\phi^i+1}^H\mathbf{y}^{(i)} \\ \vdots \\ \mathbf{h}_{N_t-i}^H\mathbf{y}^{(i)} \end{bmatrix} = \begin{bmatrix} \mathbf{h}_1^H\mathbf{y}^{(i-1)} \\ \mathbf{h}_2^H\mathbf{y}^{(i-1)} \\ \vdots \\ \mathbf{h}_{\phi^i-1}^H\mathbf{y}^{(i-1)} \\ \mathbf{h}_{\phi^i+1}^H\mathbf{y}^{(i-1)} \\ \vdots \\ \mathbf{h}_{N_t-i}^H\mathbf{y}^{(i-1)} \end{bmatrix} - \begin{bmatrix} \mathbf{h}_1^H\mathbf{h}_{\phi^i}\hat{\mathbf{s}}_{\phi^i} \\ \mathbf{h}_2^H\mathbf{h}_{\phi^i}\hat{\mathbf{s}}_{\phi^i} \\ \vdots \\ \mathbf{h}_{\phi^i-1}^H\mathbf{h}_{\phi^i}\hat{\mathbf{s}}_{\phi^i} \\ \mathbf{h}_{\phi^i+1}^H\mathbf{h}_{\phi^i}\hat{\mathbf{s}}_{\phi^i} \\ \vdots \\ \mathbf{h}_{N_t-i}^H\mathbf{h}_{\phi^i}\hat{\mathbf{s}}_{\phi^i} \end{bmatrix}. \tag{5.4}$$

The first term of (5.4) can be obtained from $(\mathbf{B}^{(i-1)})^H\mathbf{y}^{(i-1)}$ of (5.3), and $\mathbf{h}_k^H\mathbf{h}_{\phi^i}, k, \phi^i = 1, 2, \cdots, N_t$ in the second term are the components of $\mathbf{H}^H\mathbf{H}$ which are already obtained in computing $\mathbf{W} = \mathbf{H}^H\mathbf{H} + \rho_s^{-1}\mathbf{I}$. Hence there is no extra overhead required for obtaining the two terms in (5.4), and the only required complexity for computing $(\mathbf{B}^{(i)})^H\mathbf{y}^{(i)}$ is that of a vector subtraction, that scales as $\mathbb{O}(N_t - i)$. Similarly to the fast implementation of V-BLAST-SIC [70], in IO-SIC, only $(\mathbf{W}^{-1})^{(1)}$ at the first layer is required to be computed, and then $(\mathbf{W}^{-1})^{(i)}$ at $i \geq 2$ layers can be updated with low complexity. Notice that $(\mathbf{W}^{-1})^{(1)}$ can be approximated by K-SENIA/IU with low latency and simple hardware implementation.

5.2 BER Performance Comparison

Next we present the simulation results for BER performance of selection based list detection with CIS/DMS channel partition and IO-SIC sub-detection. The general setup of the computer simulations is detailed in Appendix C. For the first stage comparison, selection based list detection that uses V-BLAST-SIC sub-detection is considered. We also consider exact matrix inversion (Ei) as well as K-SENIA/IU (Ai) implementations, and hence the schemes considered for the first stage comparison are referred to as CIS-(Ei/Ai)-(IO/VBLAST)-SIC. For the second stage comparison, we consider (CIS/DMS)-IO-SIC and

the other two state-of-art LS-MIMO detection algorithms—multistage LAS and MPD.

In Fig. 5.1 we present BER results for LS-MIMO 4-QAM systems with fixed number of BS antennas $N_r = 128$ and varying number of single antenna users $N_t = 32, 64, 96$, corresponding to the system loading factors $\alpha = 0.25, 0.5, 0.75$. The number of antennas selected at the channel partition stage is $N = 1$, for K-SENIA-IU the number of iterations of K-SENIA is 3, and the initial size of the matrix inversion of IU is 16. It is observed that CIS-Ai-IO-SIC perform indistinguishable from CIS-Ei-IO-SIC at the BER$\geq 10^{-6}$ in all system configurations, demonstrating the effectiveness of K-SENIA-IU in selection based list detections with IO-SIC. Furthermore, in all the system configurations, CIS-Ei-IO-SIC outperforms CIS-Ei-VBLAST-SIC and the performance gain increases when the system loading factor increases. For example, in the 128×32 system at BER$= 1.14 \times 10^{-6}$ the performance gain achieved by CIS-Ei-IO-SIC over CIS-Ai-VBLAST-SIC is about 0.4dB, in the 128×64 system at BER$= 7.57 \times 10^{-6}$ CIS-Ei-IO-SIC is about 1dB better than CIS-Ai-VBLAST-SIC, and in the 128×96 system, CIS-Ei-IO-SIC achieves about 2.5dB SNR gain over CIS-Ai-VBLAST-SIC at BER$= 1.60 \times 10^{-5}$. The reason why the performance gain provided by selection based list detections with IO-SIC over that with V-BLAST-SIC improves in the higher loaded systems is because Type-L reliability measure converges to the optimum MAP-based reliability measure with increasing number of users [40]. These results reveal the attractiveness of selection based list detection with IO-SIC sub-detection for high loaded systems.

In Fig. 5.2 we present the results for DMS-IO-SIC with different number of antennas selected at channel partition stage ($N = 1, 2, 3$), multistage LAS algorithm—MMSE-3LAS, and MPD algorithm for a 32×32 4-QAM MIMO system. The reason we use DMS is that in medium size system, DMS is still more effective than CIS. It can be observed that all DMS-IO-SIC configurations outperform MMSE-3LAS. For example, at BER$= 1.05 \times 10^{-3}$, DMS-IO-SIC ($N = 1, 2, 3$) can achieve 0.4dB 0.65dB and 0.8dB SNR gain over MMSE-3LAS respectively. MPD is about 1.4dB worse than DMS-IO-SIC ($N = 3$) at BER$= 8.50 \times 10^{-5}$.

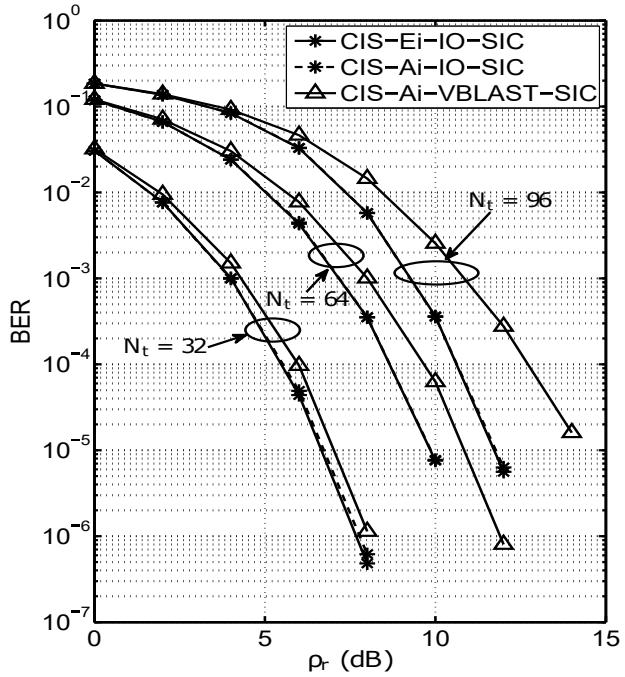

Fig. 5.1 BER performance of selection based list detection with improved ordering in $N_r = 128$, $N_t = 32, 64, 96$ 4-QAM MIMO systems with $N = 1$

Furthermore, in such medium size system, there is an observable performance improvement for DMS-IO-SIC when N increases. For example, at BER$= 2.46 \times 10^{-5}$, DMS-IO-SIC with $N = 3$ achieves about 0.7dB SNR gain over that of $N = 1$.

In Fig. 5.3 we present the results of CIS-IO-SIC ($N = 1, 2$) and MPD for $N_r = 128$ and $N_t = 32, 64, 96$ with 4-QAM. Firstly, for all the system configurations with BER$\geq 10^{-5}$, CIS-IO-SIC with $N = 1$ exhibits almost no performance loss compared with CIS-IO-SIC with $N = 2$ and the list size of the former one is only $\frac{1}{4}$ of the latter one. Then, as we can observe for all the system configurations considered, the performance loss of CIS-IO-SIC $N = 1, 2$ compared with MPD is just a fraction of dB. For example, in the 128×32 system, at BER$= 4.60 \times 10^{-5}$, CIS-IO-SIC is about 0.3dB worse than MPD, in the 128×64 system, MPD is about 0.25dB better than CIS-IO-SIC at BER$= 3.0 \times 10^{-5}$, and in the 128×96 system, at BER$= 2.0 \times 10^{-5}$, CIS-IO-SIC is about 0.4dB worse than MPD.

Therefore in large size systems, for the proposed algorithm, a small list size is enough to maintain a competitive performance.

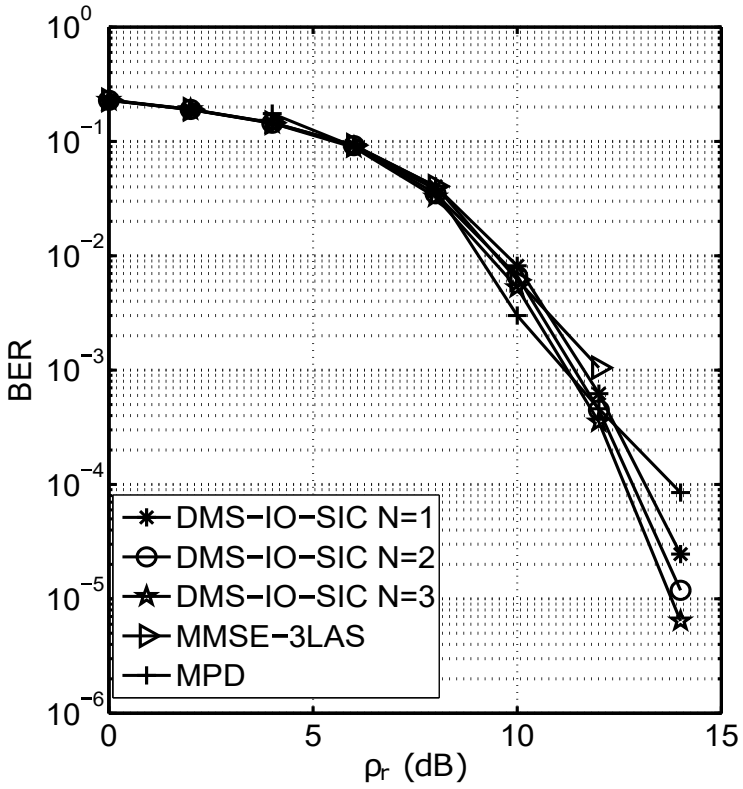

Fig. 5.2 BER performance comparison among DMS-IO-SIC, MMSE-3LAS and MPD (data for MMSE-3LAS and MPD collected from [41] and [19]) for a 32×32 4-QAM MIMO system

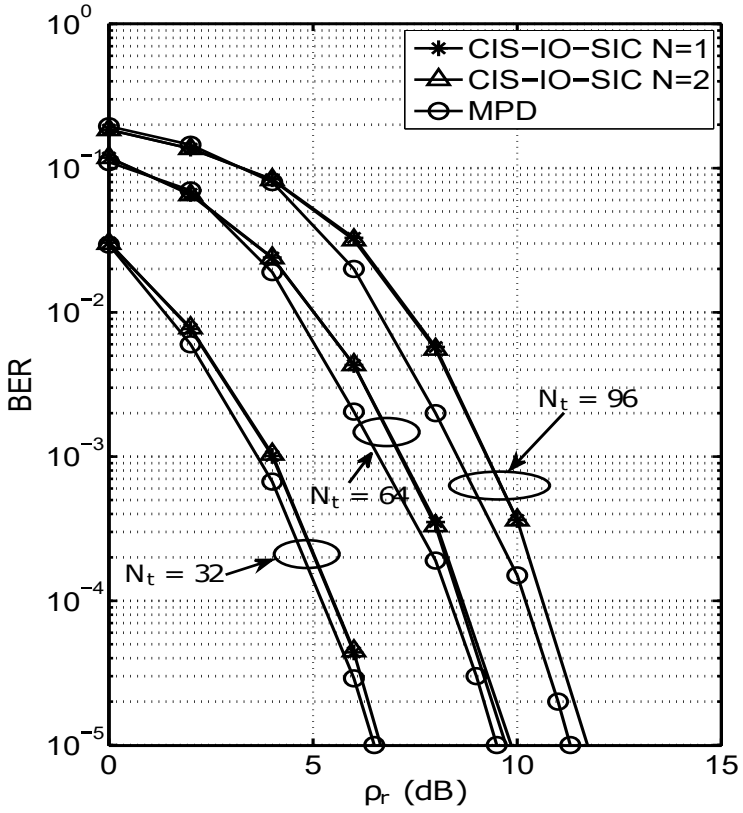

Fig. 5.3 BER performance comparison between CIS-IO-SIC and MPD (data for MPD collected from [19]) in $N_r = 128$, $N_t = 32, 64, 96$ 4-QAM MIMO systems

5.3 Complexity Analysis and Comparison

For selection based list detection, assume the number of antenna selected at the channel partition stage is N. At channel partition stage, if CIS is used, then there is no complexity overhead in this stage. At the candidate list generation stage, computation of each residual observation $\mathbf{y}^k$ in (4.5) for each sub-detector requires a complexity of order $\mathbb{O}(N_r N)$. Then consider each IO-SIC sub-detector. As seen in Algorithm 3, at the first layer, computation of $(\mathbf{W}^{-1})^{(1)}$ is required, where the use of exact matrix inversion requires a complexity of order $\mathbb{O}((N_t-N)^3)$ and the use of K-SENIA-IU, based on the analysis in chapter 3, requires a complexity of order $\mathbb{O}(N_r(N_t-N)^2)$. The computation of initial soft estimate $(\mathbf{B}^0)^H\mathbf{y}^0$ requires a complexity of order $\mathbb{O}(N_r(N_t-N))$. Then for the ith layer ($i \geq 2$), $(\mathbf{W}^{-1})^{(i)}$ can be updated based on the fast implementation of [70] , which has a complexity that scales as $\mathbb{O}((N_t-N-i+1)^2)$. The update of the soft estimate $(\mathbf{B}^{(i-1)})^H\mathbf{y}^{(i-1)}$ requires a complexity of order $\mathbb{O}(N_t-N-i+1)$, and obtaining $\tilde{\mathbf{s}}^{(i)}$ has a complexity of order $\mathbb{O}((N_t-N-i+1)^2)$. Finally the computation of the Type-L reliabilities has a complexity that scales as $\mathbb{O}(N_t-N-i+1)$, and the interference cancellation $\mathbf{y}^{(i)} = \mathbf{y}^{(i-1)} - \mathbf{h}_{\phi^i}\hat{\mathbf{s}}_{\phi^i}$ has a complexity of order $\mathbb{O}(N_r)$. Hence, the computational complexity of obtaining one candidate symbol vector in the list is of order

$$\mathbb{O}((N_t-N)^3) + \sum_{i=2}^{N_t-N}[\mathbb{O}((N_t-N-i+1)^2)] \triangleq \mathbb{O}((N_t-N)^3) \quad \text{For Ei,} \tag{5.5}$$

$$\mathbb{O}(N_r(N_t-N)^2) + \sum_{i=2}^{N_t-N}[\mathbb{O}((N_t-N-i+1)^2)] \triangleq \mathbb{O}(N_r(N_t-N)^2) \quad \text{For Ai,} \tag{5.6}$$

(the definition of the above addition operation is given by (3.36) in chapter 3). With the candidate list generation stage, where the list size is M^N, the overall complexity is of order $\mathbb{O}(M^N(N_t-N)^3)$ for Ei and $\mathbb{O}(M^N N_r(N_t-N)^2)$ for Ai. For the final decision step, notice that for each candidate, $\mathbf{y}^k - \mathbf{H}_2\hat{\mathbf{x}}_2^k$ in (4.7) is already computed in the SIC sub-detection, and thus only an Euclidean norm operation is required with a complexity of order $\mathbb{O}(N_r)$.

Hence the total complexity of this step is $\mathbb{O}(M^N N_r)$. In conclusion, the overall complexities of DMS-(Ei/Ai)-IO-SIC is of order $\mathbb{O}(M^N(N_t-N)^3)$ and $\mathbb{O}(M^N N_r(N_t-N)^2)$ respectively.

Consider the multistage LAS algorithm, which updates an initial solution iteratively that aims at increasing the likelihood function until a certain stopping criterion is satisfied [12,41]. The complexity of MMSE-3LAS algorithm comprises of two parts—the generation of the initial solution by MMSE detector and the multistage LAS updating process. The generation of MMSE initial solution $\hat{\mathbf{s}}^{(0)}$ requires a complexity that scales as $\mathbb{O}(N_r N_t^2)$ [12]. Then we consider the complexity required by multistage LAS updating process, in [12], it is shown by simulation that the average number of stages required is of order $\mathbb{O}(N_t)$, with a complexity of order $\mathbb{O}(N_t)$ for each stage. Hence, the empirical complexity of multistage LAS searching process based on simulation, is of order $\mathbb{O}(N_t^2)$. Therefore, the overall complexity of MMSE-3LAS algorithm, which comprises of obtaining initial solution by MMSE detection ($\mathbb{O}(N_r N_t^2)$) and multistage LAS updating process ($\mathbb{O}(N_t^2)$), scales as $\mathbb{O}(N_r N_t^2)$. A more detailed description of MMSE-3LAS algorithm is presented in the next section.

MPD is a belief propagation based iterative algorithm that works with a fully connected graphical model and updates all the sub-datastreams iteratively, a process called massage passing. The complexity of MPD algorithm comprises of two parts—the establishment of the graphical model and the message passing process. Firstly, the establishment of the graphical model requires the computation of $\mathbf{H}^H\mathbf{y}$ and $\mathbf{H}^H\mathbf{H}$, with complexities that scale as $\mathbb{O}(N_r N_t)$ and $\mathbb{O}(N_r N_t^2)$ respectively. Then for the message passing process with square M-QAM constellations, each iteration has a complexity of order $\mathbb{O}(\sqrt{M}N_t^2)$. Hence, the complexity of the message passing process with n_I iterations is of order $\mathbb{O}(n_I\sqrt{M}N_t^2)$. Therefore the overall complexity of the MPD algorithm, which constitutes the establishment of graphical model ($\mathbb{O}(N_r N_t^2)$) and massage passing process ($\mathbb{O}(n_I\sqrt{M}N_t^2)$), scales as $\mathbb{O}((N_r + n_I\sqrt{M})N_t^2)$. Since $n_I\sqrt{M}$ is close to N_r [19], the overall complexity after simplification is of order $\mathbb{O}(N_r N_t^2)$. A more detailed description of MPD algorithm is presented

in the next section.

5.4 Structural Issues

From the analysis above, CIS-(Ei/Ai)-IO-SIC, MMSE-3LAS and MPD algorithms have complexities that scale as $\mathbb{O}(M^N(N_t-N)^3)$ or $\mathbb{O}(M^N N_r(N_t-N)^2)$, $\mathbb{O}(N_r N_t^2)$ and $\mathbb{O}(N_r N_t^2)$ respectively. When N is small, their complexities are comparable with that of MMSE detection ($\mathbb{O}(N_r N_t^2)$). Besides, neither multistage LAS and MPD algorithms possess the same massive parallelism feature as selection based list detection. Next we provide analysis of the structures of multistage LAS and MPD algorithms.

Consider MMSE-3LAS, which is a trajectory searching algorithm that increases a likelihood function by updating the solution sequentially. The likelihood function $c(\hat{\mathbf{s}}^{(n)})$ is defined based on MED rule of (4.1), where $\hat{\mathbf{s}}^{(n)}$ denotes the solution at nth stage in LAS searching process,

$$c(\hat{\mathbf{s}}^{(n)}) = \mathbf{y}^H\mathbf{H}\hat{\mathbf{s}}^{(n)} + (\hat{\mathbf{s}}^{(n)})^H\mathbf{H}^H\mathbf{y} - (\hat{\mathbf{s}}^{(n)})^H\mathbf{H}^H\mathbf{H}\hat{\mathbf{s}}^{(n)}. \tag{5.7}$$

The procedure of MMSE-3LAS algorithm is shown in Fig. 5.4. Firstly, the initial solution $\hat{\mathbf{s}}^{(0)}$ is obtained by MMSE detection. Then MMSE-3LAS considers a set of LAS search stages, which increase the likelihood function monotonically (monotonic likelihood ascend) by updating $\hat{\mathbf{s}}^{(n)}$. In MMSE-3LAS, each LAS search stage constitutes 3 sub-stages and only the first sub-stage has more than 1 iteration (in order to control the complexity). In the first sub-stage, 1-coordinate neighbourhood update to $\hat{\mathbf{s}}^{(n)}$ (i.e. 1 component in the symbol vector $\hat{\mathbf{s}}^{(n)}$ is updated) is performed iteratively, until the local optimum of $\hat{\mathbf{s}}^{(n)}$ is reached (i.e. until the 1-coordinate update of $\hat{\mathbf{s}}^{(n)}$ can not increase the likelihood function any more). Then the second sub-stage starts, with a 2-coordinate neighbourhood update performed to $\hat{\mathbf{s}}^{(n)}$. If the likelihood function is increased by this operation, the algorithm starts the next stage by going back to 1-coordinate update. If the likelihood function

can not be increased by this operation, then the algorithm starts the third sub-stage. In the third sub-stage, a 3-coordinate neighbourhood update is performed. If the likelihood function is increased, then the algorithm initialize a new stage with 1-coordinate update, or the algorithm terminates. We can conclude that multistage LAS algorithm works as a sequence of LAS search stages. Each stage contains a set of sub-stages with one or more iterations that also works sequentially. In [12], it is shown that based on simulations, the average number of stages required scales linearly with N_t ($\mathbb{O}(N_t)$), that may induce a large processing latency. Therefore, multistage LAS algorithm is not feasible for parallel implementations.

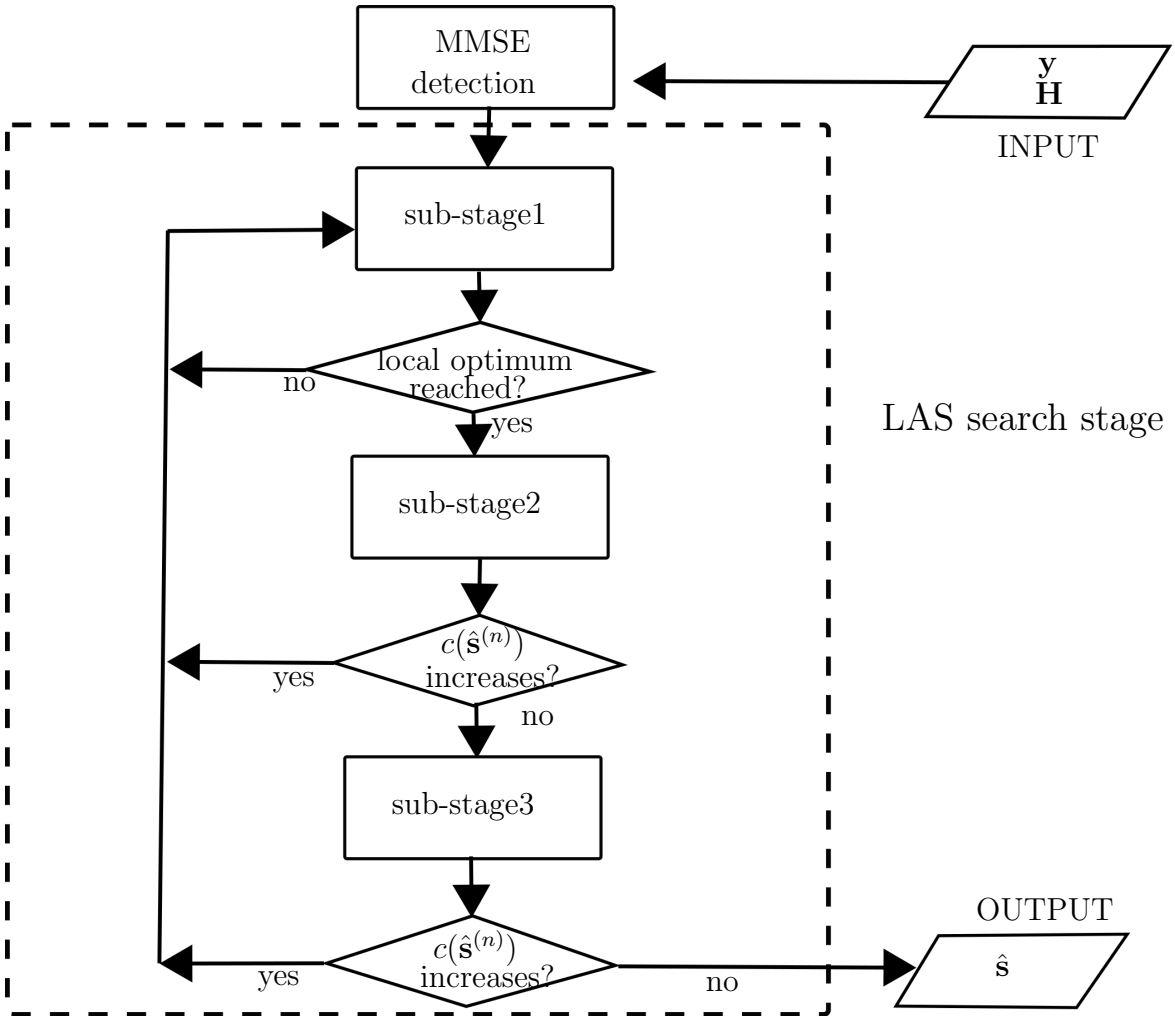

Fig. 5.4 Flowchart of MMSE-3LAS algorithm

Consider MPD, which is based on belief propagation (BP) that works with a fully connected graphical model and updates all the sub-data streams by message passing. First calculate

$$\mathbf{H}^H\mathbf{y} = \mathbf{H}^H\mathbf{H}\mathbf{s} + \mathbf{H}^H\mathbf{n}, \tag{5.8}$$

then we modify (5.8) as

$$\mathbf{z} = \mathbf{J}\mathbf{s} + \mathbf{v}, \tag{5.9}$$

where $\mathbf{z} = \frac{\mathbf{H}^H\mathbf{y}}{N_r}$, $\mathbf{J} = \frac{\mathbf{H}^H\mathbf{H}}{N_r}$ and $\mathbf{v} = \frac{\mathbf{H}^H\mathbf{n}}{N_r}$. The ith component of $\mathbf{z}$ is given by

$$\mathbf{z}_i = [\mathbf{J}]_{ii}\mathbf{s}_i + \sum_{j=1,j\neq i}^{N_t} [\mathbf{J}]_{ij}\mathbf{s}_j + \mathbf{v}_i, \tag{5.10}$$

where $\mathbf{v}_i = \sum_{j=1}^{N_r} \frac{[\mathbf{H}^*]_{ji}\mathbf{n}_j}{N_r}$. Based on the central limit theorem, for large N_r, $\mathbf{v}_i \sim \mathbb{C}\mathcal{N}(0, \frac{\sigma_o^2}{N_r})$ [19]. Define $\sigma_v^2 = \frac{\sigma_o^2}{N_r}$. Denote the interference plus noise term $g_i = \sum_{j=1,j\neq i}^{N_t}[\mathbf{J}]_{ij}\mathbf{s}_j + \mathbf{v}_i$. When N_r, N_t are large, based on the central limit theorem, the distribution of g_i can be approximated as $\mathbb{C}\mathcal{N}(u_i, \sigma_i^2)$ with [19]

$$u_i = \sum_{j=1,j\neq i}^{N_t} [\mathbf{J}]_{ij}\mathbb{E}(s_j), \tag{5.11}$$

$$\sigma_i^2 = \sum_{j=1,j\neq i}^{N_t} [\mathbf{J}]_{ij}^2 Var(\mathbf{s}_j) + \sigma_v^2. \tag{5.12}$$

Let $P_i(b), i = 1, 2, \cdots, N_t$ denote the probability of the sub-date stream $\mathbf{s}_i$ being symbol $b \in \mathbb{A}$ (e.g. for 4-QAM constellation, $b \in \{-1-\imath, -1+\imath, 1-\imath, 1+\imath\}$). Computations of $\mathbb{E}(s_j)$ and $Var(\mathbf{s}_j)$ in (5.11) and (5.12) require the knowledge of $P_j(b)$. Then based on the Gaussian approximation of g_i, the a posterior probability (APP) of $\mathbf{s}_i$ being b can be computed by [19]

$$P_i(b) = Pr(\mathbf{s}_i = b|\mathbf{z}_i) \propto exp(-\frac{1}{2\sigma_i^2}(\mathbf{z}_i - [\mathbf{J}]_{ii}b - u_i)^2). \tag{5.13}$$

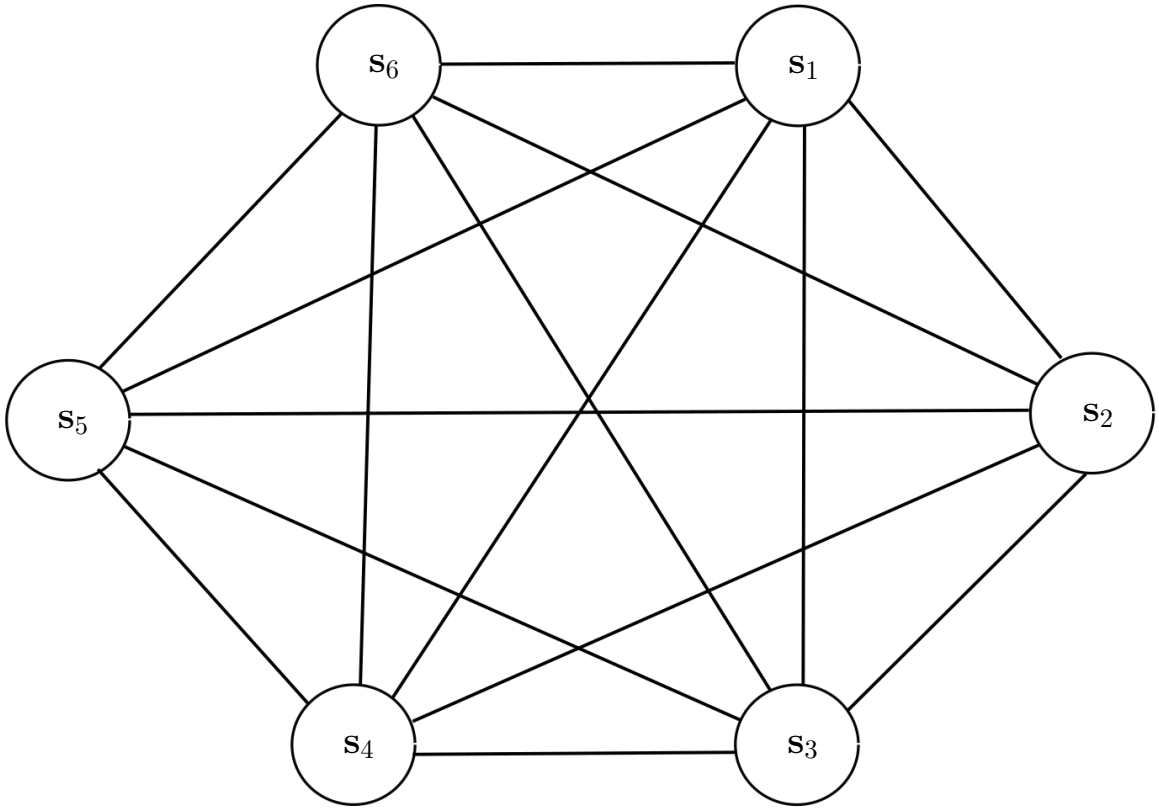

Fig. 5.5 Fully connected graph of MPD with $N_t = 6$

Each sub-datastream is modelled as a node in a fully connected graph, hence there are N_t nodes. Fig. 5.5 shows an example of the fully connected graph with $N_t = 6$. The computation of $P_i(b)$ in (5.13) requires the $P_j(b)$ from the other nodes (in order to compute $\mathbb{E}(\mathbf{s}_j)$ and $Var(\mathbf{s}_j)$ in (5.11) and (5.12)). Therefore, APP information of the possible symbols for each sub-data stream is exchanged and updated among the nodes iteratively such that improving the reliability of the solution. This process is called message passing. This message passing process is carried out for a certain number of iterations N_I, whose procedure is summarized by the following pseudo code, where $P_i^{(t)}(b)$ denotes $P_i(b)$ in the tth iteration.

As we can observe from Algorithm 4, in each iteration, the APP information (messages) at all the nodes can be updated simultaneously using the messages from the previous iteration. Hence the MPD algorithm in [19] can be classified as a synchronous BP [71], where the update of messages at each iteration can be naturally parallelized. Alternatively,

Algorithm 4 Message Passing

procedure $(\mathbf{J}, \mathbf{z})$
$P_i^{(0)}(b) = \frac{1}{M}, b \in \mathbb{A}, |\mathbb{A}| = M$ and $i = 1, 2, \cdots, N_t$ ▷ initialize APP information in each node
for $t = 1 \rightarrow N_I$ **do**
for $i = 1 \rightarrow N_t$ **do**
compute $\mathbb{E}(\mathbf{s}_j)$ and $Var(\mathbf{s}_j)$ in (5.11) and (5.12) using APP information $P_j^{(t-1)}(\mathbf{s}_j)$ from the other sub-data streams
compute u_i using (5.11)
compute σ_i^2 using (5.12)
update $P_i^{(t)}(b)$ using (5.13)
end for
end for
end procedure

asynchronous BP can be considered, where the messages of nodes are updated sequentially using the most recent updated messages in a certain order. Although synchronous BP has a parallel structure for each iteration, its efficiency is low. Since not all the updates contributes to the convergence of the algorithm and hence compared with asynchronous BP, synchronous BP has longer processing latency (number of iterations), more computational cost and higher memory consumption (for the storage of the updated messages from the previous iteration). In order to accelerate the convergence speed of synchronous BP, damping method [72] and Aitken acceleration technique [73] can be applied. Asynchronous BP uses various scheduling techniques (i.e. determine the order of the messages to be updated in each iteration) to improve the efficiency of the message passing process. For example, BP with wildfire scheduling avoids repeated updates of the nodes that have already converged [74]. Residual BP algorithm updates the nodes that will exhibit largest change with high priority [75]. Besides, asynchronous BP can be parallelized by partitioning the graphical model into separate collections of nodes and performing scheduling and updates independently [76], rendering lower processing latency. However, the advantage of asynchronous BP is not obtained with no cost. Scheduling requires more computational operations in each iteration [74–76]. Since in asynchronous BP, the messages are updated

in-place, synchronization techniques are required to avoid the read-write conflict at the same node [71]. In addition, although it is shown experimentally that MPD gives good performances in LS-MIMO systems, whose graphical models are fully connected (loopy graphs). As indicated in [77, 78], the convergence of BP in such loopy graphs is not guaranteed.

In conclusion, selection based list detection works in parallel to generate a list of solution candidates, while multistage LAS and MPD (synchronous and asynchronous) algorithms both improve the reliability of the solution sequentially. Compared with selection based list detection, the MPD algorithms can only achieve parallelism in each iteration, with higher implementation difficulties. This demonstrates the structural advantage of selection based list detection over multistage LAS and MPD algorithms.

Chapter 6

Conclusion

In this thesis, we first proposed a novel approximate matrix inversion scheme—K-SENIA, that can converge faster (exponential with iteration times) than the conventional L-term SE approximation (linear with number of expansion terms). We combined K-SENIA and matrix inversion inflate update (IU) that relax its convergence constraint, making it suitable for high loaded systems. We showed that the complexities of the proposed approximate matrix inversion schemes ($\mathbb{O}(N_t^3)$ for K-SENIA and $\mathbb{O}(N_r N_t^2)$ for K-SENIA-IU) are comparable with that of exact matrix inversion schemes ($\mathbb{O}(N_t^3)$), while the processing latency of the former ones ($\mathbb{O}(\log(N_t))$) is much lower than the latter one ($\mathbb{O}(N_t)$). In addition, K-SENIA/IU possess the advantages for more economical hardware implementation and higher energy efficiency over the exact matrix inversion schemes, making it suitable for practical applications.

To assess the performance of K-SENIA/IU in LS-MIMO detection, we first considered its application for linear MMSE detection. Simulation results show the superior performance of K-SENIA/IU compared with L-term SE approximation when they are applied to MMSE detection. We analysed the error floor problem in MMSE detection with K-SENIA/IU and further propose an alternative hybrid MMSE detector to reduce the error floor based on our statistical analysis of MIMO channel orthogonality. Simulation results reveal the

effectiveness of this hybrid MMSE detector to reduce the error floor at high SNR region. K-SENIA/IU is suitable for integration into selection based list detectors for lower latency and deeper parallelism.

Then we considered the application of K-SENIA/IU for selection based list detection in LS-MIMO systems. By studying the impacts of the channel hardening phenomenon on selection based list detection, we found that when the size of the system increases, the postprocessing SINR based DMS channel partition rule and V-BLAST ordering become less effective. Simulation results show that DMS performs almost equally as CIS in LS-MIMO systems, indicating that DMS can be replaced by CIS with negligible performance loss and significant complexity reduction. It is also shown that in LS-MIMO the ordering strategy has a larger impact on performance than the channel partition strategy. Based on these findings, we considered an improved ordering scheme for SIC sub-detection, that takes into account both postprocessing SINR and received signal vector, rendering higher diversity of the solution candidates list. Simulation results corroborate that a significant performance gain can be achieved by the selection based list detection with improved ordering-SIC over the selection based list algorithm with V-BLAST-SIC in different system configurations.

This thesis also provides a comprehensive comparison between the selection based list algorithm employing improved ordering with two state-of-art LS-MIMO detection techniques, multistage LAS and MPD algorithms. Simulation results show that our selection based list algorithm with improved ordering performs better than multistage LAS and MPD algorithms in a medium size system (32×32), and exhibits only a fraction of dB performance degradation with respect to the MPD algorithm in large size systems ($128 \times 32, 64, 96$). We also considered the effect of different numbers of antennas (N) selected at the channel partition stage. In a medium size system (32×32), for DMS-IO-SIC, increasing N from 1 to 3 results in an observable performance improvement. While in large size systems $N_r = 128, N_t = 32, 64, 96$, where DMS can be replaced by CIS with negligible performance loss and substantial complexity reduction, N can be chosen as 1 with almost no perfor-

mance loss and hence lower complexity compared with $N = 2$. The complexity of the proposed selection based list detection, multistage LAS and MPD are in the same order of magnitude. Besides BER performance and complexity, we also took a close look at the structures of multistage LAS and MPD algorithms. It was found that both multistage LAS and MPD algorithms improve the quality of the solution using a sequential structure, while selection based list algorithm can generate a list of solution candidates in parallel. Compared with selection based list detection, MPD algorithm can only achieve parallelism in each iteration, with higher implementation difficulties. This demonstrates that selection based list detection has the structural advantage of massive parallelism over multistage LAS and MPD algorithms. Therefore, from the comparisons of BER performance, complexity and structure, we can claim that the proposed selection based list algorithm is a competitive candidate for LS-MIMO detection, allowing for a parallel implementation without sacrificing any significant performance.

Appendix A

Residual Estimation Error Analysis of MMSE-SENIA

Given

$$\epsilon = \mathbb{E}(||\hat{\mathbf{s}}^{MMSE} - \hat{\mathbf{s}}^{MMSE-SENIA}||^2) = \mathbb{E}(||(\mathbf{D}^{-1}\mathbf{E})^{2^{k+1}}\mathbf{W}^{-1}\mathbf{H}^H\mathbf{y}||^2), \tag{A.1}$$

let $\mathbf{F} = (\mathbf{D}^{-1}\mathbf{E})^{2^{k+1}}$, $\mathbf{G} = \mathbf{W}^{-1}\mathbf{H}^H$, and $Tr(\mathbf{X})$ denote the trace of matrix $\mathbf{X}$. Then (A.1) can be rewritten as

$$\epsilon = \mathbb{E}(||\mathbf{FGy}||^2) = \mathbb{E}[Tr(\mathbf{FGyy}^H\mathbf{G}^H\mathbf{F}^H)] = Tr\{\mathbb{E}(\mathbf{FGyy}^H\mathbf{G}^H\mathbf{F}^H)\}, \tag{A.2}$$

then the use of $\mathbf{y} = \mathbf{Hs} + \mathbf{n}$ in (A.2) yields

$$\begin{aligned}
\epsilon &= Tr\{\mathbb{E}[\mathbf{FG}(\mathbf{Hs}+\mathbf{n})(\mathbf{s}^H\mathbf{H}^H + \mathbf{n}^H)\mathbf{G}^H\mathbf{F}^H]\} \\
&= Tr\{\mathbb{E}[\mathbf{FGHss}^H(\mathbf{FGH})^H] + \mathbb{E}[\mathbf{FGnn}^H(\mathbf{FG})^H] + \mathbb{E}[\mathbf{FGHsn}^H(\mathbf{FG})^H] \\
&+ \mathbb{E}[\mathbf{FGns}^H(\mathbf{FGH})^H]\},
\end{aligned} \tag{A.3}$$

since $\mathbf{s}$ and $\mathbf{n}$ are independent, and $\mathbf{F}, \mathbf{G}, \mathbf{H}$ are independent of $\mathbf{s}$ and $\mathbf{n}$, we have

$$\begin{aligned} \epsilon &= Tr\{\mathbb{E}[\mathbf{FGH}\mathbb{E}[\mathbf{ss}^H](\mathbf{FGH})^H] + \mathbb{E}[\mathbf{FG}\mathbb{E}[\mathbf{nn}^H](\mathbf{FG})^H] \\ &+ \mathbb{E}[\mathbf{FGH}\mathbb{E}[\mathbf{sn}^H](\mathbf{FG})^H] + \mathbb{E}[\mathbf{FG}\mathbb{E}[\mathbf{ns}^H](\mathbf{FGH})^H]\}, \end{aligned} \tag{A.4}$$

where $\mathbb{E}[\mathbf{ss}^H] = E_s\mathbf{I}_{N_t}$ and $\mathbb{E}[\mathbf{nn}^H] = \sigma_o^2\mathbf{I}_{N_r}$. Furthermore $\mathbf{s}$ and $\mathbf{n}$ have zero mean components, thus $\mathbb{E}[\mathbf{sn}^H] = \mathbb{E}[\mathbf{s}]\mathbb{E}[\mathbf{n}^H] = \mathbf{0}_{N_t \times N_r}$ and $\mathbb{E}[\mathbf{ns}^H] = \mathbb{E}[\mathbf{n}]\mathbb{E}[\mathbf{s}^H] = \mathbf{0}_{N_r \times N_t}$, where $\mathbf{0}$ denotes the zero matrix. Hence the last two terms of (A.4) are 0, and

$$\begin{aligned} \epsilon &= Tr\{\mathbb{E}[\mathbf{FGH}E_s\mathbf{I}_{N_t}(\mathbf{FGH})^H] + \mathbb{E}[\mathbf{FG}\sigma_o^2\mathbf{I}_{N_r}(\mathbf{FG})^H]\} \\ &= Tr\{E_s\mathbb{E}[\mathbf{FGHH}^H\mathbf{G}^H\mathbf{F}^H] + \sigma_o^2\mathbb{E}[\mathbf{FGG}^H\mathbf{F}^H]\} \\ &= E_sTr\{\mathbb{E}[\mathbf{FGHH}^H\mathbf{G}^H\mathbf{F}^H] + \rho_s^{-1}\mathbb{E}[\mathbf{FGG}^H\mathbf{F}^H]\} \end{aligned} \tag{A.5}$$

At high SNR region ($\rho_s \to \infty$), the second term of (A.5) vanishes, and (A.5) can be rewritten as

$$\lim_{\rho_s \to \infty} \epsilon = E_sTr\{\mathbb{E}[\mathbf{FGHH}^H\mathbf{G}^H\mathbf{F}^H]\}, \tag{A.6}$$

Furthermore, since $\lim_{\rho_s\to\infty}\mathbf{G} = \lim_{\rho_s\to\infty}\mathbf{W}^{-1}\mathbf{H}^H = \lim_{\rho_s\to\infty}(\mathbf{H}^H\mathbf{H} + \rho_s^{-1}\mathbf{I})^{-1}\mathbf{H}^H = (\mathbf{H}^H\mathbf{H})^{-1}\mathbf{H}^H$, (A.6) can be rewritten as

$$\lim_{\rho_s \to \infty} \epsilon = E_s\mathbb{E}\{Tr[\mathbf{FF}^H]\} = E_s\mathbb{E}[||\mathbf{F}||_F^2] = E_s\mathbb{E}[||(\mathbf{D}^{-1}\mathbf{E})^{2^{k+1}}||_F^2], \tag{A.7}$$

where $||\cdot||_F$ denotes Frobenius norm.

Appendix B

Distribution of OM

B.1 Exact Distribution of OM

Let

$$Y = -\ln(\breve{\phi}) = \sum_{i=1}^{N_t-1} Y_i \tag{B.1}$$

where $Y_i = -\ln(\tilde{\eta}_i), \quad i = 1, 2, \ldots, N_t - 1$. The characteristic function (c.f.) of random variable Y_i, denoted by $\varphi_{Y_i}(t)$, is given by

$$\begin{aligned} \varphi_{Y_i}(t) &= \mathbb{E}[\exp(\imath t Y_i)] \\ &= \mathbb{E}[\tilde{\eta}_i^{-\imath t}] \\ &= \frac{1}{\mathbb{B}(\tilde{k}_1^i, \tilde{k}_2^i)} \int_0^1 x^{\tilde{k}_1^i - \imath t - 1}(1-x)^{\tilde{k}_2^i - 1} dx \end{aligned} \tag{B.2}$$

where $\mathbb{B}(x, y)$ denotes beta function with parameters x and y

$$\mathbb{B}(x, y) = \int_0^1 t^{x-1}(1-t)^{y-1} dt, \tag{B.3}$$

$$= \frac{\Gamma(x)\Gamma(y)}{\Gamma(x+y)}. \tag{B.4}$$

Then the use of (B.3) and (B.4) in (B.2) yields

$$\begin{aligned}\varphi_{Y_i}(t) &= \frac{\mathbb{B}(\tilde{k}_1^i - \imath t, \tilde{k}_2^i)}{\mathbb{B}(\tilde{k}_1^i, \tilde{k}_2^i)} \\ &= \frac{\Gamma(\tilde{k}_1^i + \tilde{k}_2^i)\Gamma(\tilde{k}_1^i - \imath t)}{\Gamma(\tilde{k}_1^i)\Gamma(\tilde{k}_1^i + \tilde{k}_2^i - \imath t)}.\end{aligned} \tag{B.5}$$

Since all the Y_i are independent and have different parameters, the c.f. of Y is given by

$$\begin{aligned}\varphi_Y(t) &= \prod_{i=1}^{N_t-1} \varphi_{Y_i}(t), \\ &= \prod_{i=1}^{N_t-1} \frac{\Gamma(\tilde{k}_1^i + \tilde{k}_2^i)\Gamma(\tilde{k}_1^i - \imath t)}{\Gamma(\tilde{k}_1^i)\Gamma(\tilde{k}_1^i + \tilde{k}_2^i - \imath t)}.\end{aligned} \tag{B.6}$$

Let $x \in \mathbb{C}$, $k \in \mathbb{N}^+$ and $\Re(x) > 0$, we can write [79]

$$\frac{\Gamma(x+k)}{\Gamma(x)} = \prod_{l=0}^{k-1}(x+l), \tag{B.7}$$

then the use of (B.7) in (B.6) yields

$$\varphi_Y(t) = \prod_{i=1}^{N_t-1} \prod_{l_i=0}^{\tilde{k}_2^i-1} (\tilde{k}_1^i + l_i)(\tilde{k}_1^i + l_i - \imath t)^{-1}, \tag{B.8}$$

consider a random variable $Z \sim Gamma(k, \lambda^{-1})$, with shape parameter k and rate parameter λ. Then c.f. of Z is given by

$$\varphi_Z(t) = \lambda^k(\lambda - \imath t)^{-k}. \tag{B.9}$$

It is observed from (B.8) that $\varphi_Y(t)$ is the c.f. of the sum of $K = \sum_{i=1}^{N_t-1} \tilde{k}_2^i = \sum_{i=1}^{N_t-1} i = \frac{N_t(N_t-1)}{2}$ independent gamma random variables $G_m \sim Gamma(1, \gamma_m^{-1})$, where the rate pa-

rameters γ_m is given by

$$\begin{aligned} \gamma_m &= \tilde{k}_1^i + l_i, && \text{(B.10)} \\ l_i &= \tilde{k}_2^i - 1, \tilde{k}_2^i - 2, \ldots, 1, 0 && \text{(B.11)} \\ i &= 1, 2, \ldots, N_t - 1, && \text{(B.12)} \\ m &= \sum_{s=1}^{i-1} \tilde{k}_2^s + l_i, && \text{(B.13)} \\ m &= 0, 1, 2, \ldots, K - 1, && \text{(B.14)} \end{aligned}$$

Hence Y has a Generalized Integer Gamma (GIG) distribution [63], which is characterized by three parameters: depth, shape parameters and rate parameters.

Next we briefly introduce the definition of the GIG distribution. Let $Z = \sum_{i=1}^{p} Z_i$, where $Z_i \sim Gamma(r_i, \lambda_i^{-1})$ are independent, with all the shape parameters r_i integers and rate parameters λ_i. If each of the rate parameter λ_i has a distinct value, then Z is GIG distributed with depth p, shape parameters $\{r_i\}_{i=1:p}$ and rate parameters $\{\lambda_i\}_{i=1:p}$, denoted by $Z \sim GIG(p, \{r_i\}_{i=1:p}, \{\lambda_i\}_{i=1:p})$. In the case some of the λ_i have the same values, Z is still GIG distributed, but with a reduced depth. This is because the sum of the independent gamma random variable with identical rate parameters is still a gamma random variable, with the rate parameter unchanged and the shape parameter equals to the sum of the shape parameters of the corresponding components in the summation. Therefore, more generally, let $\{\lambda_l\}_{l=1:q}, q \leq p$ denote the distinct values of $\{\lambda_i\}_{i=1:p}$ and $\{r_l\}_{l=1:q}$ denote the shape parameters corresponding to λ_l, which is the sum of the r_i of the gamma random variables with rate parameters equal to λ_l. Thus $\Phi \sim GIG(q, \{r_l\}_{l=1:q}, \{\lambda_l\}_{l=1:q})$. The p.d.f. and c.d.f. of Z, denoted by $f_Z(z)$ and $F_Z(z)$ respectively, are given by [63]

$$f_Z(z) = f^{GIG}(z|q, \{r_l\}_{l=1:q}, \{\lambda_l\}_{l=1:q}), \qquad \text{(B.15)}$$

and

$$F_Z(z) = F^{GIG}(z|q, \{r_l\}_{l=1:q}, \{\lambda_l\}_{l=1:q}), \tag{B.16}$$

with

$$f^{GIG}(z|q, \{r_l\}_{l=1:q}, \{\lambda_l\}_{l=1:q}) = C \sum_{l=1}^{q} P_l(z) e^{-\lambda_l z}, \tag{B.17}$$

and

$$F^{GIG}(z|q, \{r_l\}_{l=1:q}, \{\lambda_l\}_{l=1:q}) = 1 - C \sum_{l=1}^{q} P_l^*(z) e^{-\lambda_l z}, \tag{B.18}$$

where

$$C = \prod_{l=1}^{q} \lambda_l^{r_l}, \quad P_l(z) = \sum_{k=1}^{r_l} c_{l,k} z^{k-1}, \quad P_l^*(z) = \sum_{k=1}^{r_l} c_{l,k} (k-1)! \sum_{i=0}^{k-1} \frac{z^i}{i! \lambda_l^{k-i}}, \tag{B.19}$$

with

$$c_{l,r_l} = \frac{1}{(r_l - 1)!} \prod_{j=1, j \neq l}^{q} (\lambda_j - \lambda_l)^{-r_j}, \tag{B.20}$$

and

$$c_{l,r_l-n} = \frac{1}{n} \sum_{j=1}^{n} \frac{(r_l - n + j - 1)!}{(r_l - n - 1)!} R(j, l, q) c_{l,r_l-(n-j)}, (n = 1, 2, \ldots, r_l - 1; i = 1, 2, \ldots, q) \tag{B.21}$$

where

$$R(j, l, q) = \sum_{k=1, k \neq l}^{q} r_k (\lambda_l - \lambda_k)^{-j}. \tag{B.22}$$

From $\tilde{k}_1^i = N_r - i$, $\tilde{k}_2^i = i$, $i = 1, 2, \ldots, N_t - 1$ and (B.10)-(B.14), we can write the rate

parameters of Y as

$$\begin{aligned}\{\gamma_0, \gamma_1, \cdots, \gamma_{K-1}\} = \{ \quad & N_r - 1, \\ & N_r - 1, \quad N_r - 2, \\ & N_r - 1, \quad N_r - 2, \quad N_r - 3, \\ & \vdots, \qquad \vdots, \qquad \vdots, \qquad \vdots, \\ & N_r - 1, \quad N_r - 2, \quad N_r - 3, \cdots, N_r - N_t + 1\}. \end{aligned} \tag{B.23}$$

For Y, let $\{\tau_l\}_{1:g}, g \leq K$ denote the distinct values of the rate parameters γ_m as shown in (B.23) and $\{\mu_l\}_{l=1:g}$ denote the corresponding integral shape parameters, from (B.23), we have

$$g = N_t - 1, \tag{B.24}$$

$$\{\tau_1, \tau_2, \cdots, \tau_g\} = \{N_r - 1, N_r - 2, \cdots, N_r - N_t + 1\} \tag{B.25}$$

$$\{\mu_1, \mu_2, \cdots, \mu_g\} = \{N_t - 1, N_t - 2, \cdots, 1\} \tag{B.26}$$

Hence $Y \sim GIG(g, \{\mu_l\}_{l=1:g}, \{\tau_l\}_{l=1:g})$, with p.d.f. $f_Y(y)$ and c.d.f. $F_Y(y)$ given by

$$f_Y(y) = f^{GIG}(y|g, \{\mu_l\}_{l=1:g}, \{\tau_l\}_{l=1:g}), \tag{B.27}$$

and

$$F_Y(y) = F^{GIG}(y|g, \{\mu_l\}_{l=1:g}, \{\tau_l\}_{l=1:g}), \tag{B.28}$$

correspondingly, the p.d.f. and c.d.f. of $\breve{\phi} = e^{-Y}$ are given by

$$f_{\breve{\phi}}(x) = x^{-1} f^{GIG}(-\ln(x)|g, \{\mu_l\}_{l=1:g}, \{\tau_l\}_{l=1:g}). \tag{B.29}$$

and

$$F_{\phi}^{\vee}(x) = 1 - F^{GIG}(-\ln(x)|g, \{\mu_l\}_{l=1:g}, \{\tau_l\}_{l=1:g}), \tag{B.30}$$

B.2 Log-normal Approximated Distribution of OM

Recall Y defined in (B.1), which is a sum of $N_t - 1$ independent negative logbeta random variables Y_i, with mean u_i and variance σ_i^2 given by [54]

$$\begin{aligned} u_i &= \mathbb{E}[Y_i] = E[-\ln(\tilde{\eta}_i)] \\ &= \psi(\tilde{k}_1^i + \tilde{k}_2^i) - \psi(\tilde{k}_1^i) \\ &= \psi(N_r) - \psi(N_r - i), \quad i = 1, 2, \ldots, N_t - 1, \end{aligned} \tag{B.31}$$

$$\begin{aligned} \sigma_i^2 &= Var(Y_i) = Var(-\ln(\tilde{\eta}_i)) \\ &= \psi_1(\tilde{k}_1^i) - \psi_1(\tilde{k}_1^i + \tilde{k}_2^i) \\ &= \psi_1(N_r - i) - \psi_1(N_r), \quad i = 1, 2, \ldots, N_t - 1, \end{aligned} \tag{B.32}$$

where $Var(X)$ denotes the variance of X and $\psi_1(x) = \frac{d}{dx}\psi(x)$ denotes the trigamma function. Based on central limit theorem for independent and non-identity random variables [64], we have

$$\lim_{N_t \to \infty} Y_{N_t} \sim \mathcal{N}(U_{N_t}, S_{N_t}^2), \tag{B.33}$$

where

$$U_{N_t} = \sum_{i=1}^{N_t - 1} u_i = (N_t - 1)\psi(N_r) - \sum_{i=1}^{N_t - 1} \psi(N_r - i), \tag{B.34}$$

and

$$S_{N_t}^2 = \sum_{i=1}^{N_t - 1} \sigma_i^2 = \sum_{i=1}^{N_t - 1} \psi_1(N_r - i) - (N_t - 1)\psi_1(N_r), \tag{B.35}$$

Therefore, the distribution of $\breve{\phi}$ converges to log-normal distribution [65] asymptotically,

$$\lim_{N_t \to \infty} \breve{\phi}_{N_t} \sim \ln \mathcal{N}(-U_{N_t}, S_{N_t}^2), \tag{B.36}$$

Appendix C

Computer Simulation Guide

This section explains the software that was used for generating the simulation results in this thesis and provides a guideline how to use it.

We consider uncoded complex LS-MIMO uplink multiuser systems. For each receive SNR level, the BER is calculated based on a minimum of 10^5 independent channel realizations and a minimum of 300 accumulated frame errors. The modulation schemes considered are rectangular M-QAM (4-QAM and 16-QAM) with Gray code labelling. In each channel realization, for each single antenna user, $n_c = \log_2(M)$ mutually independent randomly generated bits are mapped to a complex symbol. Then N_t complex symbols are transmitted by the single antenna users over randomly generated Rayleigh flat fading channels. Each component of the channel matrix is a CSCG random variable with zero mean and unit variance. The received signal vector is contaminated by AWGN.

The software testbed is implemented in C, compiled by GCC compiler version 4.9.2 on 64 bit Debian (release 8.2) Linux system. The experiments are performed on two desktops, one consisting of an Intel I5-4th generation CPU, quad cores with 3.2GHz clock rate and the other consisting of an Intel I7-5th generation CPU, six cores with 3.5GHz clock rate.

All the source files can be obtained from the author, Table.C.1 shows the major source files. “CommunicationLink.c” is the main source file. “systemConfigurations.h” and “com-

Table C.1 Major Source Files

Source Files	Descriptions
CommunicationLink.c	Integrated simulation main file
systemConfigurations.h	set the system configuration parameters
commonSettings.h	set the detection algorithms to be tested

monSettings.h" are the user interface files. "systemConfigurations.h" sets the system configuration parameters as shown Table.C.2. "commonSettings.h" contains the labels that control the detection algorithm used in simulation, as shown in Table.C.3. To simulate the selection based list detection algorithms discussed in chapter 4 and 5, activate the labels for channel partition (DMS/CIS), matrix inversion mode (SLD/SLDSENIAIU) and sub-detection(SIC/VBLASTSIC/IOSIC) accordingly. For example, to simulate algorithm"CIS-Ai-IO-SI", activate labels CIS, SLDSENIAIU and IOSIC together.

To generate the executable file on Linux operating systems, put all the source file under the same working directory and use the following command (notice these codes make use of the GNU Scientific Library (GSL) software package (version 2.1))

```
gcc CommunicationLink.c -o CIS-Ai-SIC -lgsl -lgslcblas -lm
```
(C.1)

"CIS-Ai-SIC" is the executable file, to run it, use the following command

```
./CIS-Ai-SIC &
```
(C.2)

Then a .txt output file that stores the simulation results is generated. At the beginning of this .txt file, there is a short paragraph that explains the system configuration information.

Table C.2 System configuration parameters

System configuration parameters	Descriptions
receiveAntennas	number of receive antennas
transmitAntennas	number of transmit antennas
symConstellationSize	size of rectangular M-QAM constellation $(4, 16, 64)$
minFrameErrors	minimum number of frame errors accumulated at each SNR level
minChannelRealizations	minimum number of channel realizations at each SNR level
Start_ SNR	start SNR level (dB)
End_ SNR	stop SNR level (dB)
Step_ SNR	step between two SNR levels (dB)
k	number of iterations of K-SENIA
L	initial size of the matrix inversion for K-SENIA-IU
OM	threshold value of OM setted for hybrid MMSE detection
perSENIA	usage percentage of K-SENIA/IU in hybrid MMSE detection
Nsel	number of antennas selected at the channel partition stage for selection based list detection
fileName	name of the output .txt file that stores the simulation results

Table C.3 Labels for detection algorithms

Labels	Descriptions
MMSEEMI	MMSE-EMI algorithm
MMSESE3	MMSE-SE3 algorithm
MMSESENIA	MMSE-SENIA algorithm
MMSEEMIIU	MMSE-EMI-IU algorithm
MMSESE3IU	MMSE-SE3-IU algorithm
MMSESENIAIU	MMSE-SENIA-IU algorithm
MMSEHYB	hybrid MMSE detector
DMS	DMS channel partition
CIS	CIS channel partition
SLDSENIAIU	selection based list detection employing K-SENIA/IU
SLD	selection based list detection employing exact matrix inversion
SIC	SIC sub-detection
VBLASTSIC	VBLAST-SIC sub-detection
IOSIC	IO-SIC sub-detection

References

[1] T. L. Marzetta, "Noncooperative cellular wireless with unlimited numbers of base station antennas," *Wireless Communications, IEEE Transactions on*, vol. 9, no. 11, pp. 3590–3600, 2010.

[2] F. Rusek, D. Persson, B. K. Lau, E. G. Larsson, T. L. Marzetta, O. Edfors, and F. Tufvesson, "Scaling up MIMO: Opportunities and challenges with very large arrays," *Signal Processing Magazine, IEEE*, vol. 30, no. 1, pp. 40–60, 2013.

[3] E. Larsson, O. Edfors, F. Tufvesson, and T. Marzetta, "Massive MIMO for next generation wireless systems," *Communications Magazine, IEEE*, vol. 52, no. 2, pp. 186–195, 2014.

[4] S. Yang and L. Hanzo, "Fifty years of MIMO detection: The road to large-scale MIMOs," *Communications Surveys & Tutorials, IEEE*, vol. 17, no. 4, pp. 1941–1988, 2014.

[5] C. Oestges and B. Clerckx, *MIMO wireless communications: from real-world propagation to space-time code design*. Academic Press, 2010.

[6] E. Viterbo and J. Boutros, "A universal lattice code decoder for fading channels," *Information Theory, IEEE Transactions on*, vol. 45, no. 5, pp. 1639–1642, 1999.

[7] M. O. Damen, H. El Gamal, and G. Caire, "On maximum-likelihood detection and the search for the closest lattice point," *Information Theory, IEEE Transactions on*, vol. 49, no. 10, pp. 2389–2402, 2003.

[8] J. Jaldén and B. Otterste, "On the complexity of sphere decoding in digital communications," *Signal Processing, IEEE Transactions on*, vol. 53, no. 4, pp. 1474–1484, 2005.

[9] Y.-C. Liang, S. Sun, and C. K. Ho, "Block-iterative generalized decision feedback equalizers for large MIMO systems: algorithm design and asymptotic performance analysis," *Signal Processing, IEEE Transactions on*, vol. 54, no. 6, pp. 2035–2048, 2006.

[10] Y.-C. Liang, G. Pan, and Z. Bai, "Asymptotic performance of MMSE receivers for large systems using random matrix theory," *Information Theory, IEEE Transactions on*, vol. 53, no. 11, pp. 4173–4190, 2007.

[11] Y.-C. Liang, E. Y. Cheu, L. Bai, and G. Pan, "On the relationship between MMSE-SIC and BI-GDFE receivers for large multiple-input multiple-output channels," *Signal Processing, IEEE Transactions on*, vol. 56, no. 8, pp. 3627–3637, 2008.

[12] K. V. Vardhan, S. K. Mohammed, A. Chockalingam, and B. S. Rajan, "A low-complexity detector for large MIMO systems and multicarrier CDMA systems," *Selected Areas in Communications, IEEE Journal on*, vol. 26, no. 3, pp. 473–485, 2008.

[13] B. Cerato and E. Viterbo, "Hardware implementation of a low-complexity detector for large MIMO," in *Circuits and Systems, 2009. ISCAS 2009. IEEE International Symposium on*. IEEE, 2009, pp. 593–596.

[14] P. Li and R. D. Murch, "Multiple output selection-LAS algorithm in large MIMO systems," *Communications Letters, IEEE*, vol. 14, no. 5, pp. 399–401, 2010.

[15] T. Datta, N. Srinidhi, A. Chockalingam, and B. S. Rajan, "Random-restart reactive tabu search algorithm for detection in large-MIMO systems," *Communications Letters, IEEE*, vol. 14, no. 12, pp. 1107–1109, 2010.

[16] N. Srinidhi, T. Datta, A. Chockalingam, and B. S. Rajan, "Layered tabu search algorithm for large-MIMO detection and a lower bound on ML performance," *Communications, IEEE Transactions on*, vol. 59, no. 11, pp. 2955–2963, 2011.

[17] P. Som, T. Datta, N. Srinidhi, A. Chockalingam, and B. S. Rajan, "Low-complexity detection in large-dimension MIMO-ISI channels using graphical models," *Selected Topics in Signal Processing, IEEE Journal of*, vol. 5, no. 8, pp. 1497–1511, 2011.

[18] J. Goldberger and A. Leshem, "MIMO detection for high-order QAM based on a Gaussian tree approximation," *Information Theory, IEEE Transactions on*, vol. 57, no. 8, pp. 4973–4982, 2011.

[19] T. L. Narasimhan and A. Chockalingam, "Channel hardening-exploiting message passing (CHEMP) receiver in large-scale MIMO systems," *Selected Topics in Signal Processing, IEEE Journal of*, vol. 8, no. 5, pp. 847–860, 2014.

[20] S. Wu, L. Kuang, Z. Ni, J. Lu, D. D. Huang, and Q. Guo, "Low-complexity iterative detection for large-scale multiuser MIMO-OFDM systems using approximate message passing," *Selected Topics in Signal Processing, IEEE Journal of*, vol. 8, no. 5, pp. 902–915, 2014.

[21] A. Kumar, S. Chandrasekaran, A. Chockalingam, and B. S. Rajan, "Near-optimal large-MIMO detection using randomized MCMC and randomized search algorithms," in *Communications (ICC), 2011 IEEE International Conference on*. IEEE, 2011, pp. 1–5.

[22] T. Datta, N. A. Kumar, A. Chockalingam, and B. S. Rajan, "A novel Monte-Carlo-sampling-based receiver for large-scale uplink multiuser MIMO systems," *Vehicular Technology, IEEE Transactions on*, vol. 62, no. 7, pp. 3019–3038, 2013.

[23] Q. Zhou and X. Ma, "Element-based lattice reduction algorithms for large MIMO detection," *Selected Areas in Communications, IEEE Journal on*, vol. 31, no. 2, pp. 274–286, 2013.

[24] Z. Luo, M. Zhao, S. Liu, and Y. Liu, "Generalized parallel interference cancellation with near-optimal detection performance," *Signal Processing, IEEE Transactions on*, vol. 56, no. 1, pp. 304–312, 2008.

[25] D. Radji and H. Leib, "Interference cancellation based detection for V-BLAST with diversity maximizing channel partition," *Selected Topics in Signal Processing, IEEE Journal of*, vol. 3, no. 6, pp. 1000–1015, 2009.

[26] ——, "Asymptotic optimal detection for MIMO communication systems employing tree search with incremental channel partition preprocessing," *Transactions on Emerging Telecommunications Technologies*, vol. 24, no. 2, pp. 166–184, 2013.

[27] Z.-Y. Huang and P.-Y. Tsai, "Efficient implementation of QR decomposition for gigabit MIMO-OFDM systems," *Circuits and Systems I: Regular Papers, IEEE Transactions on*, vol. 58, no. 10, pp. 2531–2542, 2011.

[28] L. Ma, K. Dickson, J. McAllister, and J. McCanny, "QR decomposition-based matrix inversion for high performance embedded MIMO receivers," *Signal Processing, IEEE Transactions on*, vol. 59, no. 4, pp. 1858–1867, 2011.

[29] S. Moussa, A. M. A. Razik, A. O. Dahmane, and H. Hamam, "FPGA implementation of floating-point complex matrix inversion based on Gauss-Jordan elimination," in *Electrical and Computer Engineering (CCECE), 2013 26th Annual IEEE Canadian Conference on*. IEEE, 2013, pp. 1–4.

[30] B. M. Hochwald, T. L. Marzetta, and V. Tarokh, "Multiple-antenna channel hardening and its implications for rate feedback and scheduling," *Information Theory, IEEE Transactions on*, vol. 50, no. 9, pp. 1893–1909, 2004.

[31] M. Wu, B. Yin, A. Vosoughi, C. Studer, J. R. Cavallaro, and C. Dick, "Approximate matrix inversion for high-throughput data detection in the large-scale MIMO uplink," in *Circuits and Systems (ISCAS), 2013 IEEE International Symposium on*. IEEE, 2013, pp. 2155–2158.

[32] M. Wu, B. Yin, G. Wang, C. Dick, J. R. Cavallaro, and C. Studer, "Large-scale MIMO detection for 3GPP LTE: algorithms and FPGA implementations," *Selected Topics in Signal Processing, IEEE Journal of*, vol. 8, no. 5, pp. 916–929, 2014.

[33] H. Prabhu, J. Rodrigues, O. Edfors, and F. Rusek, "Approximative matrix inverse computations for very-large MIMO and applications to linear pre-coding systems," in *Wireless Communications and Networking Conference (WCNC), 2013 IEEE*. IEEE, 2013, pp. 2710–2715.

[34] D. Zhu, B. Li, and P. Liang, "On the matrix inversion approximation based on Neumann Series in Massive MIMO systems," *arXiv preprint arXiv:1503.05241*, 2015.

[35] A. Ben-Israel, "An iterative method for computing the generalized inverse of an arbitrary matrix," *Mathematics of Computation*, pp. 452–455, 1965.

[36] V. Pan and J. Reif, "Efficient parallel solution of linear systems," in *Proceedings of the seventeenth annual ACM symposium on Theory of computing*. ACM, 1985, pp. 143–152.

[37] V. Pan and R. Schreiber, "An improved Newton iteration for the generalized inverse of a matrix, with applications," *SIAM Journal on Scientific and Statistical Computing*, vol. 12, no. 5, pp. 1109–1130, 1991.

[38] Y. Wang and H. Leib, "Sphere decoding for MIMO systems with Newton iterative matrix inversion," *Communications Letters, IEEE*, vol. 17, no. 2, pp. 389–392, 2013.

[39] F. Rosario, F. A. Monteiro, and A. Rodrigues, "Fast matrix inversion updates for Massive MIMO detection and precoding," *Signal Processing Letters, IEEE*, vol. 23, no. 1, pp. 75–79, 2016.

[40] L.-L. Yang, "Using multi-stage MMSE detection to approach optimum error performance in multiantenna MIMO systems," in *Vehicular Technology Conference Fall (VTC 2009-Fall), 2009 IEEE 70th*. IEEE, 2009, pp. 1–5.

[41] A. Chockalingam and B. S. Rajan, *Large MIMO systems*. Cambridge University Press, 2014.

[42] X. Ma and W. Zhang, "Performance analysis for MIMO systems with lattice-reduction aided linear equalization," *Communications, IEEE Transactions on*, vol. 56, no. 2, pp. 309–318, 2008.

[43] T. Kailath, H. Vikalo, and B. Hassibi, "MIMO receive algorithms," *Space-Time Wireless Systems: From Array Processing to MIMO Communications*, 2005.

[44] S. Loyka and F. Gagnon, "Performance analysis of the V-BLAST algorithm: an analytical approach," *Wireless Communications, IEEE Transactions on*, vol. 3, no. 4, pp. 1326–1337, 2004.

[45] Y. Jiang, X. Zheng, and J. Li, "Asymptotic performance analysis of V-BLAST," in *Global Telecommunications Conference, 2005. GLOBECOM'05. IEEE*, vol. 6. IEEE, 2005, pp. 5–pp.

[46] A. M. Tulino and S. Verdú, *Random matrix theory and wireless communications*. Now Publishers Inc, 2004, vol. 1.

[47] A. Edelman, "Eigenvalues and condition numbers of random matrices," *SIAM Journal on Matrix Analysis and Applications*, vol. 9, no. 4, pp. 543–560, 1988.

[48] G. H. Golub and C. F. Van Loan, *Matrix computations*. John Hopkins University Press, 2012, vol. 3.

[49] T. K. Moon and W. C. Stirling, *Mathematical methods and algorithms for signal processing*. Prentice hall New York, 2000, vol. 1.

[50] T. H. Cormen, *Introduction to algorithms*. MIT press, 2009.

[51] J. Arias-García, R. P. Jacobi, C. H. Llanos, and M. Ayala-Rincón, "A suitable FPGA implementation of floating-point matrix inversion based on Gauss-Jordan elimination," in *Programmable Logic (SPL), 2011 VII Southern Conference on*. IEEE, 2011, pp. 263–268.

[52] D. S. Watkins, *Fundamentals of matrix computations*. John Wiley & Sons, 2004, vol. 64.

[53] D. K. Nagar and A. K. Gupta, "Expectations of functions of complex Wishart matrix," *Acta applicandae mathematicae*, vol. 113, no. 3, pp. 265–288, 2011.

[54] A. K. Gupta and S. Nadarajah, *Handbook of beta distribution and its applications*. CRC Press, 2004.

[55] F. J. Marques, C. A. Coelho, and B. C. Arnold, "A general near-exact distribution theory for the most common likelihood ratio test statistics used in Multivariate Analysis," *Test*, vol. 20, no. 1, pp. 180–203, 2011.

[56] C. Khatri, "Classical statistical analysis based on a certain multivariate complex Gaussian distribution," *The Annals of Mathematical Statistics*, pp. 98–114, 1965.

[57] C. A. Coelho and F. J. Marques, "The Multi-Sample Block-Scalar Sphericity Test: Exact and near-exact distributions for its likelihood ratio test statistic," *Communications in Statistics-Theory and Methods*, vol. 42, no. 7, pp. 1153–1175, 2013.

[58] C. Khatri, "A test for reality of a covariance matrix in a certain complex Gaussian distribution," *The Annals of Mathematical Statistics*, vol. 36, no. 1, pp. 115–119, 1965.

[59] M. D. Springer and M. D. Springer, "The algebra of random variables," Tech. Rep., 1979.

[60] R. Bhargava and C. Khatri, "The distribution of product of independent beta random variables with application to multivariate analysis," *Annals of the Institute of Statistical Mathematics*, vol. 33, no. 1, pp. 287–296, 1981.

[61] J. Tang and A. Gupta, "On the distribution of the product of independent beta random variables," *Statistics & Probability Letters*, vol. 2, no. 3, pp. 165–168, 1984.

[62] C. A. Coelhoa and R. P. Albertob, "On the distribution of the product of independent beta random variables–applications."

[63] C. A. Coelho, "The generalized integer Gamma distributiona basis for distributions in multivariate statistics," *Journal of Multivariate Analysis*, vol. 64, no. 1, pp. 86–102, 1998.

[64] P. Billingsley, "Probability and measure," *Wiley series in probability and mathematical statistics Show all parts in this series*, 1995.

[65] N. L. Johnson and S. Kotz, *Distributions in Statistics: Continuous Univariate Distributions: Vol.: 2*. Houghton Mifflin, 1970.

[66] P. W. Wolniansky, G. J. Foschini, G. Golden, and R. A. Valenzuela, "V-BLAST: An architecture for realizing very high data rates over the rich-scattering wireless channel," in *Signals, Systems, and Electronics, 1998. ISSSE 98. 1998 URSI International Symposium on*. IEEE, 1998, pp. 295–300.

[67] H. Zhang, H. Dai, Q. Zhou, and B. L. Hughes, "On the diversity order of spatial multiplexing systems with transmit antenna selection: A geometrical approach," *Information Theory, IEEE Transactions on*, vol. 52, no. 12, pp. 5297–5311, 2006.

[68] A. Paulraj, R. Nabar, and D. Gore, *Introduction to space-time wireless communications*. Cambridge university press, 2003.

[69] S. Verdu, *Multiuser detection*. Cambridge university press, 1998.

[70] J. Benesty, Y. Huang, and J. Chen, "A fast recursive algorithm for optimum sequential signal detection in a BLAST system," *Signal Processing, IEEE Transactions on*, vol. 51, no. 7, pp. 1722–1730, 2003.

[71] R. Bekkerman, M. Bilenko, and J. Langford, *Scaling up machine learning: Parallel and distributed approaches*. Cambridge University Press, 2011.

[72] P. Som, T. Datta, A. Chockalingam, and B. S. Rajan, "Improved large-MIMO detection based on damped belief propagation," in *Information Theory (ITW 2010, Cairo), 2010 IEEE Information Theory Workshop on*. IEEE, 2010, pp. 1–5.

[73] D. Bickson, O. Shental, P. Siegel, J. Wolf, and D. Dolev, "Linear detection via belief propagation," in *Proc. 45th Allerton Conf. on Communications, Control and Computing*, 2007.

[74] A. Ranganathan, M. Kaess, and F. Dellaert, "Loopy SAM," in *Proceedings of the 20th International Joint Conference on Artificial Intelligence (IJCAI)*, 2007, pp. 6–12.

[75] G. Elidan, I. McGraw, and D. Koller, "Residual belief propagation: Informed scheduling for asynchronous message passing," *arXiv preprint arXiv:1206.6837*, 2012.

[76] J. Gonzalez, Y. Low, and C. Guestrin, "Residual Splash for Optimally Parallelizing Belief Propagation," in *AISTATS*, vol. 2, no. 2.2, 2009, p. 2.

[77] A. T. Ihler, W. F. John III, and A. S. Willsky, "Loopy belief propagation: Convergence and effects of message errors," *Journal of Machine Learning Research*, vol. 6, no. May, pp. 905–936, 2005.

[78] J. Pearl, *Probabilistic reasoning in intelligent systems: networks of plausible inference*. Morgan Kaufmann, 2014.

[79] A. Papoulis and S. U. Pillai, *Probability, random variables, and stochastic processes*. Tata McGraw-Hill Education, 2002.